University
*of Ljubljana*
Faculty
*of Civil and Geodetic Engineering*

*Jamova 2, p.o.b. 3422*
*1115 Ljubljana, Slovenia*
*telephone +386 1 47 68 500*
*fax +386 1 42 50 681*
*fgg@fgg.uni-lj.si*

**TRANSFER OF COPYRIGHT AGREEMENT**

Copyright of the master degree thesis below is hereby transferred to The University of Ljubljana, Faculty of Civil and Geodetic Engineering effective for uploading into digital repository of Faculty of Civil and Geodetic Engineering.

Seismic Performance Evaluation of a Historic Unreinforced Masonry Building Structure
Title of the Thesis

Master Sc. Thesis
Type of Thesis (Graduation Thesis, Master Sc.Thesis, Master Degree Thesis, Ph.D. Thesis)

Camathias Ueli
Name of Author

Prof. Dr. Bozidar Stojadinović
Name of the Supervisor and affiliation

Prof. Dr. Vlatko Bosiljkov ; Dr. Nebojša Mojsilović
Name of the Co-Supervisor and affiliation

Signature required by the author.

Signature

7.11.13
Date signed

Ueli Camathias
Printed Name

Title, if not author

ETH (Swiss Federal Institute of Technology Zürich)
Company or Institution

Eidgenössische Technische Hochschule Zürich
Swiss Federal Institute of Technology Zurich

University of Ljubljana
Faculty of Civil and Geodetic Engineering

# Seismic Performance Evaluation of a Historic Unreinforced Masonry Building Structure

## Master Thesis

**Swiss Federal Institute of Technology**

**Institute of Structural Engineering**

Student: Ueli Camathias

Supervisor: Prof. Dr. Bozidar Stojadinović

Advisor: Dr. Nebojša Mojsilović

**University of Ljubljana**

**Faculty of Civil and Geodetic Engineering**

Advisor: Prof. Dr. Vlatko Bosiljkov

Ljubljana, 01.07.2013

# Acknowledgments

I would like to express my deepest gratitude to my supervisor *Prof. Dr. Bozidar Stojadinovic* and my advisor *Dr. Nebojsa Mojsilovic,* representing the ETH Zürich, and to my advisor *Prof. Dr. Vlatko Bosiljkov*, representing the University of Ljubljana, for their continuous guidance and excellent cooperation during the completion of this master thesis.

# Abstract

This thesis deals with an evaluation of the seismic performance of an old unreinforced masonry building structure. For this purpose the *Bundeshaus Ost* in Bern is selected. The structure is already used in SIA D0237 as a reference building for seismic analysis. After a survey of the building, where publicly available information about the structure was collected, a deformation-based analysis was performed using 3Muri software and two building models, one with in-plane flexible and the other with in-plane rigid floor diaphragms. 3Muri was used to model the structure and then to compute a pushover force-deformation response curve for the structure. Subsequently, the available capacities are compared to the correspondent demands to demonstrate that the building pushover response is satisfactory. Finally, an evaluation procedure for analyzing the seismic performance of old masonry structures was formulated and proposed.


1st of July 2013 Ueli Camathias

# Table of content

# List of Figures

# List of Tables

# 1 Introduction

The purpose of this thesis is to conduct a seismic performance evaluation of an old unreinforced masonry building structure. Therefore the *Bundeshaus Ost* building in Bern is selected. This structure is already used in SIA D0237 [1] as a reference building for seismic analysis.

Before starting the evaluation, different existing evaluation procedures are investigated. In general, the evaluation procedures can be divided into two groups, namely configuration based checks and strength checks. Configuration based checks serve to figure out quickly the general behavior of a structure based on its configuration, while strength checks serve to compute the load carrying capacity of the structure. The methods described in Eurocode 8, Swisscode and FEMA 310 are compared. Conclusively it can be said, that FEMA includes the most advanced evaluation procedure for the evaluation of existent building structures.

The first phase of the evaluation of the *Bundeshaus Ost* in Bern is the survey of the building. In this phase, the first step concerns the seismic properties of the building. Bern lies in the lowest seismic zone Z1 of Switzerland. Therefore the seismic impact loads are relatively low. Further the structure is assigned to the soil class B and to the importance class II. In the second step, the geometry of the building is studied. For this purpose, the federal office for property, construction and logistics (BBL) provided the plans created for the building permit of the ongoing renovation. In the third step, the structural properties are investigated. It is important to understand the structural system in order to analyze the resistance of the building. In the forth step, the influence of flexible and rigid floor compositions is discussed. Then, in the fifth step, the masonry characteristics are defined. Unfortunately no values out of a materials' survey were available. Therefore, these values were estimated using provisions described in codes. The last step of this phase is the site visit. During the site visit, the collected data is verified. Remaining questions may be answered and additional information collected.

The second phase of the evaluation concerns the development of the numerical simulation. For this purpose the 3Muri software is selected, which is a numerical computation program created for the seismic analysis of masonry structures. In the first step, a simple test structure is defined and modeled. This structure is analyzed using the equivalent lateral force method, the response spectra method. Further a hand-calculated pushover curve is computed using the method developed by Bachmann und Lang [2]. Then, the results of these hand calculations are compared with the results from the 3Muri computation. This comparison shows almost equal values for the hand-calculated pushover curve and the 3Muri-computed pushover curve. After the verification, a model of the *Bundeshaus Ost* structure is developed in 3Muri.

The third phase discusses the results. In order to compare the results, the demands for the *Bundeshaus Ost* structure are computed using a UHS for Bern and by using the equations for the design response spectra of SIA 261. By applying the participation factor, the demands are transformed into the values that can be compared with the delivered values of the 3Muri computation. The *Bundeshaus Ost* structure satisfies all the required demands for the three performance levels, operational (72y), limited damage (475y) and collapse prevention (2475y). An in-plane deflection of the flexible-floor model of the third floor diaphragm was found under loading in the NS-direction.

After the structure with flexible diaphragms was analyzed, a second model was developed by making the flexible floor diaphragms rigid in their own planes. This way a flexible-floor structure can be compared with a rigid-floor structure. The results show, that the performance of the structure is better with rigid floors. However, it is difficult to compare the values for the loading in NS-direction, since the reference node, used for the computation, lies in the diaphragm deflection in the third floor of the flexible floor model. Therefore, this pushover curve shows a large elastic deformation, which is not representative of the general behavior of the structure.

Next, the story drifts are computed for the flexible-floor and the rigid-floor models. The drifts are computed on a conservative way. However, the largest drift is 0.5% in the ground floor in the NS-direction for the rigid-floor model. This value lies in the expected range of 0.4% to 0.6%. It can be observed that the rigid-floor model has a larger story-drift capacity then the flexible-floor model.

Finally, a local evaluation is performed in order to confirm the results obtained by comparing the resisting accelerations. The resistant accelerations obtained out of the out-of-plane mechanisms are expected to be smaller then those of the global evaluation. This expectation can be confirmed.

The last part of this dissertation is a proposal for an evaluation procedure for historic masonry buildings. This proposal is built upon the methods discussed in the first part of the dissertation and the experience gained through the data collection, modeling and static pushover evaluation of the *Bundeshaus Ost* building.

# 2 Masonry Structures

## 2.1 Old Masonry Structures

The investigation of an old masonry structure is often combined with several difficulties. One aspect of difficulty is to find the original design plans of the structure. Over time, changes may have occurred to the structure. These might be structural modifications due to changes of use or combined with renovations. Another reason may be the purchase of new technical installations such as a heating system. Not all modifications concern the structural system, but they often do. If modifications took place, they should be notified in the building chronology. Unfortunately, documentation on modifications of the structure is often not available either. The engineer, who is investigating the structure, needs to find the required information by collecting all the data he can find on the structure. In case of an earthquake analysis, it may also be useful to find old records reporting of historical earthquakes in the region. They may tell the engineer if the structure already underwent some seismic activity. The masonry characteristics of an old structure are also difficult to estimate, since there were no codes existing at the time of the construction, which would provide information on minimal requirements. If a material survey of the structure is too excessive, the engineer has to define the parameters using the provisions in the codes or by using reference values of similar structures.

In any case, a site visit of the structure is recommended. Under proper preparation, several questions may be answered during this inspection. Dependent on how deeply the analysis should be performed, it may be necessary to drill some holes into the walls or to open some floors to see their construction. Similarly, connections and details are often hidden from the eye, which makes it difficult to discover them. An experienced engineer might eventually be able to suggest their existence and location. In this case an investigation at the expected location may give confirmation.

Analyzing an old building means that a structure is investigated, which exists of materials that have been exposed to several influences. Hence, it would be wrong to expect from an old building to satisfy the latest design criteria. An old, intact building may already have reached its original live expectancy. If the structure presents itself still in a good shape, it could be economical to upgrade it in order to extend its life duration. On the other side, if the structure is in a bad shape, it might be uneconomical to renovate it and thus it would be better to demolish it and build something new.

Most existing buildings in Switzerland are not designed for earthquake loads. If they are investigated, they often fail to satisfy the seismic requirements for new buildings. According to the existing codes, existing buildings have to be assigned to the non-ductile structural behavior class meaning that a q-factor as low as 1.5 has to be

assumed which leads to high seismic action effects. It may be rather uneconomic to upgrade existing buildings so that they satisfy the requirements of the new codes. Therefore a separate Standard SIA 2018 [3] was introduced in 2004 in order to offer a standard with lower seismic requirements for existing buildings [4].

The lower requirements for existing buildings are justified because first, the actual strength of the components is greater than the one used in the evaluation and second, because an existing building has left a reduced life expectancy [5].

## 2.2 Methods of Evaluation

This chapter presents an overview of the seismic evaluation procedures. They can be divided into two main groups: configuration-based checks and strength checks. The configuration-based checks serve as a tool to figure out unfavorable building characteristics, while the strength checks serve to assess the load carrying capacity of the structure. If the configuration is unfavorable, the building is not performing as well during an earthquake as a regular building. Deficiencies are found in irregular geometry, a weakness in a given story, concentration of mass, or in discontinuity in the lateral force resisting system. Strength, stiffness, geometry and mass are found to involve irregularities, while horizontal distribution of lateral forces to the resisting frames or shear walls involve horizontal irregularities. [5] As seen in Figure 2.1, the checks include an investigation of the load path, weak story, soft story, geometry and effective mass as well as torsion and pounding.

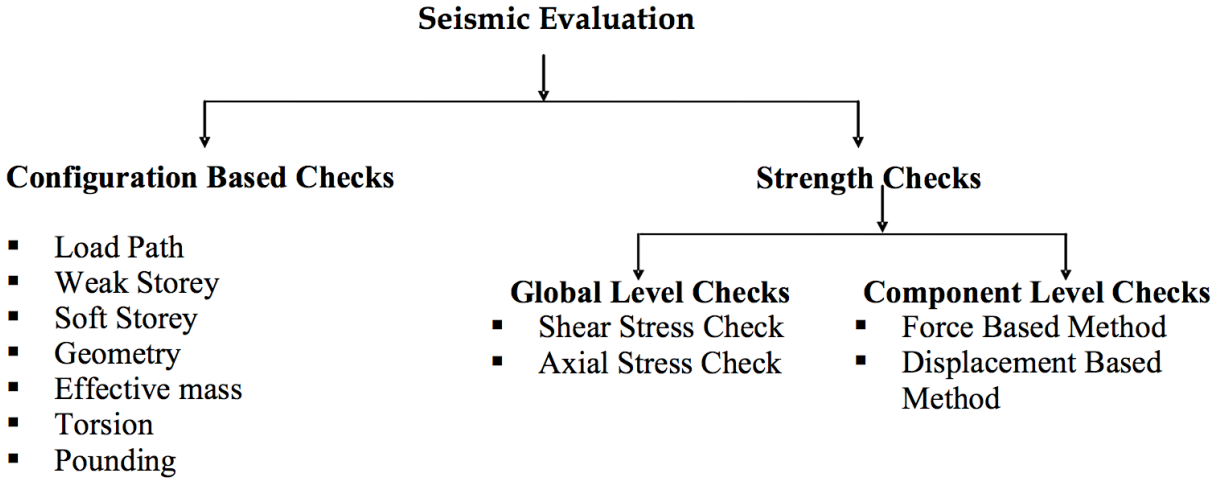


**Figure 2.1** General structure of evaluation procedures [5]

The strength checks include a more in-depth investigation. In this category two groups of investigation can be found, namely the global level and the component level checks. In general, global level checks include the estimation of the shear stress and axial stress. With the shear stress check, a quick assessment of the overall level of demand of the structure is provided. The axial stress check investigates columns that carry substantial amounts of gravity loads and that may therefore have limited additional capacity resistance against seismic forces. Columns

with high gravity loads may fail in a non-ductile manner because of excessive axial compression and especially under horizontal displacement [5].

The component level analysis gives a more detailed assessment of the building. It helps identifying the weak links of a building. These checks exist out of two types of analysis, the force-based methods and the displacement-based methods. A deformation-controlled action can be defined as an action where a deformation is allowed to exceed the yield value. The maximum deformation is limited by the ductility capacity of a component. A force-controlled action is in contrast defined as an action where the deformation is not allowed to exceed the yield point value [5].

## 2.3 Swisscode

Until the year of 1970, no regulations concerning the seismic design of structures were existent. The first one was mentioned in SIA 160 [6]. Only five years later, the recommendation SIA 160/2 [7] dealing with the seismic design, was released. In 1989 three importance classes, as well as the first response spectra, were implemented in the new SIA 160 [8]. By 1999, the development of the so-called Swisscodes, a new generation of codes, was initialized. The new codes are generally based on the Eurocodes with some adaptations. Within four years, the new codes were published. Concerning the earthquake design it seemed somewhat exaggerated to develop a self-standing document for the seismic regulations. Hence it was decided to spread the seismic information in different design codes. The regulations concerning the earthquake loads were added to the action code SIA 261 [9], while the specific material characteristics concerning seismic design were integrated into the corresponding design codes for the different materials. This way, an improved user-friendliness of the code could be achieved [4].

Because most of the existing buildings in Switzerland are not designed under earthquake considerations, Standard SIA 2018 [3] was released in the year 2004. In this document an evaluation procedure for existing buildings is explained. The process is apparent from Figure 2.2.

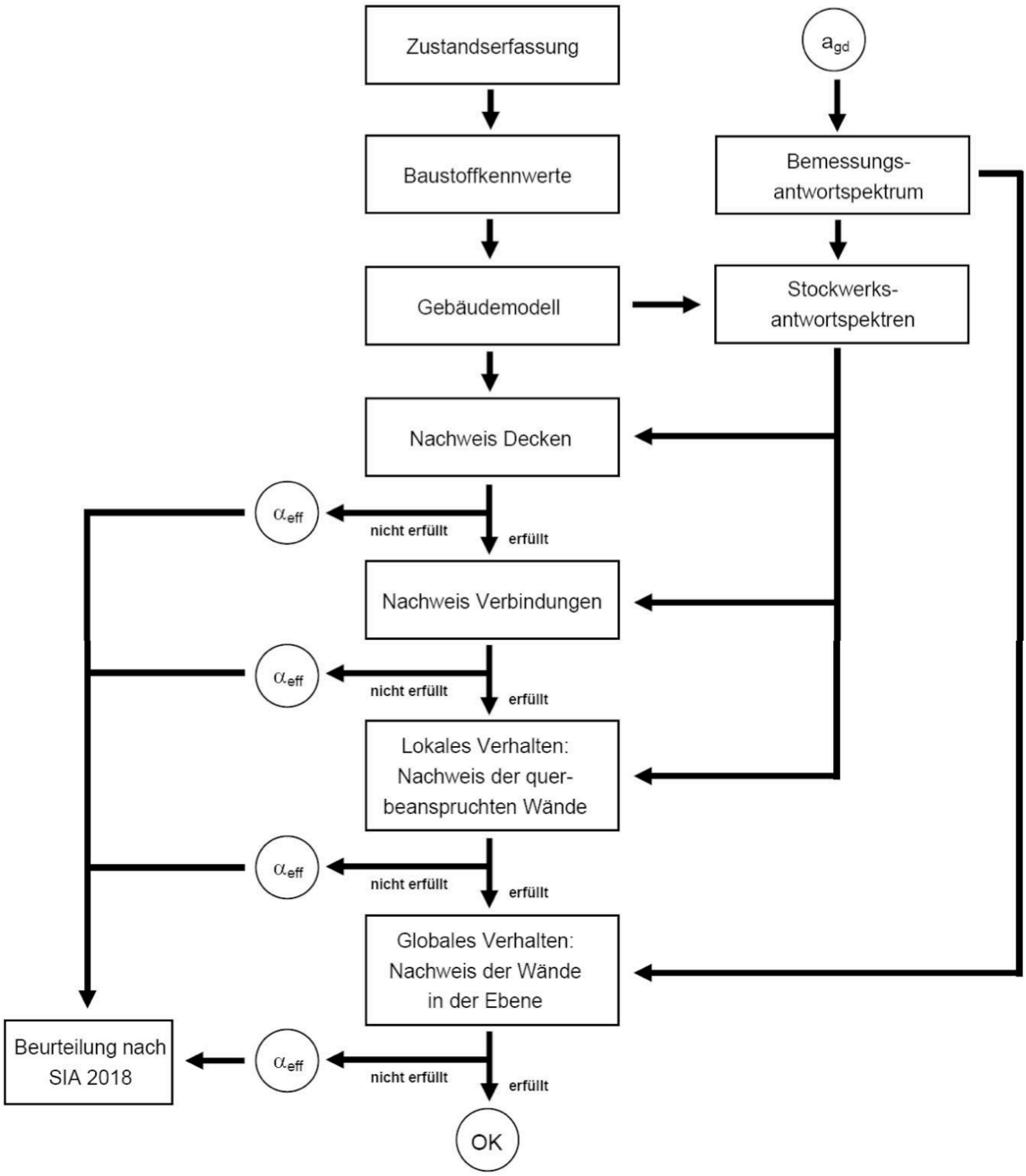


**Figure 2.2** Evaluation procedure according to SIA D0237 [1]

According to standard SIA 2018, the investigation is divided into three main steps as explained below.

The first step consists of a survey of the building. In this phase, the basic material is collected and evaluated. The structure is assigned to an importance class. Further the structural properties are analyzed. The material characteristics need to be investigated and defined for the following analysis of the building's resistance. In the second step the factor of compliance $\alpha_{eff}$ is estimated and then compared with the reduction factors $\alpha_{adm}$ and $\alpha_{\min}$. Further the evaluation of the non-structural elements

follows. Eventually an evaluation of commensurability in order to insure a proper use of mediums to reduce the general risk and reasonableness is committed.

In the third and last step, improvement recommendations follow. These recommendations concern rather general principles then detailed, practical solutions.

Standard SIA 2018 states that masonry structures are usually investigated using force-based design methods. If deformation-based design methods are selected to analyze masonry structures, which are generally preferred for existing buildings, the floor displacements are compared. The required assumptions may be taken using SIA 266 [10] and EC8-3 [11]. Further it is explained that the out-of-plane resistance is checked by comparing the wall's slenderness with the corresponding values in Table 1 of standard SIA 2018.

In order to examine the seismic resistance of existing buildings, the Federal Office for Water and Geology (FOWG) developed an evaluation procedure [12] based on the FEMA 310 [13] and the standard SIA 2018. In order to discover the deficiencies of a building as quickly as possible, it includes evaluation steps based on checklists similar to FEMA 310. Once deficiencies are discovered, standard SIA 2018 is applied for a more in-depth analysis.

## 2.4 Eurocode

Unlike the Swisscode, Eurocode 8 exists out of six parts concerning seismic rules written on not less then 638 pages. The EC8-1 [14] provides general seismic requirements for analysis and the EC8-3 [11] deals with more specific requirements and devotes a chapter to existing masonry structures. By contrast, Swisscode has only 26 pages dealing with seismic design [4].

Because Swisscode is in many issues based on Eurocode, Eurocode has a similar evaluation procedure for old masonry structures. The procedure can also be divided into three steps as shown in Figure 2.3.

The first step describes the survey of the building. It includes the same tasks as described above in Chapter 2.3. In addition to the Swisscode, the Eurocode defines three knowledge levels. A confidence factor belongs to each level. This factor is used to regard the uncertainties related to the analysis of the relevant structure. With this level, Table 3.1 of EC8-3 explains which analysis methods can be applied. The confidence factors are defined as follows:

| | |
|---|---|
| Limited knowledge | $CF_{KL1} = 1.35$ |
| Normal knowledge | $CF_{KL2} = 1.20$ |
| Full knowledge | $CF_{KL3} = 1.00$ |

In the second step the verification of the analysis is held. For plain masonry buildings, static non-linear methods are adopted. After the analysis is performed, a computational verification is made at the component level. It is based on the verification of all cross-sections. If a time domain method is used, the post yield deformations should be higher than the corresponding demand values. Further the predicted level of damage has to be kept within acceptable limits. In case that the requirements are not satisfied, the third step is required, in which structural interventions are described conceptually. In contrast to the Swisscode, they are more detailed. But Eurocode also fails to describe practical solutions in detail [5].

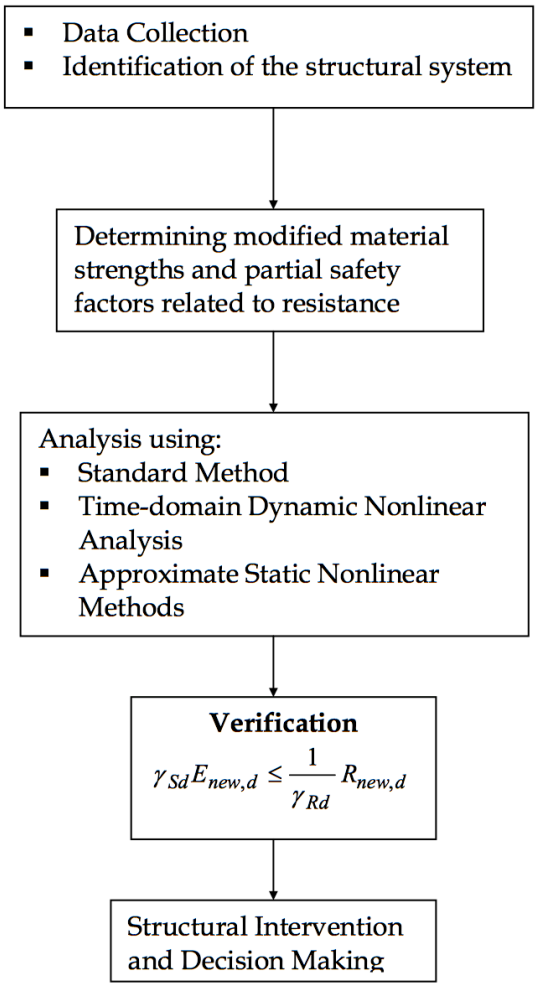


**Figure 2.3** Evaluation procedure according to Eurocode 8 [5]

## 2.5 FEMA

The Federal Emergency Management Agency (FEMA) developed an own evaluation procedure. It contains a rigorous approach to determine existing structural conditions. Like the Eurocode, it knows performance levels of design, which describe the level of damage. The performance levels are determined by the importance of the building and the consequences of damage. In the Swisscode, for instance, are no performance levels defined yet. Before beginning the seismic evaluation the data of

the building needs to be collected. Then the evaluation starts, consisting out of three tiers, as presented in Figure 2.4.

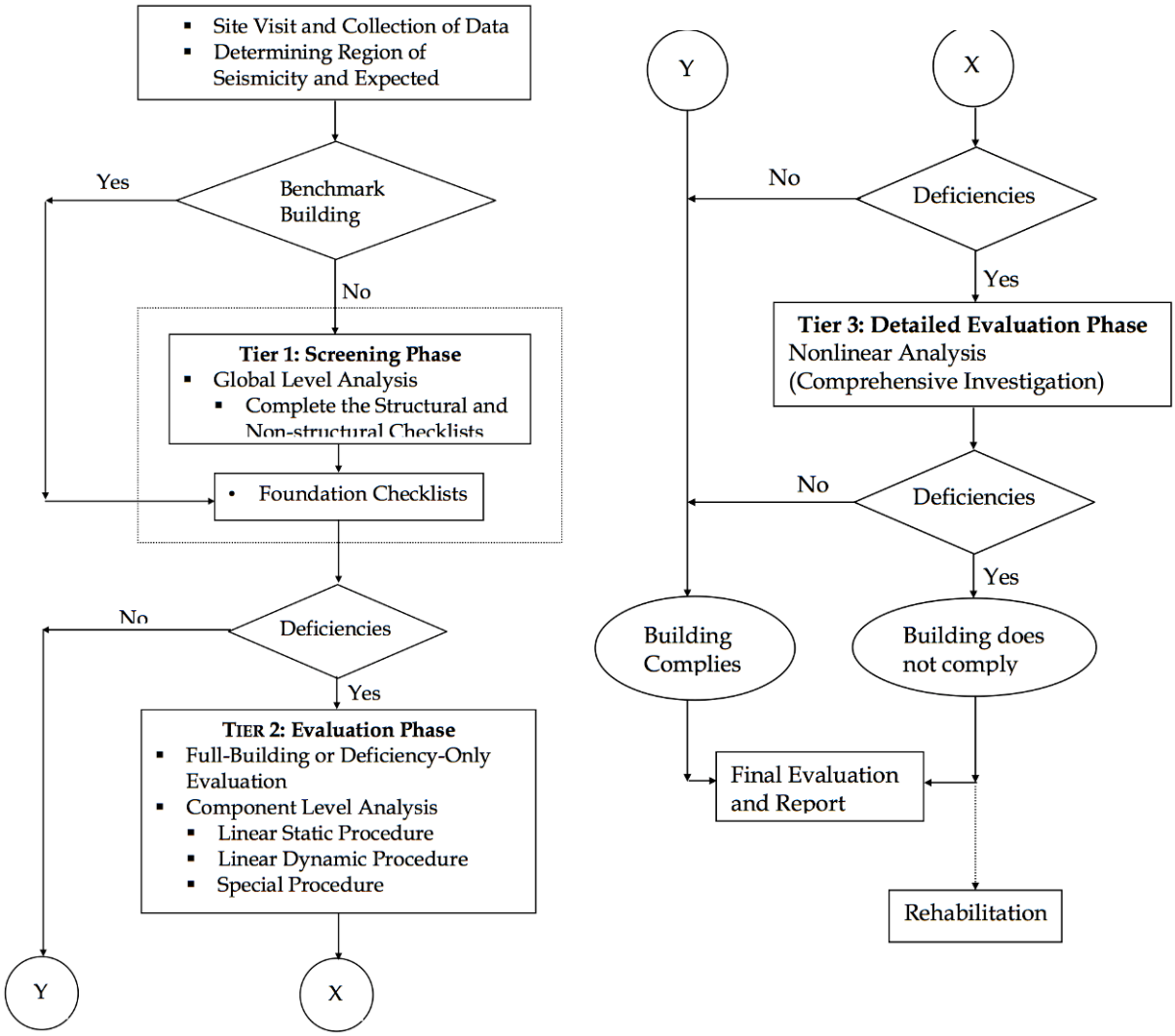


**Figure 2.4** Evaluation procedure according to FEMA 310 [5]

In the first tier, the screening phase, the building is briefly analyzed. The intention is to realize as quickly as possible if the structure complies with the provisions of the FEMA 310. The investigation follows a checklist. After its evaluation it should become clear which parts of the structure do not meet the requirements of the building codes. Where the requirements are not satisfied a deeper evaluation is required.

With tier 2, two options are available. Either a complete analysis of the building is performed concerning the deficiencies identified in tier 1 or only the deficient parts are analyzed in detail. Generally simplified linear analysis methods are applied, such as linear static or dynamic analysis methods. For unreinforced masonry buildings with flexible diaphragms, a displacement-based lateral force procedure is required. If the structure does still not satisfy the criteria, a detailed evaluation follows with tier 3. In this step, conservative assumptions should be minimized. To justify such a detailed evaluation, a significant economic or other advantage is required. If an

existing building is analyzed, a factor of 0.75 is multiplied to the conservative level used in design for new buildings [5].

## 2.6 Comparison of Eurocode 8 and FEMA 310

According to Dr. Durgesh C. Rai [5], the seismic evaluation procedure of FEMA 310 is a better option than Eurocode 8. In his comparison of analysis procedures, he notices that Eurocode 8 describes mostly the principles of evaluation but is missing specific steps of assessment and leaves a lot to the judgment of the design professional, which makes it difficult to use. Some parameters are lacking guidance provision and are therefore inquire a higher degree of understanding by the design professional. What the codes have in common is that they suggest a reduction in the force level for the analysis of existing buildings compared to new buildings. In the tier 3 of the evaluation procedure according to FEMA 310, a reduction factor of 0.75 is applied to seismic forces. Eurocode 8 mentions that considering the smaller remaining lifetime of an existing structure, the effective peak ground acceleration should be reduced for redesign purposes. However, it gives no quantitative criterion [5].

# 3 Survey of the Bundeshaus Ost Building

The so-called *Bundeshaus Ost* (from now on referred to as BHO) in Bern is part of the parliament-building complex. It has already been used in example two of the SIA D0237 as a reference building. Since the establishment of the building it has been used as an administration building. This chapter deals with the survey of the building. The goal of a survey of the building is to collect information about the object of interest. To conduct a seismic analysis of a masonry structure, it is essential to collect as much information about the structure as possible. With each lack of information, the significance of the analysis declines. The definition of the expected performance criteria requires the knowledge of the seismic situation of the location of the building. These parameters are described in Chapter 3.1. In respect of the analysis of the response of the structure, it is necessary to know the geometric properties of the structure but also to understand which elements form the load-carrying system. This part is often considered to be rather difficult for old masonry structures and is treated in Chapter 3.2 and Chapter 3.3. In Chapter 3.4 the issue of flexible and rigid floors is explained. Following, Chapter 3.5 discusses the mechanical properties of the masonry walls will be discussed. Then, Chapter 3.6 reports of the site visit of the structure, which completes the survey of the building.

This dissertation contemplates only the middle part of the structure surrounded by the red square. The side wings are neglected.

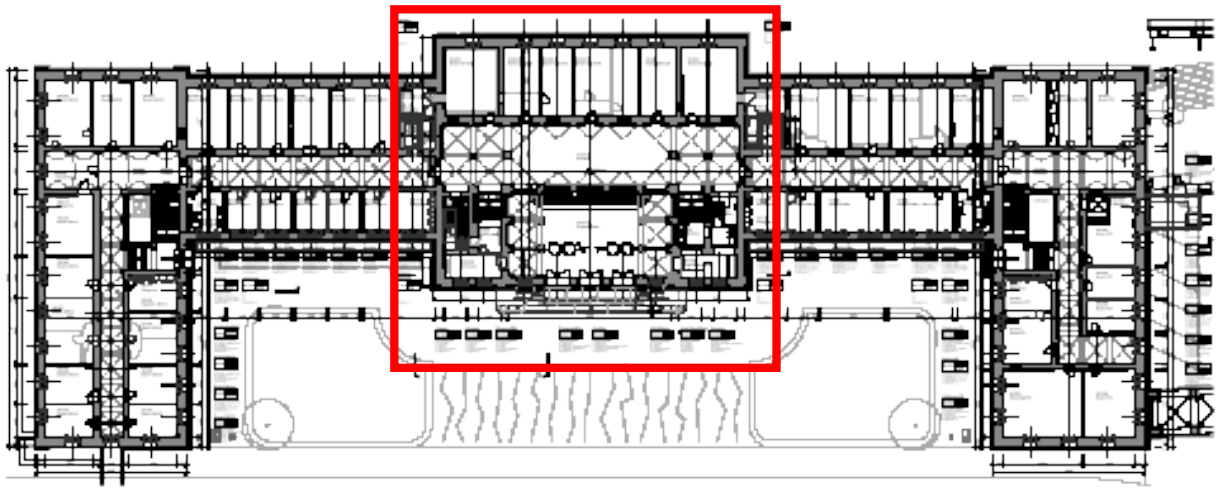

**Figure 3.1** Top view of the whole BHO-building pointing out the middle part.

## 3.1 Seismic Parameters

The BHO-structure is situated in Bern, Switzerland. According to the Swisscode, the area around Bern lays in the lowest seismic zone Z1. For the seismic zone Z1, the SIA 261 recommends a horizontal ground acceleration $a_{gd}$ of 0.6 m/s$^2$. To conduct a seismic analysis, the ground on which the structure stands needs to be classified.

According to SIA D0237, the ground on which the BHO-structure lays can be assigned to the ground class B. Table 3.1 presents the seismic parameters related to the ground class B by applying to SIA 261.

The last required seismic parameter is the importance factor. It considers the importance of the structure. The BHO-structure is assigned to the importance class II.

**Table 3.1** Seismic parameters of the BHO-structure

| | | |
|---|---|---|
| **Seismic Zone Z1** | | |
| $a_{gd}$ | 0.6 | [m/s$^2$] |
| **Ground Class B** | | |
| S | 1.2 | [-] |
| $T_B$ | 0.15 | [s] |
| $T_C$ | 0.5 | [s] |
| $T_D$ | 2.0 | [s] |
| **Importance Class II** | | |
| $Y_f$ | 1.2 | [-] |

## 3.2 Geometrical Properties

The geometry of the structure is of great importance concerning the seismic response of the structure. Hence, it is important to obtain detailed information about it. The federal office for property, construction and logistics (BBL) provided the plans created for the building permit of the ongoing renovation. Orange lines describe structural parts that will be removed and red lines describe new-constructed parts. Since this analysis is about the old structure as it was prior to the renovation, the red lines are irrelevant. The plans can be found in Appendix B. Figure 3.2 shows the north façade of the BHO-structure. It has many vaulted windows. The middle part is a floor higher then the side components. The ground plan can be seen in Figure 3.1. On the right side, a passage connects the structure with the *Bundeshaus* itself (see pictures 27 to 29 in Appendix A).

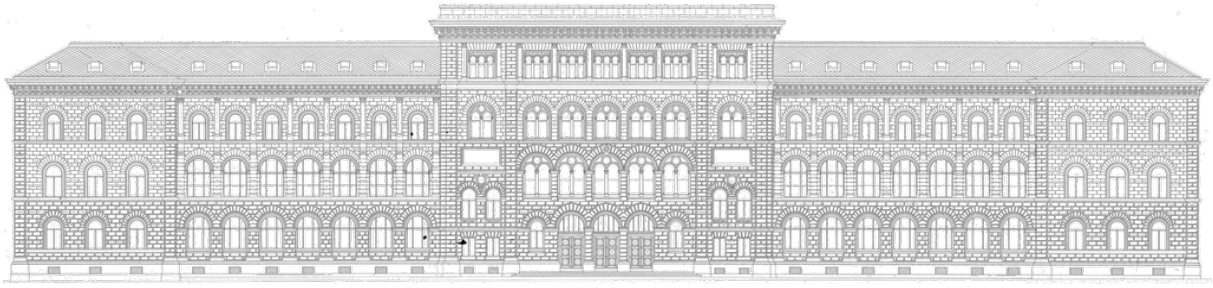

**Figure 3.2** North façade of the BHO-structure

**Table 3.2** Dimensions of the middle part of the BHO-structure

| **Main Dimensions** | |
|---|---|
| length | 30 [m] |
| width | 24 [m] |
| height | 27 [m] |

**Table 3.3** Floor heights

| Floor definition [-] | Floor ID [-] | Floor height [m] | Height [m] |
|---|---|---|---|
| Underground floor | TP | 3.9 | 3.9 |
| Ground floor | EG | 4.9 | 8.8 |
| first floor | 1.OG | 5.2 | 14 |
| second floor | 2.OG | 5.16 | 19.16 |
| third floor | 3.OG | 4.5 | 23.66 |
| fourth floor (roof) | 4.OG | 3.67 | 27.33 |

Table 3.2 shows the main dimensions and Table 3.3 the story heights of the middle part of the BHO-structure. The building has six floors (see Figure 3.4), five above and the lowest on one side below the ground level.

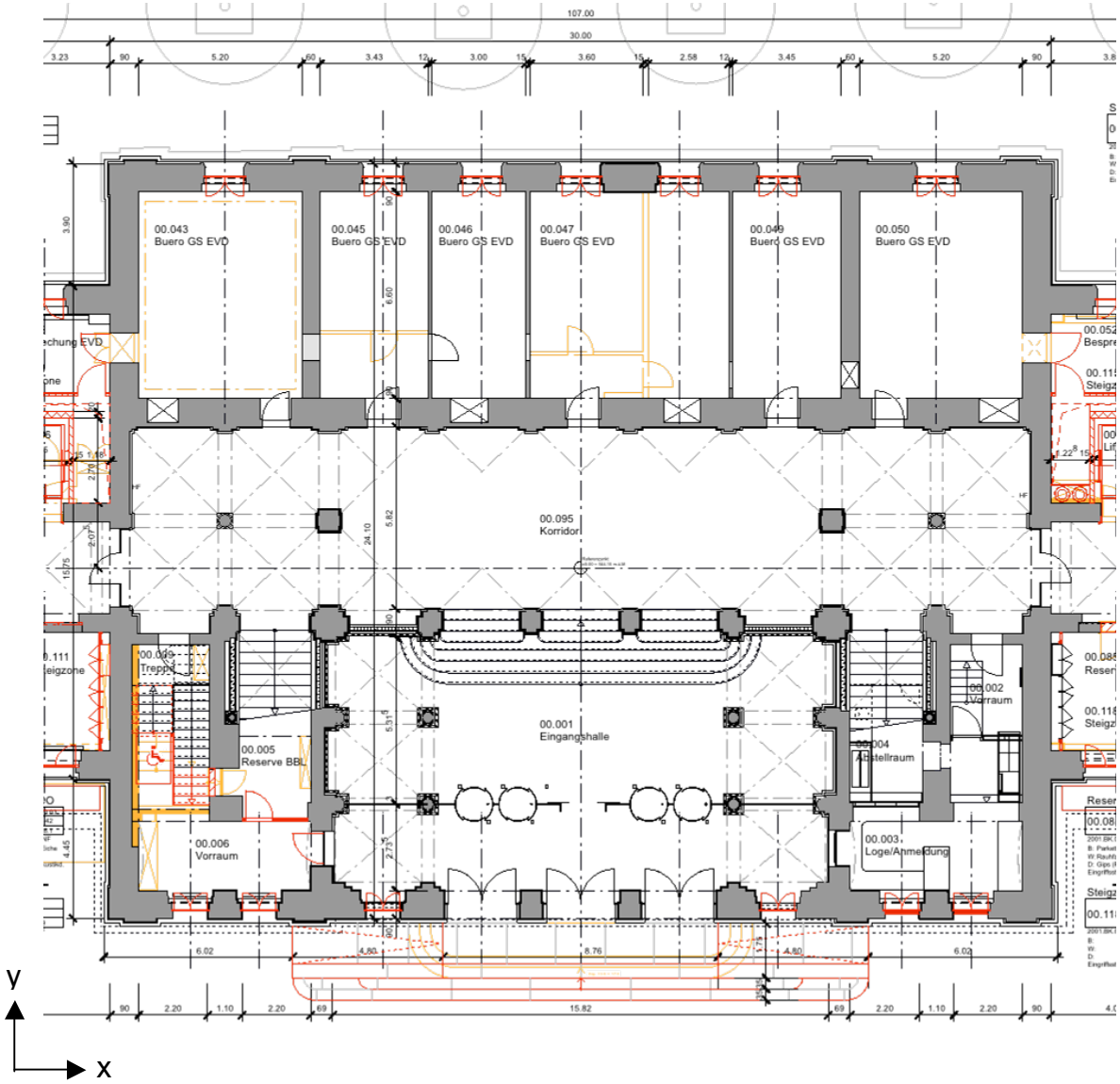


**Figure 3.3** Plan view of the ground floor

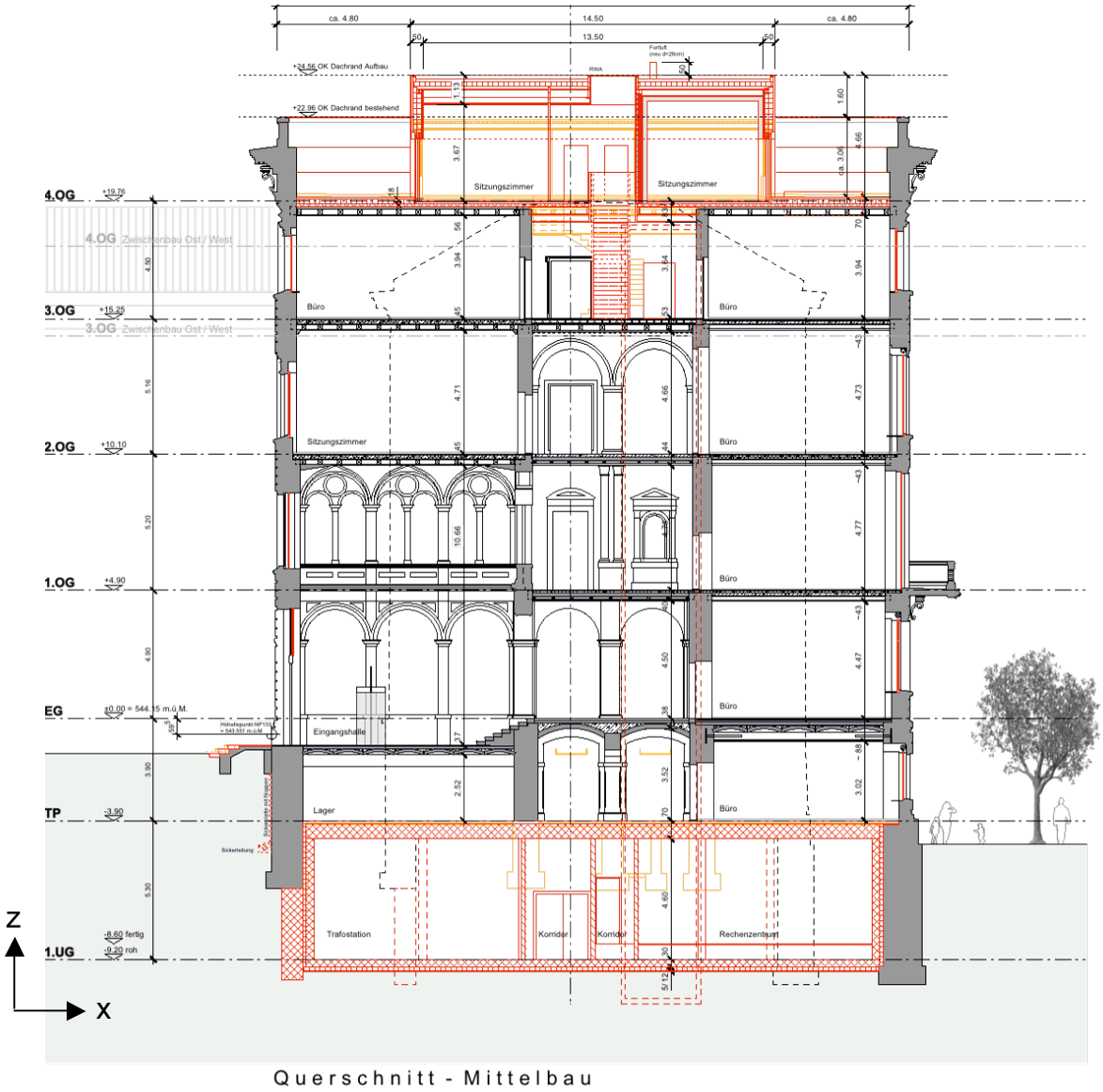


**Figure 3.4** Cross section of the middle part of the BHO-structure

Considering Figure 3.3 it becomes clear that the building has a symmetric layout. There are two staircases in both bottom corners of the plan. The horizontal space in the center of the plan forms the corridor, combining the two side wings of the whole building. This corridor is found in every floor. Across the upper part of the plan, the office facilities are found. They are situated on this side of the building in each floor. Additional office and meeting rooms can be found over the entrance hall, from the second floor upwards. On the fourth floor a roof building with office facilities situated.

The story height varies between 3.9 m in the basement to 5.2 m on the first floor. The entrance hall is visible in Figure 3.3. In the entrance hall there is no ceiling separating the entrance floor from the first floor, which is why the entrance hall has a height of 10 m.

## 3.3 Structural Properties

### 3.3.1 General

The construction of the BHO building was completed in 1892 as a masonry structure. As already mentioned above, it has been used as an administration building since then. Over the years some modifications were performed. However, these modifications did not change the original load-carrying system. There are neither statically relevant corner connections nor statically significant supplements known. The opening-overlaps are constructed using vaults according to the construction method of that time. No ring anchors are used. So far there are no lined openings known [1].

### 3.3.2 Floors

Several different floor types can be found. At the entrance, the floors consist out of pressure vaults with steel beams. Then the middle corridor lies on barrel vaults. From the first floor to the fourth floor, the offices floors are composed out of one-way timber. In the middle corridor pressure vaults can still be found, while the gallery in the entrance hall lays on cross vaults. On the second floor the corridor floor consists again out of pressure vaults, while the other floor parts are made of one-way timber. The floor over the entrance hall is also out of one-way timber supplemented by few iron girders. Then, on the third and fourth floor only one-way timber floors can be found. Later, the in-plane rigidity of the third floor diaphragm is investigated in detail. In Appendix B the different floor types and their load-carrying directions are visualized.

### 3.3.3 Walls

Figure 3.5 shows the main walls, which are responsible for the horizontal resistance of the structure. This figure presents the ground floor. The colored walls continue over the height of the building, except the ones between the stairs. Because the staircases only lead until the second floor, these walls end there. Therefore, these walls cause an additional stiffness in the lower floors. The staircases between the second and third floor are situated outside the middle part of the building in the side-wing-structures.

The masonry wall has a varying thickness. In the basement there are sections with a thickness of 1.2 m. Since the loads are smaller in higher floors, the wall thickness becomes smaller. On top of the building, the roof-surrounding wall has left a thickness of 0.5 m. The inside walls, pointing in y-direction are reduced to 30 cm on the third floor.

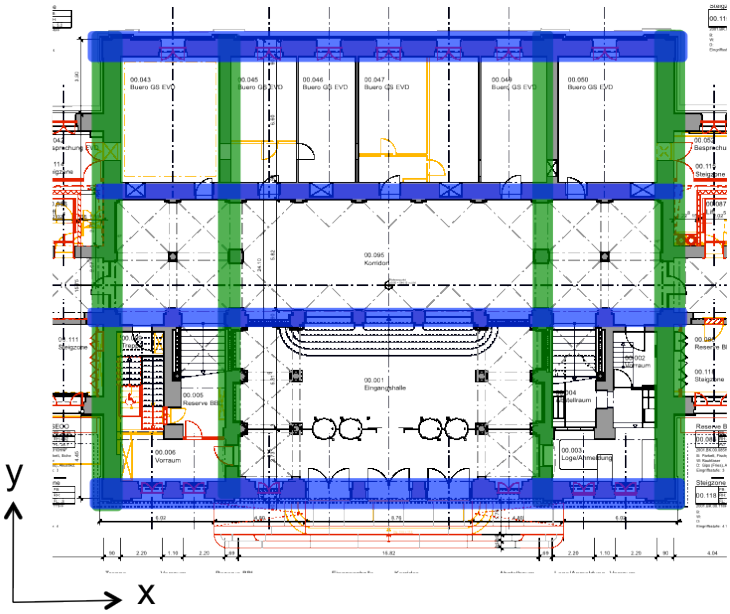


**Figure 3.5** Load carrying structural walls (blue = x-direction, green = y-direction)

## 3.4 Rigid and Flexible Floors

In case of an earthquake, a floor is supposed to transfer the acting loads, vertical as horizontal, to the walls. Then, the walls forward the loads to the foundation and into the ground. The floors may enables an interaction between single walls and thereby provide a global response behavior of the structure. The degree of interference is dependant on the composition of the floors and the connections from walls to floors and between the walls themselves. The load-carrying direction of the floors is also of great importance. In older buildings, these connections need to be examined. Next, the stiffness of the ceilings is relevant. If a floor is rigid, load redistribution can occur as single components reach their capacity. The resistance of walls and the composition of the floors define how the loads can be distributed. The floor-surrounding walls can only reach their capacity if the walls possess enough deformation capacity. This is important for displacement-related analyses. In contrast, more flexible floor-systems do not distribute the loads to the surrounding walls so well and therefore these walls have more the character of a single structure [1].

A study conducted by Tena-Colunga and Abrams [15] on three buildings showed that the diaphragm and shear-wall accelerations might increase as the diaphragm flexibility increases. They also determined that flexible in-plane shear walls vibrate at higher accelerations than stiffer walls in a flexible-diaphragm system. Further, they mention that by considering the flexibility of the diaphragms torsional effects can be reduced considerably. Another interesting observation is that in comparison to the fundamental period estimated with simplified methods, the fundamental period with flexible diaphragms appears to be longer. Moreover it is important to understand that

a design criterion, which is based on a rigid-diaphragm behavior, is not always conservative for systems based on flexible-diaphragm [15].

In Figure 3.7 the behavior of a system is presented, in which the floor is only connected to the walls A that point in the same direction as the lateral load acts. These two walls A carry the whole weight of the floor and they forward these loads into the ground. Because of that, they deform in the lateral load-acting direction, while the two perpendicular walls B, which have no connection to the wall, show no effects originating from the floor. In Figure 3.6, the opposite situation is explained. Only B-walls, which are perpendicular to the load impact, are connected to the floor and therefore carry the entire load. Because they are perpendicular to the horizontal load, it shows an out-of-plane behavior.

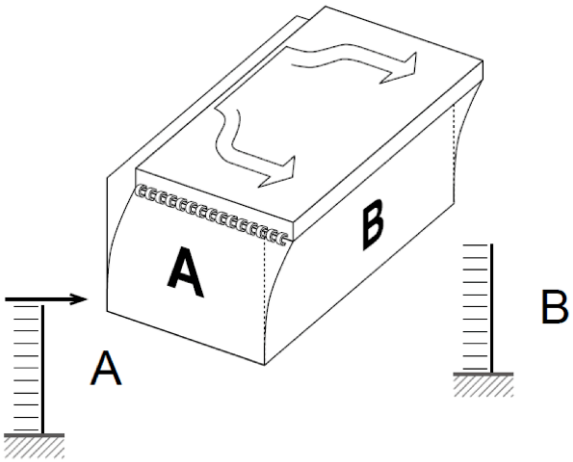


**Figure 3.7** diaphragm is connected to walls A [1]

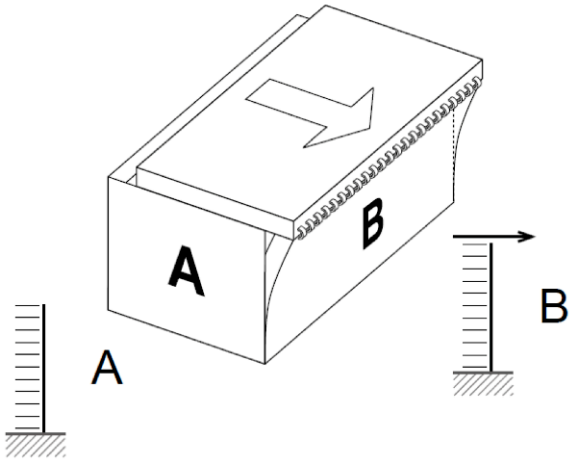


**Figure 3.6** diaphragm is connected to walls B [1]

Most of the floors of the BHO-structure consist out of one-way timber floors. In the lower elevations are also some pressure vaults with steel beams that carry the loads unidirectional as well. The only bi-directional elements of the structure are the cross vaults and the barrel vaults. For this reason, the floors affect mainly the walls the way it is described above.

According to FEMA 356 [16] classifies diaphragms according to their stiffness as flexible, rigid or stiff. It states that if the maximum horizontal deformation of the diaphragm along its length is more then twice the average interstory drift of the vertical lateral-force-resisting elements of the story immediately below the diaphragm it shall be classified as flexible. Further it says that diaphragms shall be classified as rigid when the maximum lateral deformation of the diaphragm is less than half the average interstory drift of the vertical lateral-force-resisting elements of the associated story. If a diaphragm can neither be classified as flexible nor as rigid it is classified as stiff [16].

In Figure 3.8 a diaphragm deflection is shown. The deformation $\Delta_W$ stands for the displacement of the diaphragm-wall-system. If a flexible floor is loaded horizontally with a load pointing in the same direction as the diaphragm is connected to, an

additional deflection $\Delta_d$ can be caused. This way, the diaphragm experiences in the middle a larger horizontal deformation as at the sides, where it is fixed.

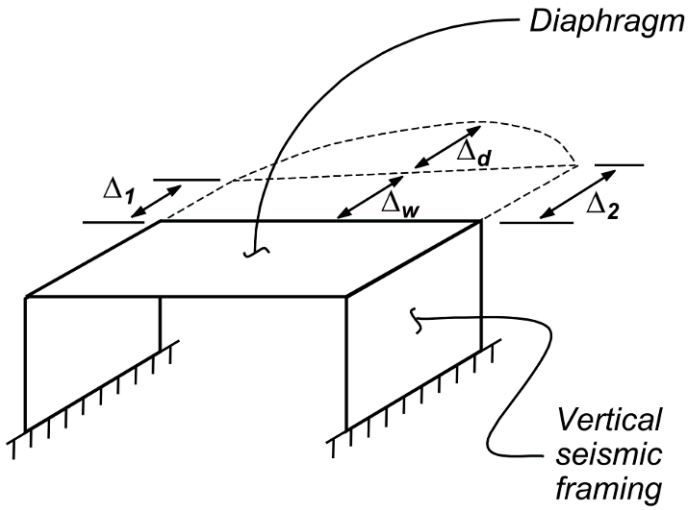


**Figure 3.8** Diaphragm and wall deformation [16]

## 3.5 Masonry Properties

The definition of the mechanical properties of the masonry of an old masonry building is rather difficult. If a detailed seismic analysis is requested, it is necessary to gain the required parameters experimentally. If such a detailed investigation is too excessive the values can be defined using reference values that describe the characteristics of the masonry as precisely as possible. Another way to obtain the required values is to use the provisions in the codes or by applying empirical formulations.

The BHO-structure masonry exists out of *Bernese sandstone* from the 19th century. Within the scope of the ongoing renovation of the BHO-structure, a material property survey is included. Unfortunately the results are not available yet. Hence, the masonry parameters are estimated as explained below.

According to EC6 [17], the characteristic compressive strength of the masonry can be obtained from the normalized mean compressive strength of the unit $f_{unit}$ and the compressive strength of the mortar $f_{mortar}$ using:

$$f_{xk} = K \cdot f_{unit}^{0.7} \cdot f_{mortar}^{0.3} \tag{3.1}$$

The value of $K$ is found in Table 3.3 of EC6. For dimensioned natural stone it is 0.45. Since the mortar joints are quite thick and because the quality of the used mortar is unknown, the compressive strength of the mortar is selected conservatively as 2 N/mm$^2$. In Appendix 3 of SIA V178 [18], the characteristic compressive strength of Bernese sandstone is recommended to be between 25 N/mm$^2$ and 40 N/mm$^2$. For

the BHO-structure a value of 30 N/mm$^2$ is chosen. With this values a characteristic compressive strength of the masonry of the BHO-structure of 6 N/mm$^2$ results.

Applying SIA 266 [10], the design values follow out of equations (3.2) and (3.3).

$$f_{xd} = \eta_1 \cdot \eta_3 \cdot \frac{f_{xk}}{\gamma_m} \tag{3.2}$$

$$f_{yd} = \eta_1 \cdot \eta_3 \cdot \frac{f_{yk}}{\gamma_m} \tag{3.3}$$

Where $\eta_1$ and $\eta_2$ are equal to 1 and $\eta_3$ is selected as 1.5 since the masonry has filled joints. In SIA 266 the partial factor $\gamma_M$ is defined as 2. Compared with the Eurocode, this value may be a little confusing. According to the Eurocode, $\gamma_M$ depends on the quality of the unit and on the quality of the brick laying. The quality of the brick laying can only be judged during the construction. For old masonry structures as this one here, it is rather impossible to make a statement about the laying quality of more then 100 years ago. As already mentioned in Chapter 2, the Eurocode defines a knowledge level, which includes all kind of uncertainties for the analysis of old structures. In the Swisscode such knowledge level factors do not exist yet. Therefore the factor $\gamma_M$, which is actually a material uncertainty factor, is here used to cover the general uncertainties.

The values of the coefficient of the inner friction of the bed joints and the specific weight of the masonry are chosen from the table in the second example of SIA D0237.

The estimation of the modulus of elasticity of the masonry is based on the approximation presented in SIA 266/2 [19].

$$E_{xk} = k_E \cdot \sqrt{\frac{f_{xk}}{5N/mm^2}} \tag{3.4}$$

The code recommends a value $k_E$ between 3000 N/mm$^2$ and 4000 N/mm$^2$. For the BHO-structure the middle value $k_E$ of 3500 N/mm$^2$ is used. Knowing the elastic modulus $E$ of the masonry the shear modulus $G$ can easily be estimated using the following equation (3.5).

$$G_k = 0.4 \cdot E_{xk} \tag{3.5}$$

For the numerical analysis, which follows later, the average compression strength $f_m$ of the masonry is required. The acronym $f_m$ should not be confused with the compression strength of the mortar as in SIA 266. Like 3Muri, this dissertation defines $f_m$ as the mean compression strength of the masonry. According to EN 1052-1 [20] three identical specimens are tested in order to evaluate the compression strength of masonry. If the compression strength of masonry units and

mortar differ within ± 25% of the specified strength, the mean compression strength $f_m$ is adjusted. With this in mind, the compression strength $f_m$ of the BHO-masonry is approximated using equation (3.6) [21].

$$f_m \approx f_{xk} \cdot 1.2 \tag{3.6}$$

Table 3.4 summarizes the mechanical properties of the masonry of the BHO-structure.

**Table 3.4** Characteristic parameters of the BHO masonry

| | | | |
|---|---|---|---|
| characteristic compression strength of sandstone unit | $f_{unit}$ = | 30 | [N/mm2] |
| characteristic compression strength of the mortar | $f_{mortar}$ = | 2 | [N/mm$^2$] |
| characteristic compressiv strength of masonry | $f_{xk}$ = | 6.0 | [N/mm$^2$] |
| partial factor for materials | $\gamma_M$ = | 2.0 | [-] |
| design compressiv strength of masonry in x-direction | $f_{xd}$ = | 3 | [N/mm$^2$] |
| design compressiv strength of masonry in y-direction | $f_{yd}$ = | 1.35 | [N/mm$^2$] |
| mean compressiv strength of masonry | $f_m$ = | 7.2 | [N/mm$^2$] |
| modulus of elasticity | E = | 3834 | [N/mm$^2$] |
| Shear modulus | G = | 1534 | [N/mm$^2$] |
| inner friction | $\mu = \tan \phi$ = | 0.6 | [-] |
| specific weight of the masonry | $\rho_m$ = | 25 | [kN/m$^3$] |

## 3.6 Site Visit

### 3.6.1 Basics

The site visit is an important part of the survey of the building. Its main goal is to verify the collected data on its actuality. During the inspection, measurements of some elements should help to verify the accuracy of the dimensions on the plans. Before the site visit is performed, it is recommended to study the collected data and to prepare for the site inspection. A useful tool is to write down all the lacking information, which the site visit should clarify. This way the site visit can proceed most effectively.

As mentioned in Chapter 2, existing buildings have often experienced modifications over time. Bigger modifications are probably recorded somewhere but also smaller ones may have occurred, which are not always recorded. Therefore small modifications are often very difficult to discover. For a seismic analysis they might be relevant if they affect the original load-carrying system. If a detailed analysis is requested, it may be necessary to take a detailed look at some walls or floors, which means that they need to be opened. Connections are often hidden from the normal eye.

### 3.6.2 BHO-Structure

The use of photographs is a powerful tool for site visits. Unfortunately it was not permitted to take pictures inside the building. Hence, the pictures of the site investigation in Appendix A show only the outside of the building.

In general there are several questions about the structure of this building. These questions concern the detailed composition of floors and walls as well as possible hidden reinforcements. Some of them could be answered by the site visit, while others remain unanswered. If an old masonry structure is analyzed, another important question concerns the properties of the used masonry. During the inspection, masonry wall sections were studied in terms of its composition. The head joints are about 5 cm thick while the bed joints show a thickness of about 2-3 cm. Thus, the shear modulus of the structure depends probably mostly on the quality of the mortar. The masonry stones are 60 cm high and over 1 m long in general. The stones could be identified to be sandstones as mentioned in SIA D0237. During the inspection it became clear that the foundation of the BHO-structure is build on some old masonry walls of the previous hospital, called *Inselspital.* While the foundation of the BHO-structure was built, some openings of these old walls were lined with usual clay-brick masonry of that time. On the plan shown in Figure 3.3, the wall between the stairs appears to be solid. During the site visit these walls turned out to consist out of vaulted openings. For this reason, they will later be modeled with openings. On the third floor, some investigation holes conducted in the walls pointing in the x-direction showed clay-brick masonry. This information is confusing since the main structural walls were assumed to consist out of sandstone masonry. For the following analysis, these walls will be assumed to consist out of sandstone masonry as the rest of the structural walls. The steel beams between the compression vaults in the basement ceiling could be found, as they are showed in the plans. Moving up the building, the declination of the wall thickness over the height of the building can be confirmed as well. The one-way timber floors were found to be as they are described in the example of SIA D0237. One floor differs from the original composition and was, according to the site engineer, modified some time ago due to a heating system replacement. However, this floor is irrelevant for the analysis since it is situated in a side corridor of the building. Another modified ceiling could be found on the third floor. This modification is connected with the renovation of the roof, which took place several years ago. During this renovation, the “roof-house” was built. In order to increase the floor strength for the roof-house, steel beams were inserted.

In accordance to Chapter 3.6.1, some walls of the building were measured during the inspection and they confirmed the dimensions presented on the plans.

# 4 Seismic Analysis Procedures

In this chapter, the existing analysis procedures that serve for evaluation of individual buildings are briefly described according to Lang [22]. They can be divided into linear and nonlinear procedures.

## 4.1 Linear Static Procedures

The linear static procedure is based on the method of the equivalent force. It models a building as an equivalent single-degree-of-freedom (SDOF) system. This SDOF system has a linear elastic stiffness and an equivalent viscous damping. Using empirical relationships or Rayleigh's method, the fundamental period is estimated. With this period, the spectral acceleration $S_a$ is determined from the appropriate response spectrum. Then the equivalent lateral force $V$ is computed by multiplying the spectral acceleration with the mass of the building.

$$V = S_a \cdot m \cdot \sum_i C_i \tag{4.1}$$

The equivalent lateral force represents the horizontal seismic input, which the earthquake causes to the structure. By choosing adequate values for the coefficients $C_i$, second order effects, stiffness degradation as well as force reduction due to anticipated inelastic behavior, can be regarded. Once the equivalent lateral force is known, it is distributed over the height of the building. By using linear static analysis the corresponding internal forces and displacements are determined.

The applicability of linear static procedures is restricted to regular buildings for which the first period is predominant. However they are incorporated in most of the design codes and serve next to this specific type of structures as a useful tool for the preliminary design [22].

## 4.2 Linear Dynamic Procedures

The linear dynamic procedure models a building as a multi-degree-of-freedom (MDOF) system with a linear elastic stiffness matrix and an equivalent viscous damping matrix. The seismic input can be determined using modal spectral analysis or time-history analysis.

If modal spectral analysis is selected, the dynamic response of the building can be found by analyzing the independent response of the natural modes of vibration using linear elastic response spectra. Therefore only the natural modes of vibration, which contribute considerably to the response, need to be considered. After that, the selected modal responses can be combined using a modal combination rule.

Chopra [23] describes such rules in his book *Dynamics of Structures*. A common combination rule is the square-root-of-sum-of-squares (SRSS) rule shown below.

$$r_0 \approx \left( \sum_{n=1}^{N} r_{no}^2 \right)^{1/2} \tag{4.2}$$

If time-history analysis is selected, a time-step-by-time-step evaluation of the building response needs to be carried out. As base motion input, recorded or synthetic earthquake records, can be used.

The corresponding internal forces and displacements are again determined using linear static analysis.

The main benefit of the linear dynamic procedures in comparison to the linear static procedures is that higher natural modes can be considered. Hence, this procedure is more adequate for the seismic analysis of irregular structures. However, they are still based on linear elastic response and therefore as the nonlinear behavior increases, the applicability decreases. The nonlinear behavior is estimated using global force reduction factors [22].

## 4.3 Nonlinear Static Procedures

The nonlinear static procedure incorporates directly the nonlinear force-deformation characteristics of individual components and elements based on inelastic material response. There are several methods existing. What combines all of them is the nonlinear force-deformation characteristic of the structure, which is represented by a pushover curve. A pushover curve is a curve showing the relation between the base shear and the top displacement of the structure. This relation is obtained by increasing monotonically the horizontal load impact or the horizontal displacement to the structure model in correspondence to its first mode of vibration until it collapses. By using either highly damped or inelastic response spectra, the maximum displacements are determined, which are likely to be expected during a given earthquake event.

The main advantage of this procedures in respect to the linear procedures is certainly the fact, that the effects of nonlinear material response are directly included. Hence the internal forces and deformations are more realistic approximations of those expected during an earthquake. However, in these procedures usually only the first mode of vibration is regarded and therefore these procedures are not appropriate for irregular structures, where higher modes obtain greater importance [22].

## 4.4 Nonlinear Dynamic Procedures

The nonlinear dynamic procedure uses a similar building model as the nonlinear static procedure. It incorporates directly the inelastic material response by using in general finite elements. The major difference is the seismic input that is in contrast to

the nonlinear static procedure in using a time-history analysis. As mentioned in Chapter 4.2, a time-step-by-time-step evaluation needs to be performed in a time-history analysis.

The application of a nonlinear dynamic procedure is rather challenging for predicting forces and displacements under seismic input. The computed response tends to be quite sensitive to the characteristics of the individual ground motion used as seismic input. It is necessary to perform several time-history analysis using different ground motion records in order to obtain satisfying results. Since this analysis procedure is so demanding it serves mainly as a research tool. Especially its objective to simulate the behavior of a building structure in detail is of great use. Details of interest may be the exact displacement behavior, the propagation of cracks, the distribution of vertical and shear stresses as well as the shape of the hysteresis curves and other [22].

# 5 Numerical Simulation

For the numerical simulation of the seismic behavior of masonry structures the 3Muri software is selected. The following subchapters deal with a brief overview of the program, followed by a verification calculation using a simple test building structure. Afterwards the development of the BHO-structure will be discussed.

## 5.1 3Muri

### 5.1.1 General Description

3Muri is a numerical computation program created for the seismic analysis of masonry structures. It uses nonlinear static procedure analysis, where a pushover curve of the building structure is generated. The nonlinear static analysis procedure is based on the N2 method. N2 methods are simplified procedures where a multi-degree-of-freedom system is investigated by analyzing an equivalent single-degree-of-freedom system, which represents the real structure. The program can examine large and small structures composed out of masonry with elements out of other materials, such as reinforced concrete, iron or wood. The software is used for the design of new structures as well as for the examination of existing structures [24].

As theoretical model the FME method was chosen. FME stands for Frame by Macro Elements. This method is considered to be the most advanced method available in the sector of masonry calculation. It is capable of considering the different failure mechanisms of masonry. Further a wall can be divided into three types of elements: Piers, spandrel beams and rigid elements. Pier elements are located at the sides of openings and spandrel beams represent the elements above openings. The remaining parts of the wall form rigid elements (see Figure 5.1). Profound theoretical studies have shown that the behavior of piers and spandrel beams can be expressed as linear elements. By connecting these different elements the equivalent frame is obtained. This frame simplifies the analysis since it reduces the degrees of freedom [24].

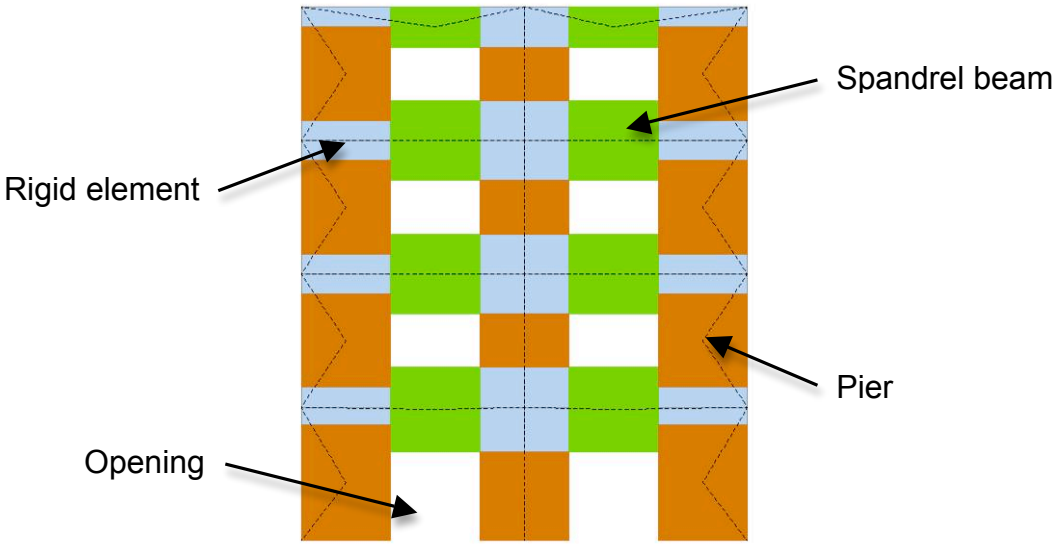


**Figure 5.1** Types of macro-elements

### 5.1.2 Masonry Macro-elements

To represent masonry piers and spandrels, modeled as masonry macro-elements, a nonlinear beam element model is implemented. According to the general description of 3Muri [24], the main characteristics of such a nonlinear beam element are:

1. initial stiffness given by elastic (cracked) properties,
2. bilinear behavior with maximum values of shear and bending moment as calculated in ultimate limit states,
3. redistribution of the internal forces according to the element equilibrium,
4. detection of damage limit states considering global and local damage parameters,
5. stiffness degradation in plastic range,
6. ductility control by definition of maximum drift based on the failure mechanism, according to the Italian seismic code [26] and EC8,

$$\delta_m^{DL} = \frac{\Delta_m}{h_m} = \delta_u \begin{cases} 0.004 \text{ Shear} \\ 0.006 \text{ Compression - bending} \end{cases} \tag{5.1}$$

7. element expiration at ultimate drift without interruption of global analysis.

As soon as one of the nodal generalized forces reaches its maximum value, the nonlinear behavior is activated. The maximum value corresponds to the minimum strength value obtained by computing the resistance of each failure mechanism [24].

According to the user manual of 3Muri [25], the different failure mechanisms and the resistance of masonry elements are computed using the following equations.

Ultimate bending moment:

$$M_u = \frac{l^2 \cdot t \cdot \sigma_0}{2}\left(1 - \frac{\sigma_0}{0.85 \cdot f_m}\right) = \frac{N \cdot l}{2}\left(1 - \frac{N}{N_u}\right) \tag{5.2}$$

Shear resistance according to Eurocodes and Italian codes:

$$V_R = (f_{v0} + 0.4 \cdot \sigma_0) \cdot l' \cdot t = f_{v0} \cdot l' \cdot t + 0.4 \cdot N \tag{5.3}$$

According to the Italian code, the shear failure of an existing building can be computed according to the Turnsek and Cacovic criterion [27].

$$V_u = l' \cdot t \cdot \frac{1.5 \cdot \tau_0}{b} \cdot \sqrt{1 + \frac{\sigma_0}{1.5 \cdot \tau_0}} \tag{5.4}$$

$l$: length of the wall

$t$: thickness of the wall

$b$: coefficient defined according to the ratio of height and length of the wall

$\tau_0$: shear value of masonry

$\sigma_0$: normal compressive stress on the whole area

$f_{v0}$: shear resistance of the masonry without compression

$f_m$: average compression strength of the masonry

$N$: axial compressive load

$N_u$: ultimate axial compressive load

### 5.1.3 Influence of Rigid and Flexible Floors

3Muri allows assigning floor stiffness. The simplest way is to choose a rigid diaphragm, which may not necessarily represent the real structure correctly, and also needs no further knowledge of the composition of the floors. A better option is to enter the properties of the floors in 3Muri. With this information, 3Muri automatically calculates the correspondent floor stiffness. A third option is to enter user defined stiffness properties manually.

Afterwards the user sets the floor in the building model with defining its death and live loads and its load-carrying direction. For some types of floors it is possible to choose a ratio for the bi-directional load distribution.

### 5.1.4 Computation Phase

Figure 5.2 shows the different steps required for a computation. The analysis of a building structure can be divided into three computation phases.

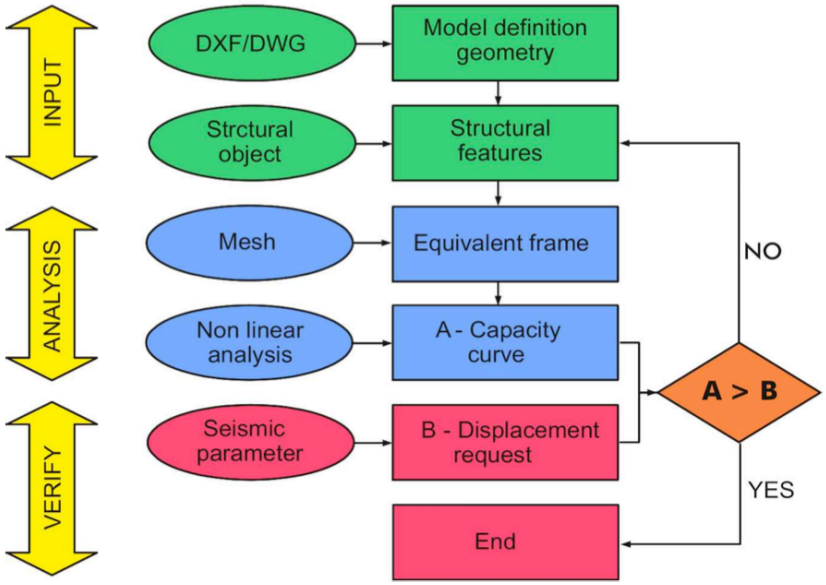


**Figure 5.2** Computation steps [24]

The first phase stands for the input. Here the geometry of the model is defined, followed by its structural characteristics. Having prepared a dxf- or dwg-file including the geometrical properties of the load carrying walls as well as the openings, the first step can be accomplished without any difficulty. Once the geometry of the walls is defined, the material properties need to be defined. Meanwhile 3Muri has three different design codes implemented. Those are: Italian code, Eurocode and Swisscode. When it comes to define the material properties, the program offers for each code some standard materials, from which the user can choose. This is quite useful especially for new buildings. However, if an old masonry structure is to be analyzed, the masonry material properties need to be defined additionally. They can be added manually or by choosing the corresponding masonry type out of a list. In that case the program sets the values according to Eurocode. If the user enters manually, he needs to select between the two options existing or new building. In both cases the masonry parameters such as the modulus of elasticity, the shear modulus, the characteristic compression strength of the masonry, the mean compression strength etc. need to be entered. After the material properties are set, they need to be assigned to all the walls of the structure. After that, the openings are added. If balconies are existent, they are also added at this point. Next, the floors are defined with their death and live loads and with the corresponding mechanical

properties. 3Muri includes the most frequently used types of floors. It automatically calculates the required values starting from its geometry. Further there are some options for taking into account if they are, for example, linked by the masonry or not. Next to the common floor types, it also includes brick vaults such as cross vaults, ribbed vaults and others [24].

The second phase deals with the analysis. In the first step, the three-dimensional structure building needs to be transformed into a three-dimensional equivalent frame model. This happens using the auto-generate function of the program. If the auto-generated mesh is not satisfactory, it can be adjusted manually. In the second step the vertical loads of each floor need to be assigned to the equivalent frame model. Afterwards, the model is ready for the evaluation process. There are 24 different analysis combinations all together, as shown in Table 5.1. From these 24 combinations, 12 are in x- and 12 in y-direction. In each direction four analyses neglect accidental eccentricity while eight consider it. In accordance with Swisscode, the amount of accidental eccentricity is five per cent of the corresponding building side. Further the program offers two different patterns for the horizontal load distribution. One is the first-mode load pattern, the second the uniform mass-proportional load pattern. At last the program also considers bi-directional loading for each combination. After choosing the desired analysis combinations, the program computes the horizontal displacements of the structure by monotonically increasing the horizontal loads. The results are presented in terms of a front view of the selected wall, a table showing the numeric results, the general deformed plan based on the load steps and a pushover curve.

**Table 5.1** The 24 analyses combinations for the 3Muri evaluation

| No. | Earth-quake | Uniform pattern of lateral load | Eccentri-city | No. | Earth-quake | Uniform pattern of lateral load | Eccentri-city |
|---|---|---|---|---|---|---|---|
| 1 | +X | Masses | 0 | 13 | +Y | Masses | 0 |
| 2 | +X | First Mode | 0 | 14 | +Y | First Mode | 0 |
| 3 | -X | Masses | 0 | 15 | -Y | Masses | 0 |
| 4 | -X | First Mode | 0 | 16 | -Y | First Mode | 0 |
| 5 | +X | Masses | + 5 % | 17 | +Y | Masses | + 5 % |
| 6 | +X | Masses | - 5 % | 18 | +Y | Masses | - 5 % |
| 7 | +X | First Mode | + 5 % | 19 | +Y | First Mode | + 5 % |
| 8 | +X | First Mode | - 5 % | 20 | +Y | First Mode | - 5 % |
| 9 | -X | Masses | + 5 % | 21 | -Y | Masses | + 5 % |
| 10 | -X | Masses | - 5 % | 22 | -Y | Masses | - 5 % |
| 11 | -X | First Mode | + 5 % | 23 | -Y | First Mode | + 5 % |
| 12 | -X | First Mode | - 5 % | 24 | -Y | First Mode | - 5 % |

In the third phase the obtained capacities need to be verified with the demands. Hence the seismic parameters of the analyzed building structure need to be entered into the program. Using Swisscode these parameters are the seismic zone, the soil type with its corresponding parameters S, $T_B$, $T_C$ and $T_D$ as well as the importance factor $\gamma_f$. With this information, the program calculates the requested displacement

according to the code. Then it performs a check where it compares this requested displacement with the displacement offered by the structure. If the check is satisfied it means that the structure can withstand an earthquake event according to the selected seismic parameters. If the check is not satisfied a step-by-step analysis of the damage process helps finding the wall areas which need improvement.

## 5.2 Verification of 3Muri

This chapter deals with a verification analysis. The intention of this verification analysis is to define a fictive test building structure, to model it with 3Muri and then to compare its results with a hand calculation. The hand calculation analysis contains an equivalent lateral force analysis, a response spectrum analysis and a development of a pushover curve according to the method developed by Lang [22]. It is expected to show more conservative results than the deformation capacity achieved with 3Muri. The seismic properties of the test structure are chosen the same as those of the BHO-structure described in Chapter 3.1.

### 5.2.1 Geometry

The dimensions of the test building presented in Figure 5.3 can be found in Table 5.2.

**Table 5.2** Dimensions of test building

| | | | |
|---|---|---|---|
| length | L | 4 | m |
| width | B | 3 | m |
| height | H | 3 | m |
| opening length | $L_p$ | 2 | m |
| opening height | $h_p$ | 2.25 | m |
| wall thickness | $t_w$ | 0.2 | m |
| surface | A | 12 | $m^2$ |

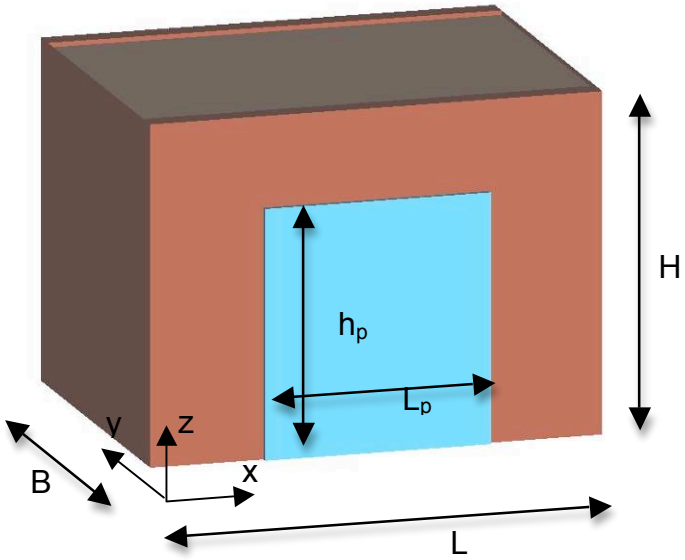


**Figure 5.3** Test building structure

The side walls with the surface B times H are necessary for the model in 3Muri. Every ceiling needs an element definition on each side. Because only the front side of this building is of interest, the sidewalls are defined as very thin masonry walls. With this assumption the influence of these sidewalls can be neglected.

## 5.2.2 Masonry Wall Characteristics

The test structure is assumed to consist out of masonry with bricks and clay MB according to SIA 266. The material characteristics are presented in Table 5.3.

**Table 5.3** Material characteristics of the test building structure

| | | | |
|---|---|---|---|
| partial factor for materials | $\gamma_m$ = | 2.0 | [-] |
| characteristic compressiv strength of masonry | $f_k$ = | 7.0 | [N/mm$^2$] |
| design compressiv strength of masonry in x-direction | $f_{xd}$ = | 3.5 | [N/mm$^2$] |
| design compressiv strength of masonry in y-direction ($f_{yd} = f_{xd} * 0.3$) | $f_{yd}$ = | 1.05 | [N/mm$^2$] |
| avarage resistance to compression of masonry (3Muri) | $f_m$ = | 10 | [N/mm$^2$] |
| characteristic initial shear strength of masonry, under zero compressive stress (3Muri) | $f_{vm0}$ = | 0.29 | [N/mm$^2$] |
| limit of the shear strength (3Muri) | $f_{v,lim}$ = | 2.2 | [N/mm$^2$] |
| inner friction | $\mu = \tan \phi$ = | 0.6 | [-] |
| modulus of elasticity (uncracked) | E = | 7000 | [N/mm$^2$] |
| Shear modulus (G = E * 0.4) | G = | 2800 | [N/mm$^2$] |
| specific weight of the masonry | $\rho_m$ = | 13 | [kN/m$^3$] |

## 5.2.3 Load Carrying System and Vertical Loads

Since the BHO-structure has many one-way timber floors, the floor of this structure is also assumed to be a one-way timber floor. Under this assumption, the ceiling carries its load directly into the front and back walls, which transfer the vertical loads into the ground. The vertical loads are calculated with equation (5.5). This formula is based on formula (40) of SIA 261. $\psi_2$ is the reduction factor according to Table 2 of SIA 260. For office floors the reduction factor $\psi_2$ is 0.3.

$$q_d = g_k + \sum \psi_2 \cdot q_k \qquad (5.5)$$

The vertical load of the floor is computed as follows:

Death load: $g_{Floor}$ = 2.43 kN/m$^2$

Live load: $q_{NL}$ = 3.00 kN/m$^2$

Using formula (4.5), the total vertical floor loads $q_{d,Floor}$ amount to 3.33 kN/m$^2$.

The masonry wall contribute with its own weight as follows:

Death load: $q_{d,Wall}$ = 13 kN/m$^3$ * $t_w$ = 2.60 kN/m$^2$

### 5.2.4 Equivalent Lateral Force Analysis

In Chapter 4.1 this type of procedure is described. To estimate the first natural period of vibration the formula (38) of SIA 261 is used.

$$T_1 = C_t \cdot h^{0.75} \tag{5.6}$$

$C_t$ is set as 0.05. With an idealized building height of 2.625 meters a first natural period of vibration of $T_1$ = 0.103 s is obtained. The following equation (5.7) corresponds to formula (25) of SIA 261. By filling in the correspondent parameters, the spectral acceleration $S_a$ of the structure reaches 1.46 m/s$^2$ ($\eta$ is assumed to be 1).

$$S_a = a_{gd} S \left[ 1 + \frac{(2.5\eta - 1)T}{T_B} \right] \leq T_B \tag{5.7}$$

For the computation of the equivalent lateral force, the weight of the structure is required. To calculate a concentrated weight of the structure, the assumption is made that the weight of the lower half of the wall height is directly transferred into the ground, whereas the upper half is contributing to the center weight point of the SDOF system. With this assumption, the concentrated weight is assembled in the following way:

| | | | | | |
|---|---|---|---|---|---|
| Floor weight: | $w_{Floor}$ | = | $q_{d,Floor}$*L*B | = | 39.96 kN |
| Walls weight: | $w_{Walls}$ | = | | | |
| | | | 2*$q_{d,Wall}$*((L-$L_p$)*H/2 + $L_p$*(H-$h_p$)) | = | 23.40 kN |
| Total weight: | $w_{tot}$ | = | | | 63.36 kN |
| Total mass: | $m_{tot}$ | = $w_{tot}$/g | | = | 6336 kg |

Dividing the weight of the structure through the gravity g provides the mass of the structure. Knowing the mass of the structure, the equivalent lateral force is calculated by multiplying the mass with its spectral acceleration.

$$F_d = S_a \cdot m_{tot} \tag{5.8}$$

This calculation delivers an equivalent lateral force $F_d$ of 9.45 kN. The elastic displacement $u_{el,ELF}$ of the structure can be estimated by applying the following equation:

$$u_{el,ELF} = S_d \cdot \Gamma_1 = \frac{S_a}{\omega_1^2} \cdot \Gamma_1 \tag{5.9}$$

The natural circular frequency $\omega_1$ follows out of equation (5.10).

$$\omega_1 = \frac{2 \cdot \pi}{T_1} \tag{5.10}$$

Since the test structure is already a SDOF system, the participation factor $\Gamma_1$ in equation (5.9) is equal to 1. This way, equation (5.9) delivers an elastic displacement $u_{el,ELF}$ of 0.4 mm. This value shows that the test structure is rather strong against the assumed loads.

### 5.2.5 Response Spectrum Analysis

A more advanced procedure for seismic analysis is the response spectrum method. As described in Chapter 4.2 the opportunity to consider higher natural periods of vibration is one of the major advantages. But since the test structure is only a SDOF system, this advantage is of no use for the analysis of the test structure. However, by performing a modal analysis the first natural period of vibration emerges out of an estimation of the stiffness and the mass of the structure. Hence, the value of the first natural period of vibration is expected to be a closer estimation to the one of the real structure.

According to Tomazevic [21], the effective stiffness of a masonry wall can be obtained by using equation (5.11).

$$K_e = \frac{G \cdot A_W}{1.2 \cdot h \cdot \left[1 + \alpha' \cdot \frac{G}{E}\left(\frac{h}{l}\right)^2\right]} \tag{5.11}$$

In this formulation α' represents a coefficient that determines the position of the bending moment's inflection point along the height of the wall. For cantilever walls, such as those of the test structure, the value of α' is recommended to be 3.33.

Table 5.4 shows the values used in equation (5.11). With these values the effective stiffness $K_e$ of one wall element is calculated to 17,466 kN/m.

**Table 5.4** Parameters for effective stiffness

| | | | |
|---|---|---|---|
| idealized story hegiht | $h_{st}$ = | 2.625 | [m] |
| pier length | $L_w$ = | 1 | [m] |
| pier cross section area | $A_w$ = | 200000 | [$mm^2$] |
| Masonry elasticity modulus | E = | 7000 | [$N/mm^2$] |
| Masonry shear modulus | G = | 2800 | [$N/mm^2$] |
| bending moment's inflection point coefficient | α' = | 3.33 | [-] |

Knowing the stiffness $K_e$ and using the structure mass calculated above the natural circular frequency $\omega_1$ can be computed using equation (5.12).

$$\omega_1 = \sqrt{\frac{k}{m}} \tag{5.12}$$

In this equation, $k$ is equal to four times the stiffness $K_e$. $K_e$ is the stiffness of one pier of the test structure and since there are four of them, $k$ is four times In this assumption, the spandrel beam combining the two walls is assumed flexible. Once $\omega_1$ is known, the first natural period of vibration $T_1$ is obtained by using the transformed equation (5.10). This way a $T_1$ of 0.06 s results, which is approximately 40% less than with the equivalent lateral force method. Using equations (5.6) to (5.8) from above, a spectral acceleration $S_a$ of 1.15 m/s$^2$, an equivalent lateral force $F_d$ of 7.3 kN and an elastic displacement $u_{el,RSA}$ of 0.1 mm is obtained.

### 5.2.6 Hand-Calculated Capacity Curve

Bachmann and Lang [2] describe a procedure, developed for the design of masonry structures, where the required capacity is compared to the capacity given by the provisional structure. The developed procedure is only valid for structures with regular geometry. In addition to the models according to SIA V177 [28], the additional stiffness coming from the coupling between the individual walls through ceilings and spandrel beams is considered. This influence can be considerable.

According to Bachmann and Lang [2], the procedure consists out of the following steps:

1. Initial data
2. Identification of the structure
3. Computation of the normal forces and story masses
4. Capacity curve of the walls
5. Capacity curve of the building
6. Equivalent SDOF
7. Capacity demand
8. Verification

Below, the test structure is analyzed following these steps using the explications of Bachmann and Lang.

**1. Initial Data**

The initial data requires the geometrical properties, the material characteristics as well as the vertical loads. These data is already described in Chapter 5.2.1 and Chapter 5.2.3.

**2. Identification of the Structure**

This step defines the load-carrying walls of the structure. For the test building, the load-carrying walls are the two in the x-direction (see Figure 5.3). As mentioned before, the two walls in the y-direction are neglected and the timber floor transfers the vertical loads two the two walls pointing in the x-direction.

**3. Computation of the Normal Forces and Story Masses**

The story mass is already computed in Chapter 5.2.4 with a value of 6,336 kg. The weight is also already known at 63.36 kN. If this weight is distributed over the four piers of the structure, each one obtains an axial force of 15.8 kN.

**4. Capacity Curve of the Walls (**see Appendix D)

Since the test building has only two load-carrying walls and because they are identical to each other, this procedure needs only to be done once. If there were more walls with different properties, a capacity curve would need to be done for each of them.

First, the point of zero moment is requested for the piers. This point is found by calculating the ratio of the flexural stiffness of the spandrel to the flexural stiffness of the piers and by using Figure 5.4. It leads to a $h_{op}$ of 1.92 m.

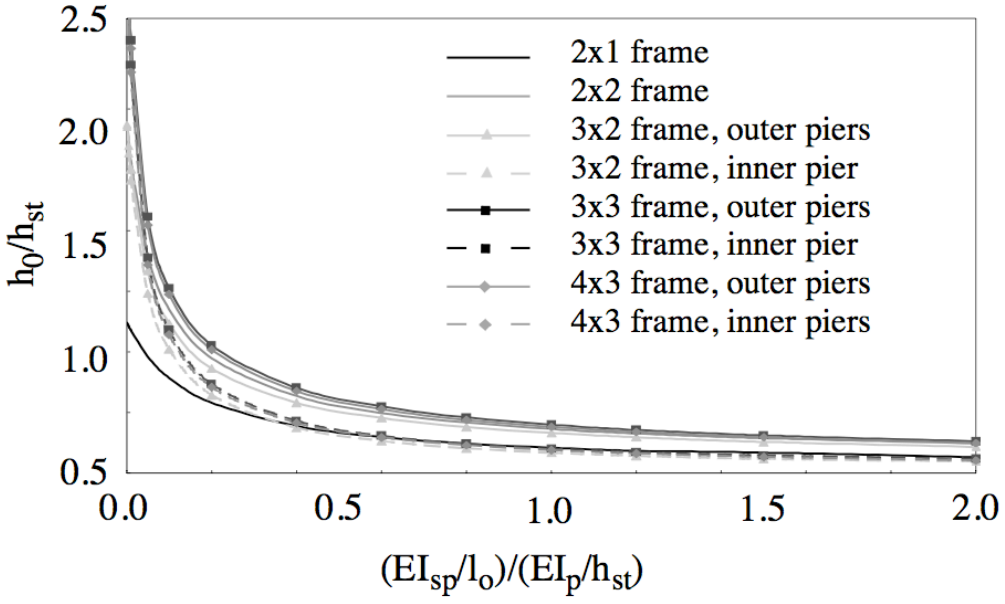


**Figure 5.4** Ratio of $h_0/h_{st}$ as a function of the ration of the flexural stiffness of the spandrels to the flexural stiffness of the piers [22]

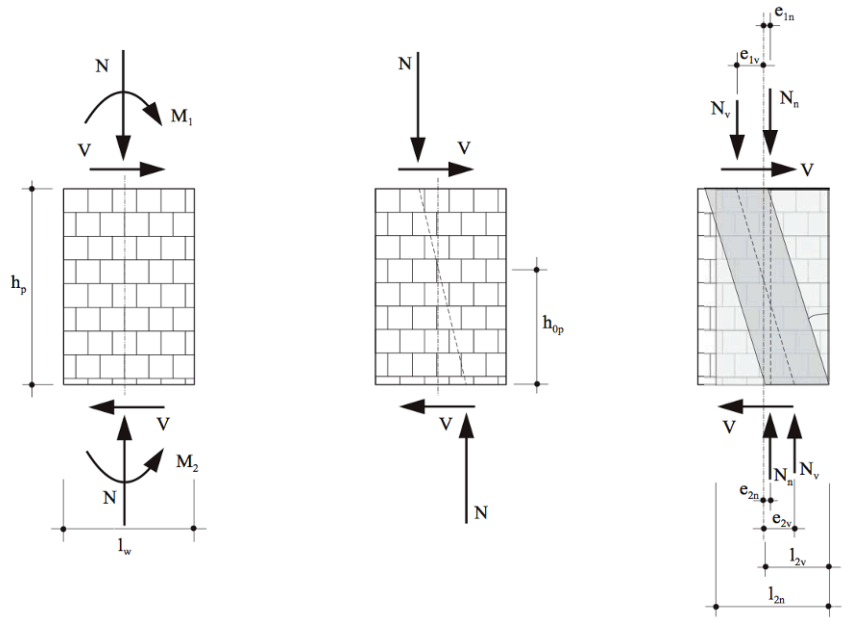


**Figure 5.5** Geometry of the piers and interacting forces [2]

Next, the horizontal resistance force $V_m$ is determined.
If $h_{op}$ is known, $M_1$ and $M_2$ can be expressed in dependence on $V_m$.

$$M_1 = V_m \cdot (h_{op} - h_p) \tag{5.13}$$

$$M_2 = V_m \cdot h_{op} \tag{5.14}$$

The maximum lateral load that a pier can undergo can be calculated by using the lower limit set of the theory of plasticity with a vertical and inclined compression brace according to Figure 5.6.

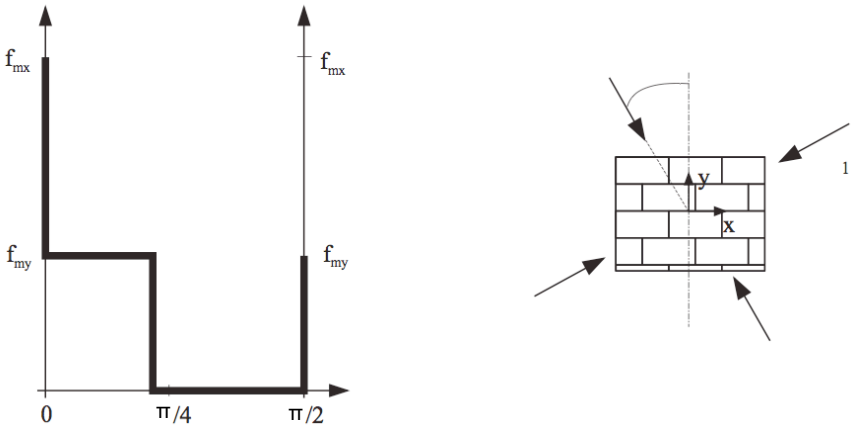


**Figure 5.6** Compression strength as a function of the inclination of the angle α [2]

The angle ratio of the inclined compression brace follows with:

$$\tan\alpha = \frac{V}{N_v} \tag{5.15}$$

The tensions, which result out of the internal forces in the inclined and vertical compression brace, $\sigma_v$ and $\sigma_n$, are not allowed to exceed the compression strength of the masonry according to Figure 5.6.

$$\sigma_v = \frac{N_v}{l_2 \cdot t \cdot \cos^2\alpha} \leq f_{my} \tag{5.16}$$

$$\sigma_n = \frac{N_n}{l_2 \cdot t} \leq f_{mx} - f_{my} \tag{5.17}$$

Further, the capability of sliding in the bed joint needs to be checked.

$$\tan\alpha \leq \tan\phi \tag{5.18}$$

Now, by using equations (5.13) to (5.15) the conditions of equations (5.16) to (5.18) are solved in respect to the horizontal resistance force. Finally, the horizontal resistance force $V_m$ follows out of the conditions expressed in equations (5.13) and (5.15):

$$V_m = \frac{f_{yd} \cdot L_w \cdot t_w \cdot N \cdot \tan\phi_d}{N + N \cdot \tan^2\phi_d + 2 \cdot f_{yd} \cdot t_w \cdot H_{op} \cdot \tan\phi_d} \tag{5.19}$$

This way the result of $V_m$ is 3.96 kN.

The bending moments $M_1$ and $M_2$ follow by using equations (5.13) and (5.14).

*$M_1$ = -1.3 kNm*

*$M_2$ = 7.6 kNm*

If the pier is rather thin, it is possible that the inclination angle α is limited by its geometry. This is the case with the test building.

$$\tan\alpha_{max} = 0.43 \leq \tan\Phi_d = 0.6$$

With the inclination ratio of 0.43, the axial force $N_V$ of the compression brace is 9.3 kN. The vertical force of 6.5 kN in the vertical compression brace is obtained out of the vertical equilibrium. Therewith, the vertical compression check of the compression brace can be performed.

$$\sigma_n = 0.77\ \text{N/mm}^2 \leq f_{xd} - f_{yd} = 2.45\ \text{N/mm}^2$$

Generally, the sliding check should be carried out at the top floor of the structure since the vertical load is there the lowest. The test building has only one floor and hence, the shear force that needs to be resisted is equal to $V_m$. Dividing $V_m$ by $N$ delivers a ratio of 0.25 which is less than the coefficient of the inner friction $\mu$ of 0.6 and hence satisfies the sliding check.

The next step in the computation of the capacity of the wall is the estimation of the effective Stiffness. There are different ways to do that, such as by using a finite element program, statics or by using Tomazevic's equation (5.11).

For the test structure, a static analysis is selected (see Appendix D). The static analysis delivers a pier stiffness $k$ of 17,081 kN/m. Bachmann and Lang recommend the use of a stiffness reduction factor of 0.5 to 0.7 to estimate the effective stiffness. These values have been confirmed by experimental results.

$$k_{eff} = (0.5 \div 0.7) \cdot k_0 \tag{5.20}$$

Appling the middle factor of 0.6 delivers an effective stiffness of $k_{eff}$ of 10,249 kN/m.

The yield displacement $\Delta_y$ of 0.386 mm is obtained by dividing the horizontal resistance force $V_m$ through the effective stiffness.

$$\delta_u = \alpha \cdot (0.8 - 0.25 \cdot \sigma_n) \tag{5.21}$$

In the last step, the plastic deformation capacity of the wall is estimated. In equation (5.21) $\sigma_n$ represents the axial tension in N/mm$^2$. Factor α serves as a safety factor since the formulation in equation (5.21) is derived on a single test series. If the formulation is used for design purpose, α should be selected between 0.5 and 0.7. The test structure serves as a verification model and therefore the value of α is selected equal to 1. This leads to a $\delta_u$ of 0.78.

Equation (5.22) shows how the displacement ductility μ can be found.

$$\mu = \frac{\delta_u}{\delta_y} \tag{5.22}$$

Assuming a linear elastic displacement behavior, the ultimate displacement $\Delta_u$ follows out of equation (5.23).

$$\Delta_u = \left\{1 + \frac{h_p}{h_{st}} \cdot (\mu - 1)\right\} \cdot \Delta_y \tag{5.23}$$

With the ultimate displacement $\Delta_u$ of 20.1 mm and with the yield displacement $\Delta_y$ of 0.386 mm the capacity curve of the wall is defined.

## 5. Capacity Curve of the Building

The capacity curve of the whole test structure is obtained by overlapping the capacity curves of single walls. Since the test building has two identical walls, the displacement capacity of the structure remains the same, while the horizontal shear force of the structure grows with each wall. With four piers capable of resisting a shear force of 3.96 kN, the whole structure is capable of resisting 15.8 kN.

The total stiffness is equal to the sum of the single walls stiffness. Thus, k is 40,996 kN/m.

$$k = \sum_{j} k_{eff,j} \tag{5.24}$$

Knowing the yielding and ultimate displacement capacity of the structure, an idealized capacity curve can be drawn. Figure 5.7 shows the capacity response of the test structure under the assumption of a 0.7 stiffness reduction.

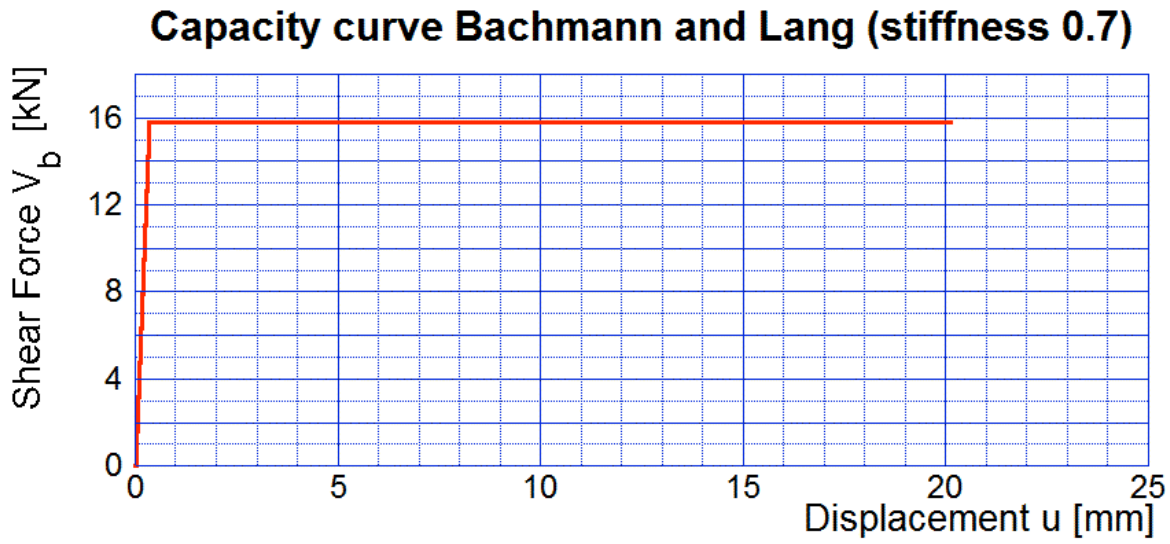


**Figure 5.7** Capacity curve of the test structure computed with a 0.7 stiffness reduction.

## 6. Equivalent SDOF

This step of the analysis deals with the development of an equivalent single-degree-of-freedom (SDOF) system. Since the mass of the structure and the total stiffness of the structure are known, the natural circular frequency can be estimated using equation (5.12). Therewith, a value of 80.44 $s^{-1}$ results for $\omega_1$. From this, by using the transformed equation (5.10), the natural period of vibration $T_1$ of the structure can be found to be 0.078 s. Because the structure has only one floor, the participation factor $\Gamma_1$ is again equal to 1.

**7. Capacity Demand**

The capacity demand is estimated for three performance levels. With the knowledge of the first period of vibration and by using the corresponding hazard spectra for Bern, the capacity demands can be calculated. In the first step the spectral acceleration is obtained. Then, with the use of equation (5.25) the spectral displacement follows.

$$S_d = \frac{\omega^2}{S_a} \tag{5.25}$$

Once the spectral displacement is known, it only needs to be multiplied with the participation factor $\Gamma_1$, which is equal to 1 for this structure, and the displacement demand results. In Table 5.5, the capacity demand is presented for the different performance levels.

**Table 5.5** Capacity demand of the test structure with a stiffness reduction of 0.7

| **Bachmann und Lang (0.7)** | $T_1$ = 0.072 s | | | |
|---|---|---|---|---|
| | $S_a$ | $S_d$ | $\Gamma$ | $\Gamma * S_d$ |
| Performance Level | [g] | [mm] | [-] | [mm] |
| Operational | 0.22 | 0.29 | 1 | 0.29 |
| Limited Damage | 0.32 | 0.42 | 1 | 0.42 |
| Collapse Prevention | 0.65 | 0.84 | 1 | 0.84 |

**8. Verification**

To verify, if the structure satisfies the expected criteria, the capacity response of the structure is compared with the corresponding capacity demand.

In Figure 5.7 it is easy to see that the highest capacity demand of 0.84 mm for the performance level of collapse prevention can easily be satisfied, since the structure has a capacity response of 20.1 mm.

## 5.2.7 3Muri Computation

For the 3Muri computation, a model of the test structure is developed according to the geometrical properties, the masonry characteristics and the loads described in Chapter 5.2.1 to 5.2.3. This delivers a structure as shown in Figure 5.3.

The program is set to use Swisscode and as seismic input, the same parameters are selected as known from the BHO-structure, described in Chapter 3.1.

To be able to compare the results with the hand calculations, it is only required to run two analysis combinations. The reason is that the eccentricity is neglected in the hand calculations and that the first-mode-load-pattern and uniform-mass-

proportional-load-pattern deliver identical results for a SDOF structure. Further, the seismic input in x-direction is only investigated. The combinations can be seen in Appendix D.4. The yellow bar shows the decisive combination, which is in this case the one in minus of the x-direction. Figure 5.8 presents the capacity curve of the test structure, calculated with 3Muri. The red line shows the idealized bi-linear curve, that 3Muri calculates for the equivalent SDOF system. As reference node, node 2 was selected.

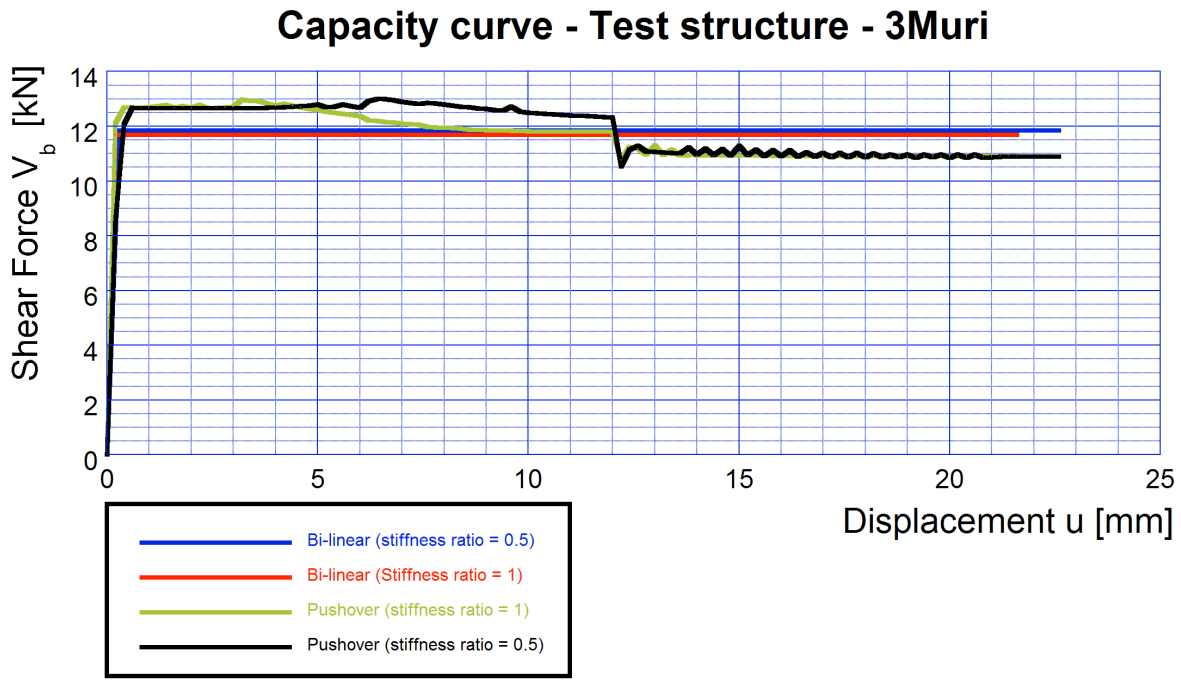


**Figure 5.8** Pushover curve of the test structure computed with 3Muri

The shear force loss at a displacement of 12 mm can be explained with the bending failure of the spandrel element. When the structure reaches its ultimate displacement, the piers fail under bending and the structure collapses. The test structure has a first period of vibration $T_1$ of 0.082 s. The yield displacement $\Delta_y$ of the equivalent SDOF system is 0.31 mm and the ultimate displacement $\Delta_u$ is 22.6 mm.

## 5.2.8 Discussion

To receive more values to compare, the hand calculation of the capacity curve is repeated for different stiffness ratios. The results are presented in Table 5.6.

**Table 5.6** Displacement response of the test building for different stiffnesses

| | uncracked stiffness | | cracked stiffness (0.5) | | cracked stiffness (0.6) | | cracked stiffness (0.7) | |
|---|---|---|---|---|---|---|---|---|
| | d [mm] | $V_b$ [kN] | d [mm] | $V_b$ [kN] | d [mm] | $V_b$ [kN] | d [mm] | $V_b$ [kN] |
| $\Delta_0$ | 0.00 | 0.00 | 0.00 | 0.00 | 0.00 | 0.00 | 0.00 | 0.00 |
| $\Delta_y$ | 0.23 | 15.83 | 0.46 | 15.83 | 0.39 | 15.83 | 0.33 | 15.83 |
| $\Delta_u$ | 20.10 | 15.83 | 20.13 | 15.83 | 20.12 | 15.83 | 20.11 | 15.83 |

In the following Table 5.7, the first period of vibration is presented for the different analysis. The last two columns show the displacement demands for the corresponded period of vibration for the two performance levels Limited Damage and Collapse Prevention. These demands are computed using the acceleration spectra for Bern, showed in Figure 6.23.

**Table 5.7** First period of vibration and capacity demands for two performance levels

| | k [kN/m] | $\omega_1$ [$s^{-1}$] | $T_1$ [s] | $u_{LD}$ [mm] | $u_{CP}$ [mm] |
|---|---|---|---|---|---|
| Equivalent Lateral Force Analysis | - | 60.9 | 0.103 | - | - |
| Response Spectra Analysis | 17466 | 105.0 | 0.060 | - | - |
| Bachmann und Lang (uncracked) | 68326 | 103.8 | 0.061 | 0.30 | 0.50 |
| Bachmann und Lang (cracked 0.7) | 47828 | 86.9 | 0.072 | 0.42 | 0.84 |
| Bachmann und Lang (cracked 0.6) | 40996 | 80.4 | 0.078 | 0.50 | 1.00 |
| Bachmann und Lang (cracked 0.5) | 34163 | 73.4 | 0.086 | 0.60 | 1.30 |
| 3Muri - equivalent SDOF (uncracked) | | 96.7 | 0.065 | 0.30 | 0.60 |
| 3Muri - equivalent SDOF (cracked 0.5) | - | 76.7 | 0.082 | 0.40 | 0.70 |

The equivalent lateral force analysis and the response spectra analysis are different from the other analyses. Its displacements are computed based on the elastic response spectra for the limited damage performance level with a return period of 475 years. Therefore the displacement of the structure satisfies automatically its required displacement. However, the knowledge of the ultimate displacement capacity of the structure is lacking. If the first periods of vibration of the different analysis are compared, the period of the response spectra analysis seems almost identical to the one of the hand calculation with uncracked stiffness. It is also practically identical to the period of the 3Muri calculation with uncracked stiffness. This is reasonable since the stiffness was estimated using the structure properties in the response spectra analysis. In contrast the first period of vibration of the equivalent lateral force analysis is estimated too high with the used empirical approach according to SIA.

The two achieved capacity responses of the hand and 3Muri analysis of the structure need to be checked with the requested capacity demand for the correspondent performance levels. Therefore, the capacity demand values in Table 5.7 are compared with the capacity responses in Table 5.8 and Figure 5.8. Consequently, all performance criteria are satisfied.

**Table 5.8** Displacement response of the equivalent SDOF with 3Muri

| | uncracked stiffness | | cracked stiffness (0.5) | |
|---|---|---|---|---|
| | d [mm] | $V_b$ [kN] | d [mm] | $V_b$ [kN] |
| $\Delta_0$ | 0.00 | 0.00 | 0.00 | 0.00 |
| $\Delta_y$ | 0.19 | 11.68 | 0.31 | 11.84 |
| $\Delta_u$ | 21.59 | 11.68 | 22.59 | 11.84 |

If Table 5.7 is compared with Table 5.8, the results for the unreduced stiffness appear to be quite similar. The displacements are almost identical, whereas 3Muri computes a smaller shear force. Further, the comparison of the two 50% cracked stiffness analyses present higher elastic displacements. This could be expected. However, the elastic displacement values differ from each other. An interesting observation is that the hand calculation with a stiffness reduction factor of 0.7 delivers almost identical displacement values as the 50% reduced stiffness analysis of 3Muri. The first period of vibration of the 50% reduced stiffness analyses are close to each other. Therefore, the difference in the displacement value is most probably connected with the somewhat higher estimated building mass in 3Muri. Another reason is probably the more advanced analysis that 3Muri performs during the evaluation. Another fact that needs to be considered while comparing these values is that the elastic displacement presented in 3Muri is the value of the idealized bi-linear capacity curve. If the effective pushover curve is analyzed in detail, it becomes clear that the precise yield point of the structure is difficult to define.

Another interesting observed fact is that if the factor α is selected at 0.6 in equation (5.21), the calculation delivers an ultimate displacement $\Delta_u$ of 12.1 mm. In Figure 5.8, the spandrel fails under bending at this value. With this safety factor the ultimate displacement capacity could be redefined as the state where the structure starts to fail partially. At this point it would still satisfy all capacity demands.

In general, the verification analyses show that 3Muri appears to deliver good results. At the same time it shows that Bachmann and Lang method is a useful tool for hand calculations.

## 5.3 Development of the 3Muri-model of the BHO-structure

In the first step the received plans of the BHO-structure are studied. Then a dwg-file for each floor is prepared, containing only the relevant walls and openings. Afterwards, these files are inserted in 3Muri and therewith the walls of the structure are defined. Next, the wall properties need to be defined. Most of the walls are out of Bernese sandstone masonry. The masonry is defined manually using the option of existing buildings and with the parameters defined in Chapter 3.5. The option to regard the initial cracked stiffness is selected. This means that the initial stiffness is equal to 50% of the entered modulus of elasticity and the shear modulus. On some floors, there are also steel and wood girders used in the ceilings. Once the wall properties have been defined, all the openings such as doors and windows can be added. Unfortunately 3Muri has no option for modeling vaulted windows. Therefore all vaulted windows are simplified and modeled as rectangular windows with a height equal to their corresponding real windows maximum vault height. It would be interesting to know the effect of this simplification on the results.

In the next step the floors are added. Therefore the knowledge of the floor properties is required. Since the detailed composition of the floors is uncertain, some characteristics were assumed in respect to the general floor composition of that time.

The composition of the timber floors is selected according to the information presented in SIA D0237. It states that the timber floors are unidirectional, with beams in a distance of 60 cm to each other and with a height of 28 cm and width of 20 cm. The beams are immured 24 cm in the masonry walls. In Appendix B.3 the selected floor parameters of the different floor types are shown. The load carrying direction of each floor is also visible. With the floors, also the vertical loads are defined. The vertical loads of the different floors are presented in Table 5.9. The balcony's composition on the first floor is rather massive. Therefore it is assumed to have a high dead load of 5 kN/m$^2$ overlapped by a 3 kN/m$^2$ live load for balconies, as the Swisscode recommends.

**Table 5.9** Interacting vertical loads on the different floor types according to their location

| Story | Floor type | Dead load [kN/m$^2$] | Live load [kN/m$^2$] | Total [kN/m$^2$] |
|---|---|---|---|---|
| TP | Steel beam and vault (office) | 3.7 | 3.0 | 6.7 |
| | Steel beam and vault (entrance hall) | 3.7 | 5.0 | 8.7 |
| | Barrel Vault | 8.0 | 4.0 | 12.0 |
| | Rock plate | 4.0 | 4.0 | 8.0 |
| EG | Steel beam and vault | 3.7 | 4.0 | 7.7 |
| | One-way timber floor with single wood plank (office) | 3.0 | 3.0 | 6.0 |
| | stairs plate | 3.5 | 4.0 | 7.5 |
| | cross vaults | 8.6 | 3.0 | 11.6 |
| 1.OG | Steel beam and vault | 3.7 | 4.0 | 7.7 |
| | One-way timber floor with single wood plank (office) | 3.0 | 3.0 | 6.0 |
| | One-way timber floor with single wood plank (hallway) | 3.0 | 4.0 | 7.0 |
| | stairs plate | 3.5 | 4.0 | 7.5 |
| | Balcony | 5.0 | 3.0 | 8.0 |
| 2.OG | One-way timber floor with single wood plank (office) | 3.0 | 3.0 | 6.0 |
| | One-way timber floor with single wood plank (hallway) | 3.0 | 4.0 | 7.0 |
| 3.OG | One-way timber floor with single wood plank (office) | 3.0 | 3.0 | 6.0 |
| | One-way timber floor with single wood plank (hallway) | 3.0 | 4.0 | 7.0 |

The roof structure is situated on the fourth floor. There is no further information available about its composition. Thus, it is assumed to consist out of rather light materials, such as timber. One reason is that the walls of this roof house do not follow the structural walls of the third floor above. In 3Muri it is only modeled in terms of its estimated gravity loads and introduced as point loads on the structural elements above (see Figure 5.9). The different loads are presented in Table 5.10. The area load is an assumption including the construction of the roof of the roof house as well as the different walls.

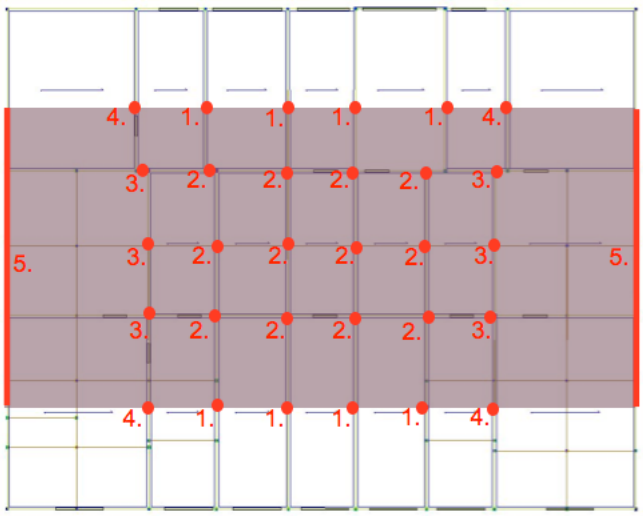


**Figure 5.9** Assignment of the point loads of the roof structure

**Table 5.10** Load assignments of the roof structure

| id [-] | Influence area [$m^2$] | Area load [$kN/m^2$] | Point load [kN] | Line load [kN/m] |
|---|---|---|---|---|
| 1 | 6 | 4 | 24 | - |
| 2 | 11.2 | 4 | 44.8 | - |
| 3 | 16.5 | 4 | 66 | - |
| 4 | 8.5 | 4 | 34 | - |
| 5 | 3.2 | 4 | - | 12.8 |

During the development of the model, some limits of the program could be detected. For example needed some windows in the staircase to be moved upwards to the next story-level because else, there would be two windows located over each other in the same story-level (see first floor in Figure 5.11). But this is something the program refuses.

In order to provide a working model of the structure, all the floors need defined elements surrounding them. If there is no existing wall, as for example on one side of the stair-floors, it is helpful to define a timber beam with a negligible cross section (see Figure 5.10). This way the simulation works while the fictive beam is too small to have any influence on the results.

The floors of the stairs in the staircase are modeled on half of the height of the floors. They are shown in blue color in Appendix B.2. Since the floors in the staircase are in general designed to be rather stiff and because there is no information available about their composition, they are assumed to be rigid. The wall between two stairs is respected in the model. As recognized during the site visit, they have vaulted openings. To consider them, openings were integrated in the model. For an unknown reason, the assumption to add a timber beam in terms of the frame definition of the stair floor, the program was not able to run the calculation. Luckily it worked after programming a solid wall element with an opening reaching from the bottom to the top (see Figure 5.10).

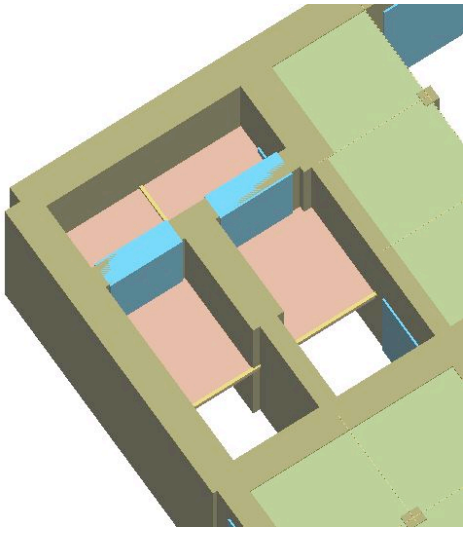

**Figure 5.10** Staircase model

The pillars in the entrance hall are modeled as masonry pillars. This assumption is probably not corresponding to the real pillars, but because detailed information is lacking and since they only carry the vertical loads from the gallery above, it should suffice.

In Figure 5.11 the 3D-model of the structure is presented. Figure 5.12 shows the 3D-mesh-model of the structure.

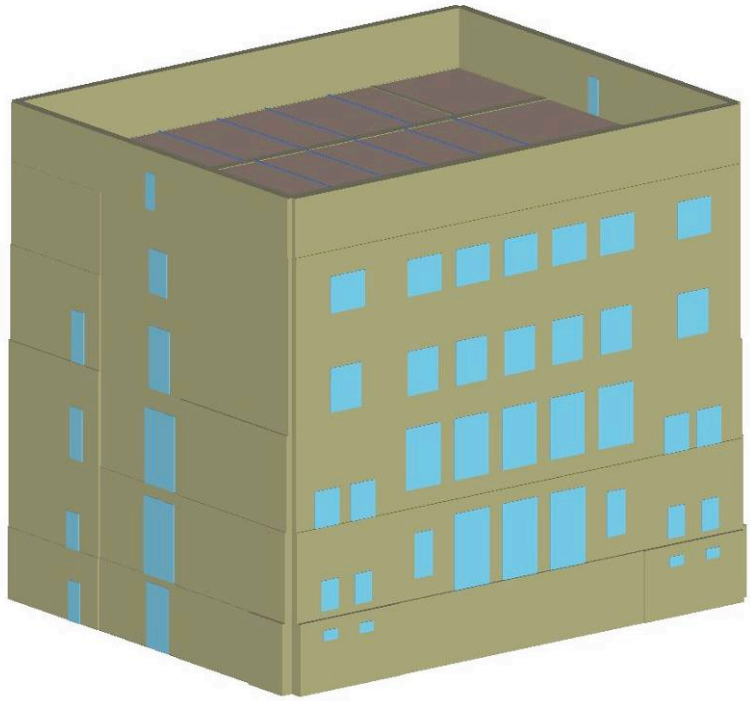

**Figure 5.11** 3D-model of the BHO-structure

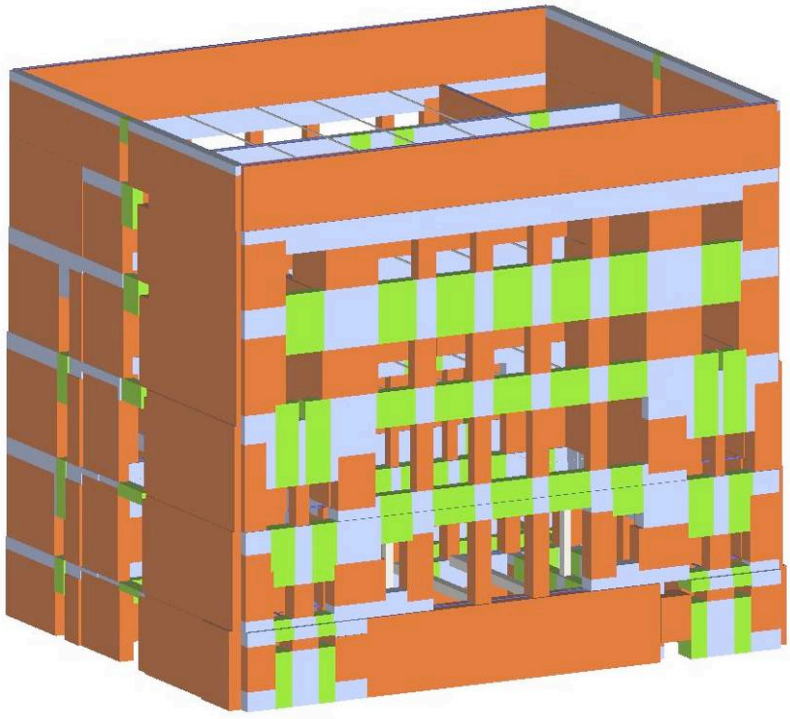

**Figure 5.12** 3D-mesh of the BHO-structure

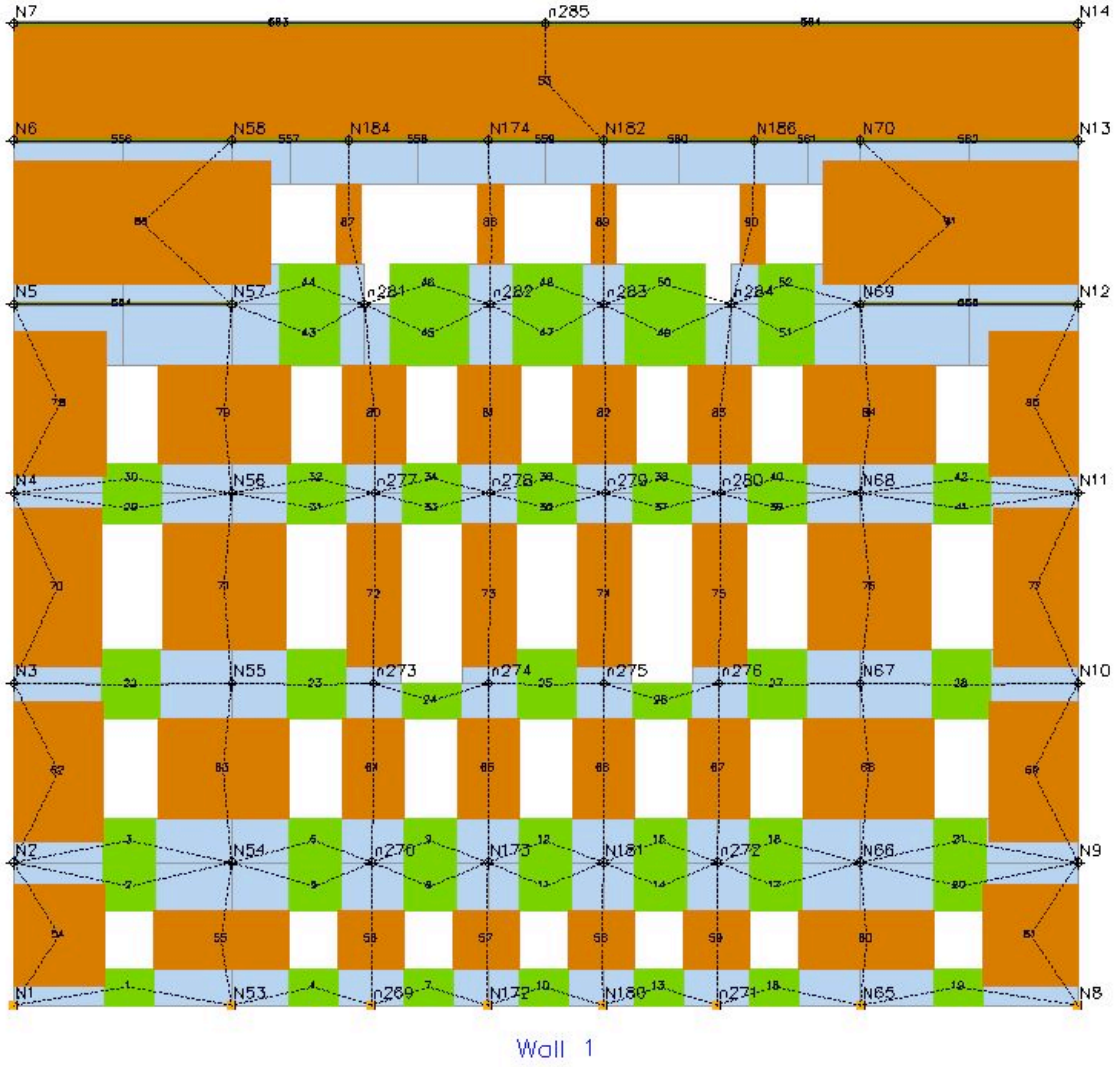


**Figure 5.13** Mesh of the south wall

After the mesh of the BHO-structure is generated, it needs to be verified. In Figure 5.13, the wall pointing south is shown representative. The divided line between nodes N4 and N56 can be explained with the changing wall thickness between the upper and lower wall. Further, the thick line found between nodes N5 and N57 is created to split the load from the big pier wall over the two smaller piers below. Similarly the generated mesh can be studied and understood.

With the generation of the mesh, the development of the structure ends and the evaluation phase starts.

# 6 Evaluation

## 6.1 Seismic Hazard

A seismic hazard is a physical hazard. Wikipedia defines a hazard as an event posing a threat to life, health, property or environment [29]. When a design engineer needs to design or evaluate a building on its seismic behavior, he needs to know to what seismic hazard the structure is exposed. The investigation of the seismic hazard for a location is an excessive task. Therefore the codes offer seismic maps, telling which region belongs to what degree of hazard. Further, they offer seismic design spectra, which help the design professional to compute the pseudo acceleration or pseudo displacement, respectively. A seismic hazard is either analyzed in a deterministic or probabilistic way. In the deterministic analysis, a particular earthquake scenario is assumed, while the probabilistic explicitly considers uncertainties. Either way, the earthquake source needs to be identified. The source is identified using all possible sources such as fault maps giving geological, tectonic and historic information as well as instrumental records of seismicity of the past. Further, understanding of the wave propagation is necessary. In Figure 6.1 the uniform hazard spectra (UHS) for Bern is shown [30].

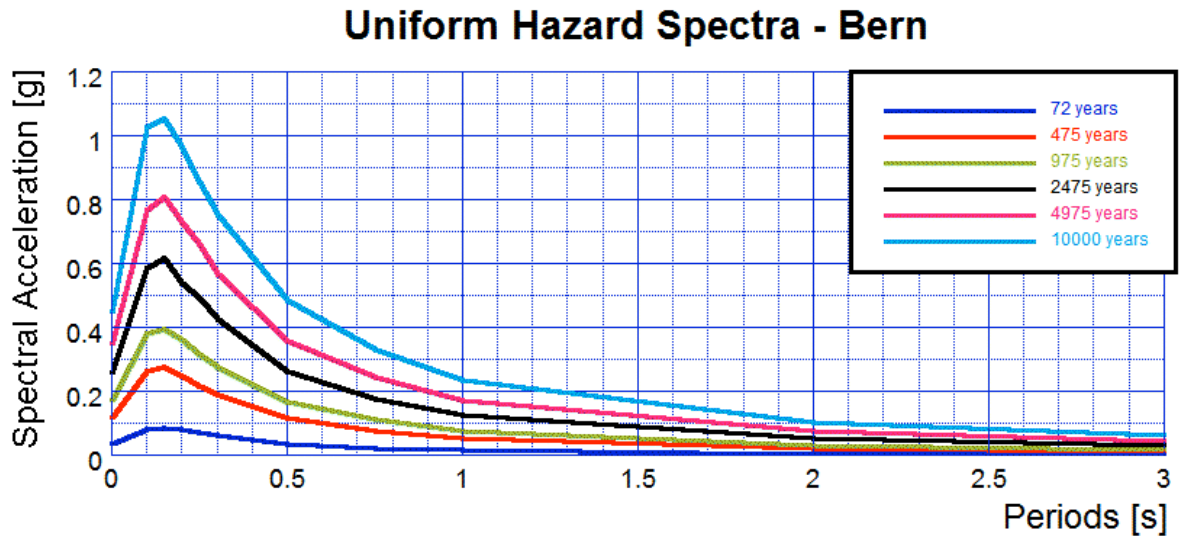


**Figure 6.1** Uniform hazard spectra (UHS) for Bern

To receive design spectra for the BHO-structure, showing the demands for the three performance levels operational (72 years), limited damage (475 years) and collapse prevention (2475 years), the uniform hazard spectra of Bern are used. The performance levels are discussed later in this chapter. For the period of one second, the spectral accelerations are obtained from the UHS for all three performance levels. These values are used as the constant $S$ in SIA 261 in order to compute the

seismic design spectra for the BHO-structure. This is not totally correct but gives a good approximation. The following equations are from SIA 261.

$$S_d = \gamma_f \cdot \frac{a_{gd}}{g} \cdot S \cdot \left[0.67 + \left(\frac{2.5}{q} - 0.67\right)\frac{T}{T_B}\right] \qquad (0 \le T \le T_B) \qquad (6.1)$$

$$S_d = 2.5 \cdot \gamma_f \cdot \frac{a_{gd}}{g} \cdot \frac{S}{q} \qquad (T_B \le T \le T_C) \qquad (6.2)$$

$$S_d = 2.5 \cdot \gamma_f \cdot \frac{a_{gd}}{g} \cdot S \cdot \frac{T_C}{T \cdot q} \qquad (T_C \le T \le T_D) \qquad (6.3)$$

$$S_d = 2.5 \cdot \gamma_f \cdot \frac{a_{gd}}{g} \cdot S \cdot \frac{T_C \cdot T_D}{T^2 \cdot q} \ge 0.1 \cdot \gamma_f \frac{a_{gd}}{g} \qquad (T_D \le T) \qquad (6.4)$$

By applying equations (6.1) to (6.4) for a period range from zero to three seconds, the design response spectra for the BHO-structure in Bern are obtained (see Figure 6.23). The corresponding seismic parameters of the BHO-structure used in these equations are described in Chapter 3.1. According to Swisscode the parameter $q$ is equal to 1.5 for unreinforced masonry structures. The acronym $S_d$ stands for the ordinate value of the design spectral acceleration.

Dependent on the importance of a building, it needs to satisfy different requirements. In Figure 6.2, the different performance goals for design are visualized. For example a hospital needs to have a greater earthquake resistance then an ordinary building. If a rare earthquake occurs, it is most important that hospitals are functional in order to treat the casualties. Figure 6.3 shows the damage progression of a building in dependence of the structural displacement. As long as a structure withstands an earthquake in its elastic range, there is no remaining structural damage. If the loads overpass the structures elastic displacement capacity it starts to deform in its inelastic range. Under small inelastic deformations the structure may still be usable after the earthquake. Maybe some specific components need to be exchanged. If the load is larger and the building undergoes large inelastic deformations, it reaches its ultimate displacement capacity. The point of collapse prevention defines the state, where the building is heavily damaged and any further displacement leads to the collapse of the structure. According to this performance model, the three performance levels are defined with the following return periods:

| | |
|---|---|
| Operational | 72 years |
| Limited Damage | 475 years |
| Collapse Prevention | 2475 years |

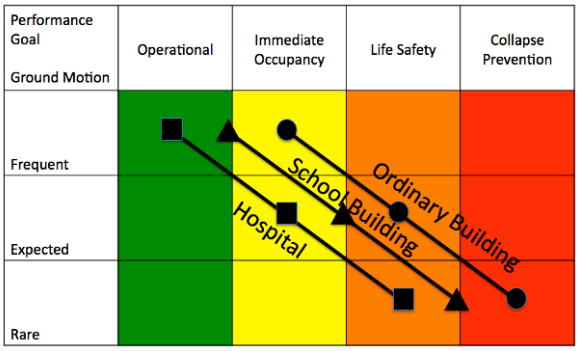


**Figure 6.2** Performance goals for design

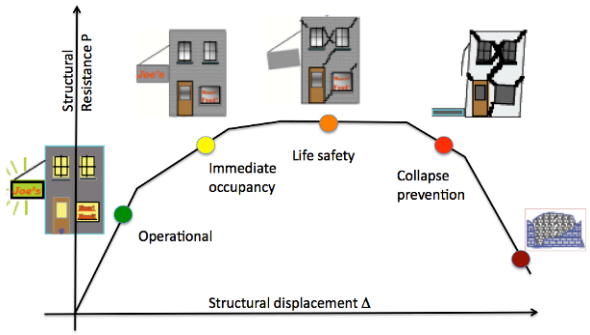


**Figure 6.3** Structural performance model

## 6.2 Equivalent Static Loading

The global analysis of the BHO-structure succeeds with a nonlinear static procedure. As described in Chapter 3.3, the result is presented in form of a pushover curve showing the relation between the base shear and the top displacement of the structure. To perform the analysis, a reference node needs to be selected on top of the structure. Therefore the closest node to the mass center of the structure is selected on the third floor. Since the roof house is only taken into account with the additional vertical loads, this reference node represents the highest point. The relation between the base shear and the top displacement is obtained by increasing monotonically the horizontal load until the building collapses. 3Muri offers two options for the horizontal load distribution. Either the horizontal load is applied according to the first mode of vibration of the structure or based on a uniform mass-proportional pattern. In this evaluation both ways are used.

Since the building is practically symmetric in the x-direction, the mass center needs only to be estimated in y-direction. The computation in Appendix C shows that the mass center moves in y-direction about 1 m forwards and backwards, dependent on which floor is contemplated. In Figure 6.4, the red point shows the mass center with its moving direction. The node number 259 is the closest node to the mass center and therefore it is selected as the first reference node. The evaluation considers all 24 analysis combinations described in Chapter 5.1.4.

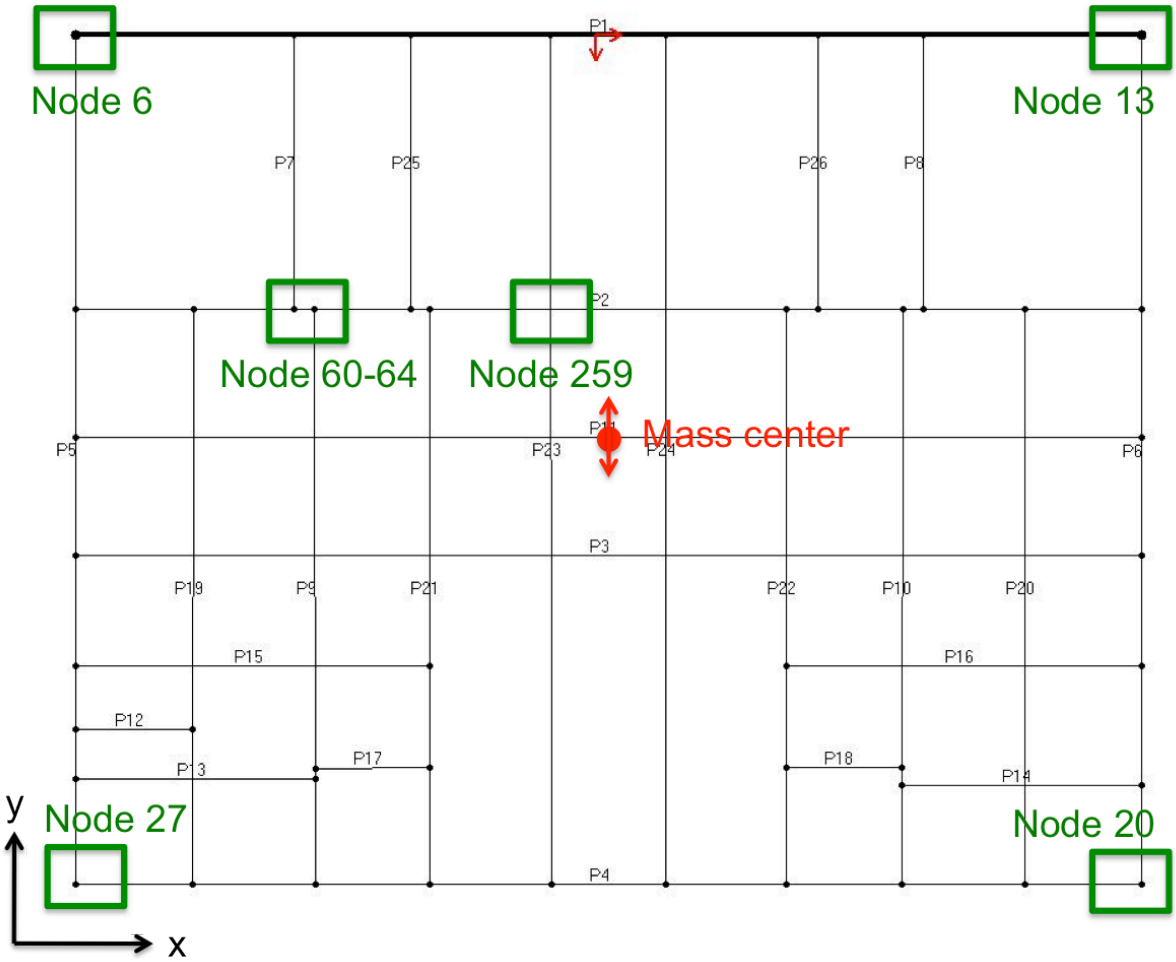


**Figure 6.4:** Reference nodes, used for the global evaluation and the mass center

The four corner nodes visible in Figure 6.4 (6, 13, 20 and 27) are used to compare and discuss the displacements. They are expected to undergo higher displacements than the reference node 259, which is close to the mass center. Further an average pushover curve is computed by 3Muri. It should provide an additional source of information in order to evaluate the behavior of the BHO-structure.

To compare the influence of a building with flexible floors to one with rigid floors, all flexible floors of the BHO-structure are replaced in the second model by rigid floors. Everything else remains the same. The structure is analyzed like before, in respect to reference node 259. Since the corner nodes are the most eccentric nodes, they should be useful in the examination of the behavior between the model with flexible and the one with rigid floors. For investigating the diaphragm behavior additional nodes may become relevant during the evaluation.

At last, the story drifts are investigated. Therefore, a representative node is required, which is close to the mass center but also existent in every floor. This way the drift between two floors can be calculated. For this purpose, the nodes 60 to 64 are selected (see Figure 6.4).

## 6.3 Global Evaluation

### 6.3.1 Flexible Floors Model

The results of the reference node 259 deliver the general behavior of the structure. In Figure 6.6, the pushover curve of the relevant analysis combination, with loading in the x-direction, is presented. The relevant analysis combination is based on the horizontal loading according to the first mode of vibration.

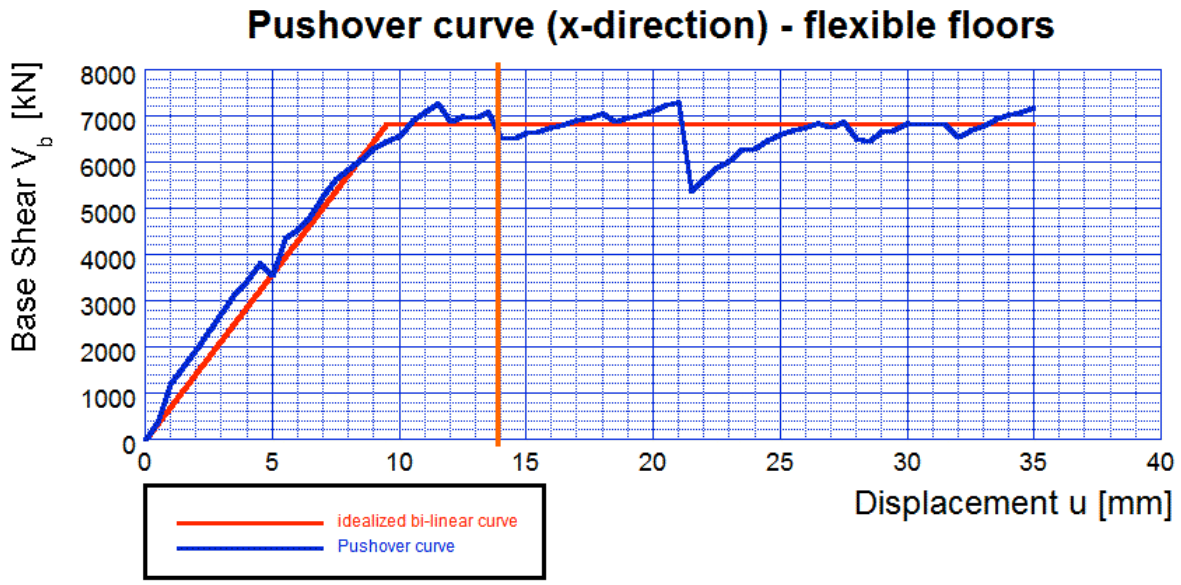


**Figure 6.5** Pushover curve with flexible floors and loading in the x-direction (analysis nr.12)

The analysis shows that the structure reaches its ultimate displacement at 35 mm. At this point, the structure collapses under shear failure (orange marked elements) of the Wall 2 (see Figure 6.6).

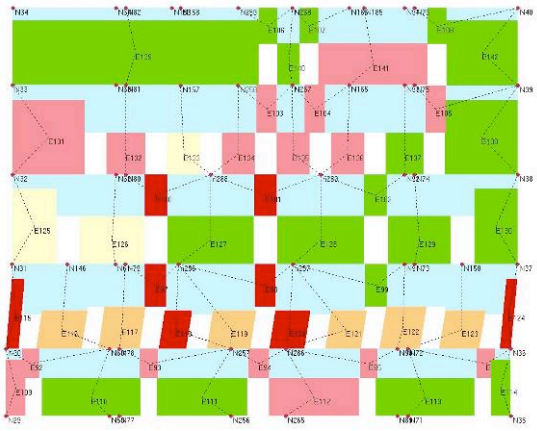

**Figure 6.6** Collapse mechanism of Wall 2 in Figure 6.5

However, at a horizontal displacement of 14 mm, the front Wall 1 already starts to collapse. In Figure 6.8 it becomes clear that Wall 4 is experiencing a large horizontal deformation. The building starts to collapse on the third floor when the piers fail under bending. As the deformation goes on the piers on the ground floor show the same failure and soon the whole wall collapses long before the shear failure at a deformation of 35 mm of Wall 2 is reached. If the front wall collapses, a large part of the front side of the BHO-structure collapses as

well. Thus, the ultimate displacement of the structure is redefined manually to 15 mm.

Figure 6.7 visualizes the collapse mechanisms of Wall 4 at a horizontal displacement of 14 mm. The walls are numerated based on their numbers in the 3Muri model. In Figure 6.8, the floor plan of the deformed structure is presented.

The deformations visible in Figure 6.8 show a flexible-floor structure-behavior. The outside walls deform stronger in the x-direction than those in the center of the building. This shows that the walls act at least partially as single structural elements, with reduced interaction between each other. This is to be expected by flexible diaphragms.

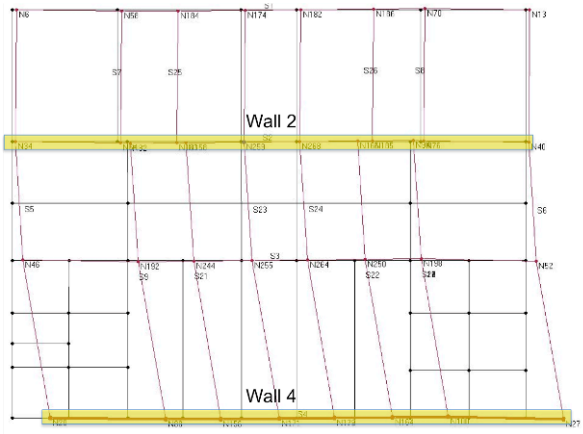


**Figure 6.8** Floor plan of the deformed third floor

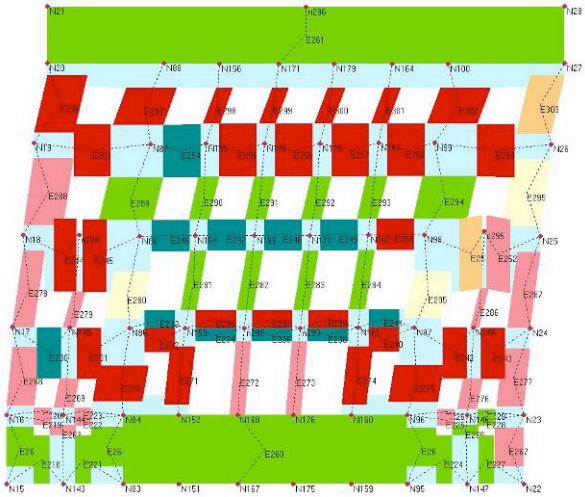

**Figure 6.7** Collapse mechanism of the Wall 4 in Figure 6.8

The pushover curve presented in Figure 6.9 is based on the average displacement of all the nodes of the reference node level. In the average of all points, the ultimate displacement according to 3Muri amounts to 117 mm. If the same manual redefinition is performed as for the analysis of the displacement of the reference node 259, an ultimate displacement of 43 mm is found. This shows that, in general, the structure undergoes a larger deformation than the reference node. However, the reference node is selected close to the mass center and is therefore also expected to show small deformations in contrast to the corner nodes.

The base shear is found around 6,800 kN for the pushover curve based only on the displacement of the reference node as well as for the one based on the average displacements.

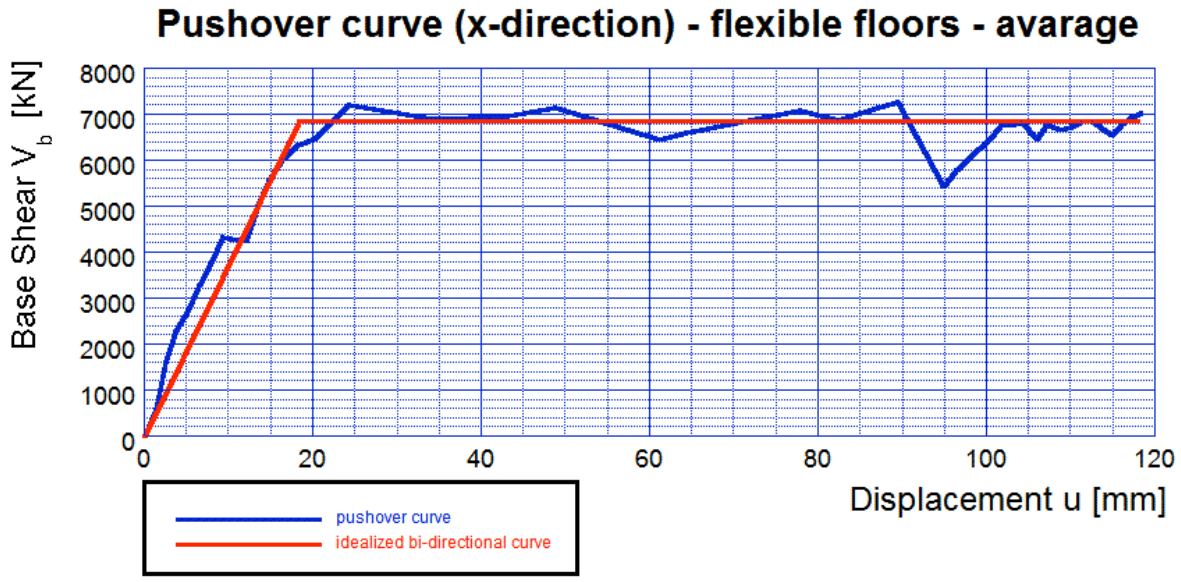


**Figure 6.9** Average pushover curve with flexible floors and loading in the x-direction (analysis nr. 18)

In Table 6.1 the displacement of the corner nodes in relation to the reference node 259 can be found for the model with flexible floors. The yellow-marked fields point out the deformations in the loading direction. For the nodes 20 and 27 a displacement of 174 mm in x-direction can be found.

**Table 6.1** Displacements of the corner nodes in relation to the reference node 259 for the flexible model

| Flexible floors | | | | | | |
|---|---|---|---|---|---|---|
| 1st Modus | loading in X-direction (analysis nr.12) | | | | | |
| T = 0.706 s | $U_x$ | $U_y$ | $U_z$ | $\Delta_X$ | $\Delta_Y$ | $\Delta_Z$ |
| Node-Nr. | [mm] | [mm] | [mm] | [%] | [%] | [%] |
| 259 | 14.00 | -2.26 | -5.57 | 100 | 100 | 100 |
| 20 | 174.04 | 0.56 | -0.94 | 1243 | -25 | 17 |
| 27 | 174.04 | -3.79 | -1.35 | 1243 | 168 | 24 |
| 13 | 20.22 | -1.82 | -3.71 | 144 | 81 | 67 |
| 6 | 20.22 | 0.52 | -2.39 | 144 | -23 | 43 |
| masses | loading in y-direction (analysis nr.18) | | | | | |
| T = 0.614 s | $U_x$ | $U_y$ | $U_z$ | $\Delta_X$ | $\Delta_Y$ | $\Delta_Z$ |
| Node-Nr. | [mm] | [mm] | [mm] | [%] | [%] | [%] |
| 259 | 1.91 | 254.53 | -4.44 | 100 | 100 | 100 |
| 20 | 1.66 | 32.99 | 0.80 | 87 | 13 | 118 |
| 27 | 1.64 | 16.19 | -1.56 | 86 | 6 | 35 |
| 13 | -0.01 | 16.20 | -4.43 | 101 | 6 | 100 |
| 6 | -0.03 | 32.49 | -5.78 | 102 | 13 | 130 |

By contemplaiting Figure 6.10, a considerably larger displacement can be noticed in the y-direction. The ultimate displacement amounts to 256 mm and is caused by the horizontal loading based on the uniform mass-proportional pattern. However, on the third floor a diaphragm deflection can be observed as shown in Figure 6.13 and

because the reference node is situated in the middle of this deflection, the pushover curve shows an unexpected large elastic deformation. The structure experiences a soft-story collapse mechanism on the ground floor. Both, shear (orange elements) and bending (red elements) failure can be observed.

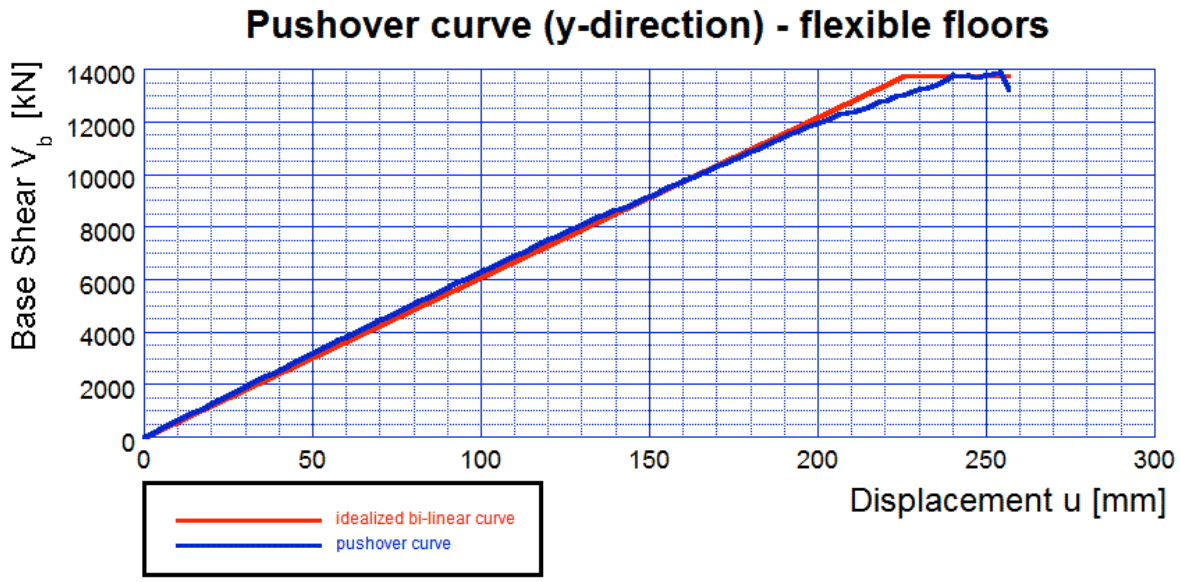


**Figure 6.10** Pushover curve with flexible floors and loading in the y-direction (analysis nr.18)

In Figure 6.12, the floor plan of the failure mechanism is shown. A torsion-effect can be observed. Since the structure is rather symmetric it is probably caused by the initial accidental eccentricity.

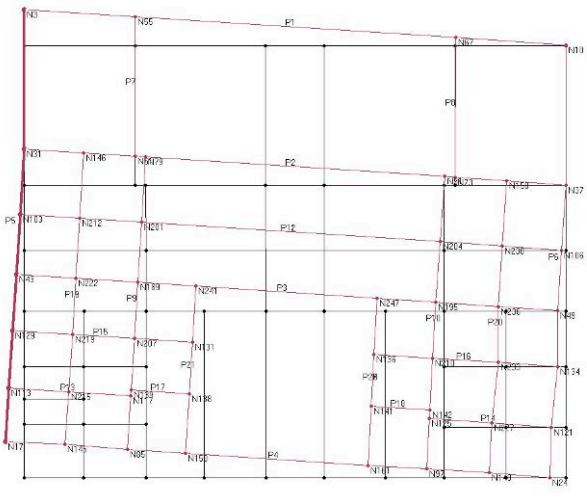

**Figure 6.12** Floor plan of the collapse mechanism of the ground floor

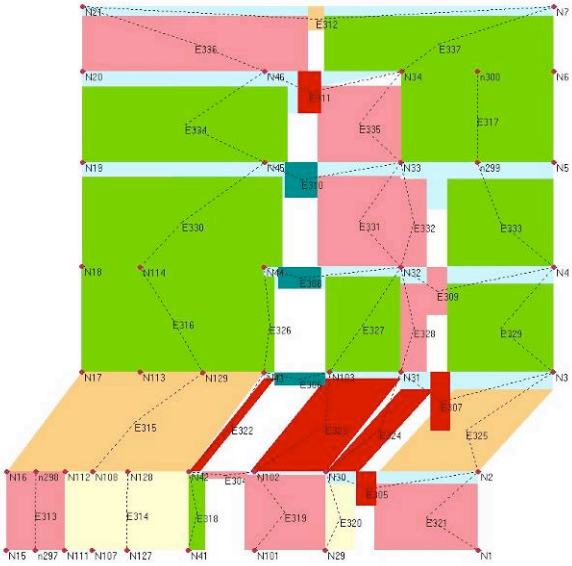

**Figure 6.11** Collapse mechanism of the red-marked wall in Figure 6.12

Through the additional loading of the point loads of the roof structure and the unidirectional load carrying of the steel beams shown in Figure 6.13 with red arrows, a diaphragm deformation results. It is only found on the third floor. With the four walls supporting these steel beams, a deformation shape results surprisingly close to the one presented in Figure 3.8 of Chapter 3.4. By comparing the displacement in the y-direction of the nodes 259 and 64, the diaphragm deflection $\Delta_d$ results in 184 mm.

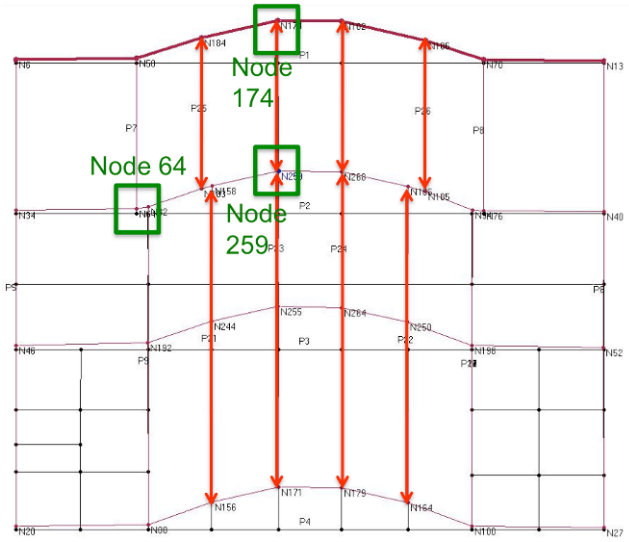


**Figure 6.13** Floor plan of the deformation behavior of the third story

**Table 6.2** Diaphragm displacement

| Node-nr. | $U_y$ [mm] |
|---|---|
| 259 | 256.9 |
| 64 | 73.2 |
| $\Delta_d$ | 183.7 |

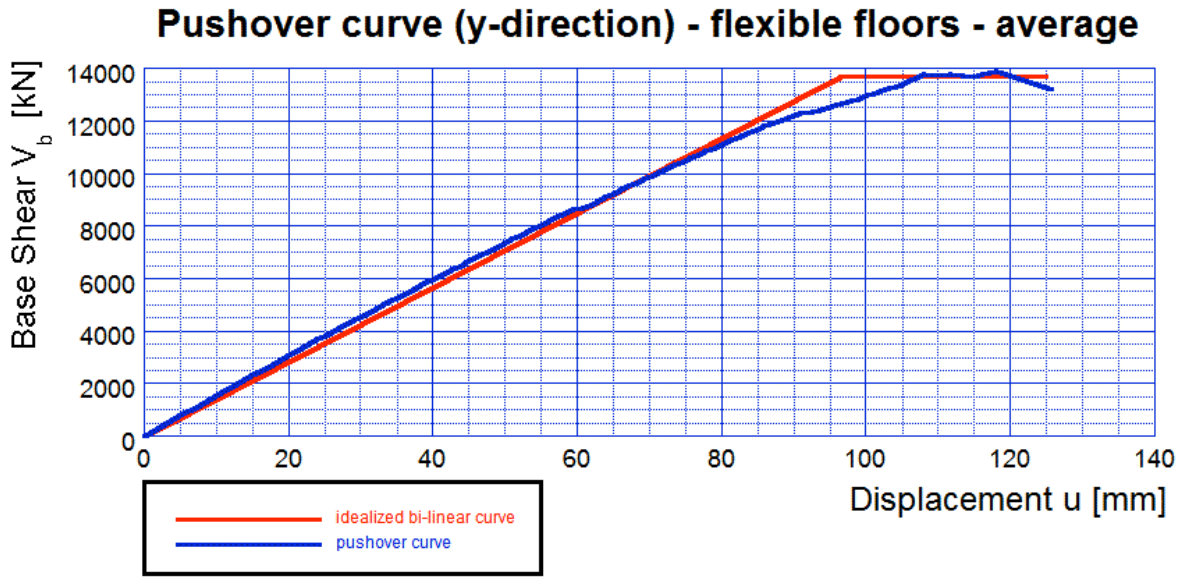


**Figure 6.14** Average pushover curve with flexible floors and loading in y-direction

The average curve of the flexible model in the y-direction is found to be similar to the one based only on the reference node. The main difference is the displacement capacity. Since the reference node is part of the diaphragm deflection, its displacement is larger and not representative for the structure itself. In Figure 6.14 an

average ultimate displacement of 125 mm is found. As before, the displacement at the mass center is expected to be lesser. The mass center displacement can be estimated with the displacement of node 64, which is relatively close to the mass center and not part of the deflection of the diaphragm on the third floor. This node shows an ultimate displacement of 58 mm in y-direction, which is approximately half the average ultimate displacement.

### 6.3.2 Rigid Floors Model

This chapter presents the results of the structure with rigid floors. Figure 6.15 shows the pushover curve in the x-direction. The curve is similar to the one of the building with flexible floors shown in Figure 6.9. The major difference is the larger deformation capacity in the inelastic range. The ultimate deformation is reached at 43 mm. The base shear is found at 10,000 kN. This is around 1,000 kN higher than with the structure with flexible floors. At 22 mm a partial failure can be found. At this point the ultimate displacement is reached in analysis 16 of the flexible structure. Even though analysis 16 is not decisive for the flexible structure a possible interpretation is that the same failure begins at this point in the building with rigid floors, but then the rigid floors redistribute the loads and therefore the structure can withstand a larger deformation.

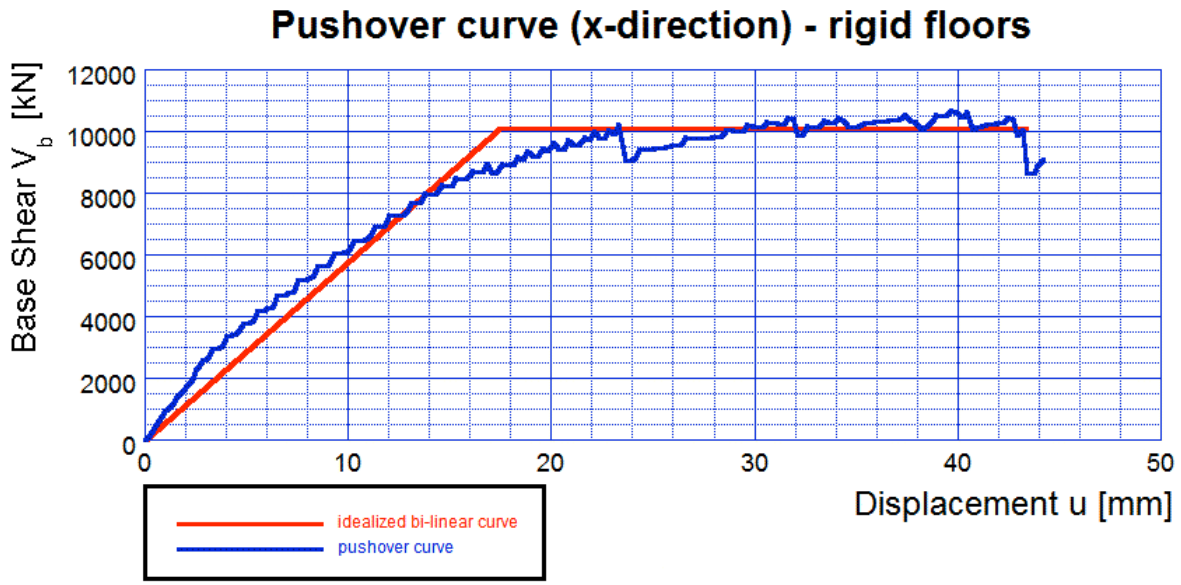


**Figure 6.15** Pushover curve with rigid floors and loading in the x-direction (analysis nr.16)

In Figure 6.16 it can be seen that the structure deforms as a global structure. The deformations appear to be the same through the whole floor. The building collapses when the piers of Wall 2, shown in Figure 6.16 in red, collapse under shear failure on the ground floor (see Figure 6.17). Shear failure is indicated by orange color in 3Muri.

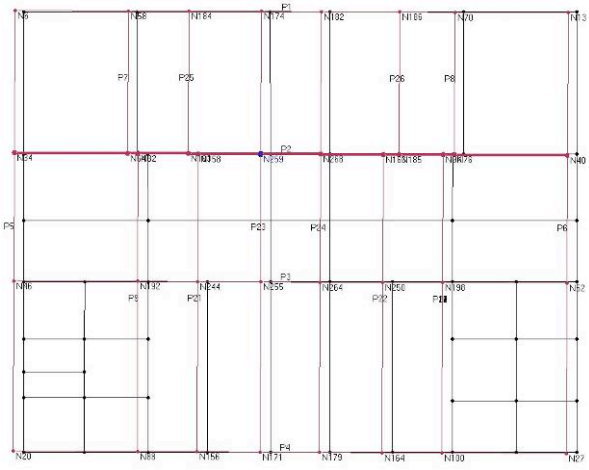

**Figure 6.16** Floor plan of the collapse mechanism

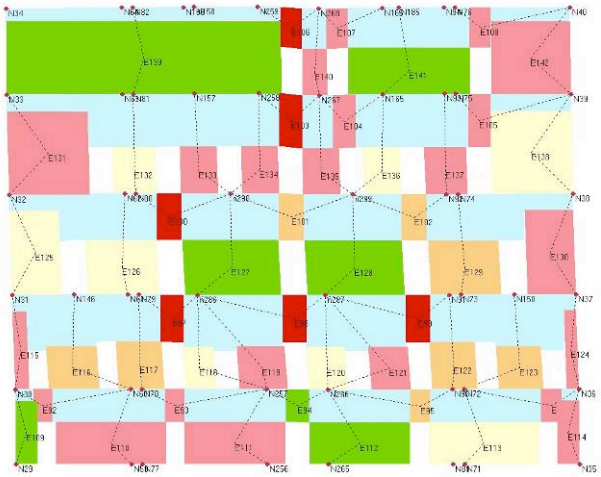

**Figure 6.17** Collapse mechanism of the red-marked wall in Figure 6.16

Figure 6.18 shows the pushover curve of the BHO-structure in the y-direction for the rigid-floors model. It is interesting, that the horizontal displacement capacity is smaller than the one for the building with flexible floors in Figure 6.10. In contrast to the decisive analysis combination for the flexible structure, the horizontal load is here assigned according to its first mode of vibration. The here obtained displacement capacity is approximately one fifth of the capacity for the flexible building.

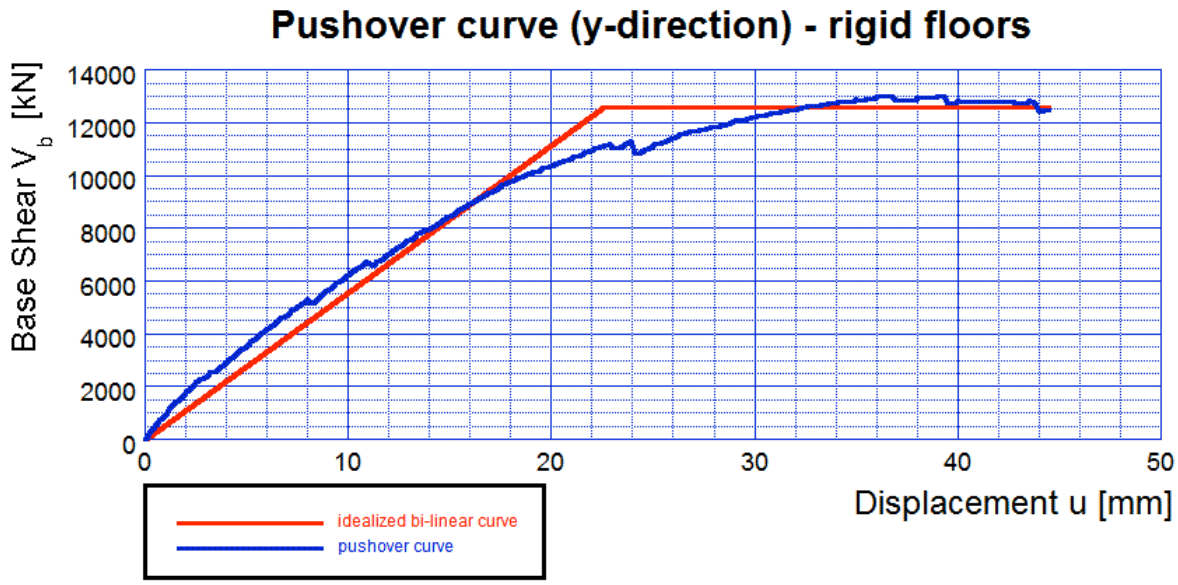


**Figure 6.18** Pushover curve with rigid floors and loading in y-direction (analysis nr.20)

Figures 6.19 and 6.20 present the same collapse mechanism as the model with flexible floors. Shear and bending failure is also observed here.

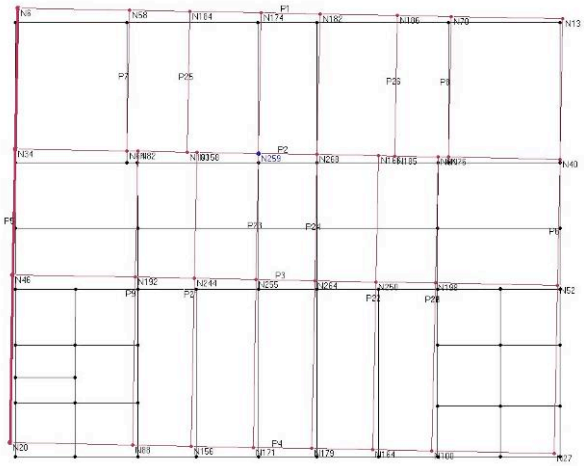

**Figure 6.19** Floor plan of the collapse mechanism

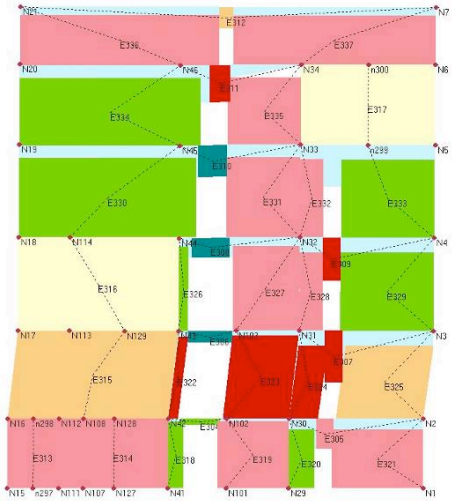

**Figure 6.20** Collapse mechanism of the red-marked wall in Figure 6.19

Table 6.3 shows the relations of the displacements between the corner nodes and the reference node 259 for the rigid model. The yellow-marked fields point out the deformations in the loading direction. The deformations for the rigid building show a more uniform response then those of the flexible model in Table 6.1. This could be expected. The corner displacements for the flexible model in y-direction show a quite smaller deformation than the reference node close to the mass center. But these values are only valid for the third floor. As discussed above, the diaphragm shows deflection on this floor. The maximum deviations from the reference node 259 to the corner nodes are for the rigid model in the y-direction 30% and can be found with node 13 and 27. This confirms again a more uniform building response for a structure with rigid floors, where loads are redistributed once a component reaches its capacity.

**Table 6.3** Displacements of the corner nodes in relation to the reference node 259 for the rigid model

| Rigid floors | | | | | | |
|---|---|---|---|---|---|---|
| 1st Modus | loading in X-direction (analysis nr.16) | | | | | |
| T = 0.696 s | $U_x$ | $U_y$ | $U_z$ | $\Delta_X$ | $\Delta_Y$ | $\Delta_Z$ |
| Node-Nr. | [mm] | [mm] | [mm] | [%] | [%] | [%] |
| 259 | -43.22 | 1.09 | 3.04 | 100 | 100 | 100 |
| 20 | -49.62 | 5.48 | -3.12 | 115 | 503 | 203 |
| 27 | -49.63 | -4.70 | -3.04 | 115 | 531 | 200 |
| 13 | -40.43 | -4.65 | -1.12 | 94 | 929 | 137 |
| 6 | -40.43 | 5.67 | -5.14 | 94 | 520 | 269 |
| 1st Modus | loading in y-direction (analysis nr.20) | | | | | |
| T = 0.6 s | $U_x$ | $U_y$ | $U_z$ | $\Delta_X$ | $\Delta_Y$ | $\Delta_Z$ |
| Node-Nr. | [mm] | [mm] | [mm] | [%] | [%] | [%] |
| 259 | 1.34 | 44.78 | -4.41 | 100 | 100 | 100 |
| 20 | -11.44 | 54.83 | 3.53 | 954 | 122 | 180 |
| 27 | -11.45 | 31.56 | 1.37 | 954 | 70 | 131 |
| 13 | 6.7 | 31.28 | -6.12 | 500 | 70 | 139 |
| 6 | 6.67 | 54.26 | -6.01 | 498 | 121 | 136 |

Figure 6.21 visualizes the pushover curves between the model with flexible and the one with rigid floors. It becomes clear that the structure with rigid floors can withstand a higher base shear force. The rigid-floors structure can also undergo a larger displacement. Unlike the pushover curve of the flexible-floors structure, which shows a partial collapse of the structure already at 14 mm, the rigid-floors structure remains relatively intact until it reaches the ultimate displacement at 44 mm. With the adjusted ultimate displacement of 14 mm of the flexible structure, the rigid structure has a three times larger displacement capacity. An interesting observation is that the flexible and rigid curve are almost identical up to a deformation of 12 mm, where the flexible one reaches its maximum base shear capacity. This means that until this deformation the composition of the diaphragms is of no relevance, as they do not contribute to the response of the structure.

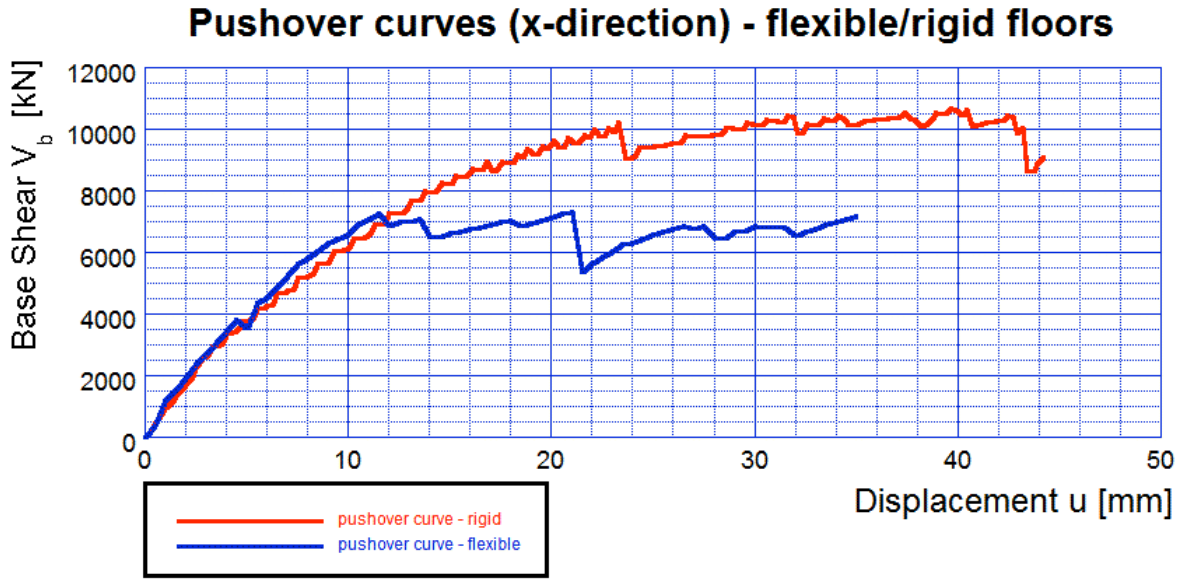


**Figure 6.21** Comparison of the pushover curve in the x-direction for the flexible and rigid model

Figure 6.22 presents the two pushover curves for the flexible and rigid structure in the y-direction. These two curves are rather difficult to compare, since the reference node 259 is part of the diaphragm deflection in the third floor. Thus, the blue curve is not the pushover curve representing the relation between the base shear and the displacement of the reference node but the average displacement of the nodes of its level as shown in Figure 6.14. This curve is a better estimation of the general displacement response of the flexible structure. Comparing the curves in Figure 6.22 shows that the flexible structure can withstand the same base shear forces as the rigid structure, but only under considerably larger horizontal deformations.

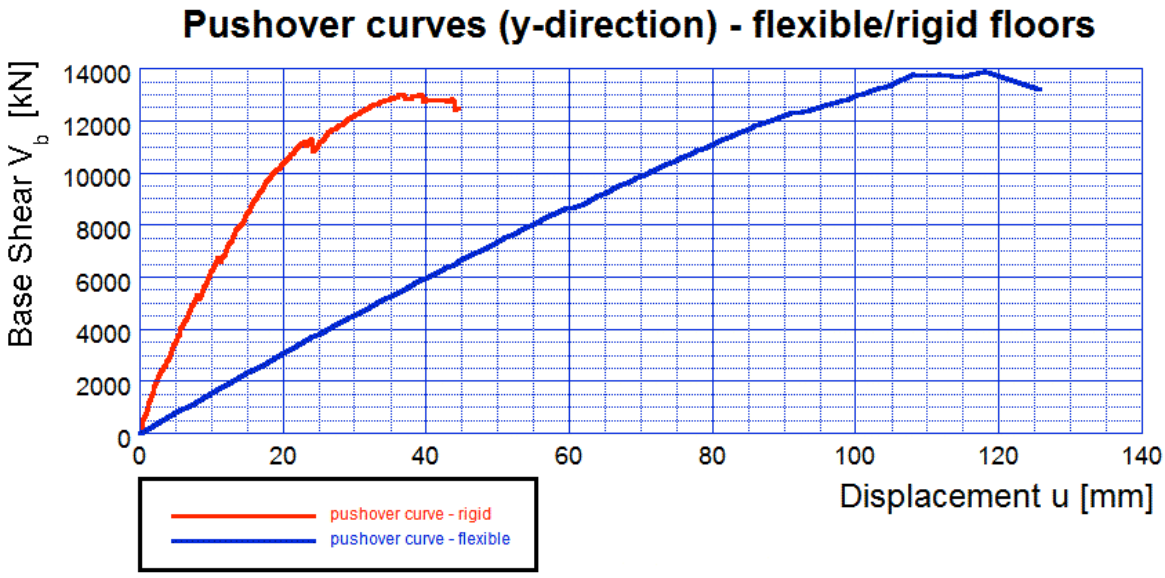


**Figure 6.22** Comparison of the pushover curve in the y-direction for the flexible and rigid model

In Table 6.4 the demands and capacities are summarized for the flexible and rigid model of the BHO-structure, based on the displacements of reference node 259. The demands are computed with the design response spectra in Figure 6.23. The spectral acceleration $S_a$ for each performance level is found in Figure 6.23 by using the correspondent first period of vibration and then by following the red arrows. By applying equations (5.10) and (5.25) the spectral displacement $S_d$ is found. Then, using the participation factor for the first period of vibration, given by 3Muri, the correspondent displacement value is obtained. Comparing the demands with the capacities it becomes clear that the demands can be satisfied by the BHO-structure. Only the manually modified capacity of the flexible structure in the x-direction is close to the demand. The verification is only performed for the real BHO-structure with the flexible floors. In the last column, the ultimate acceleration resistance is given. These values become important in the next chapter, where the local performance is investigated.

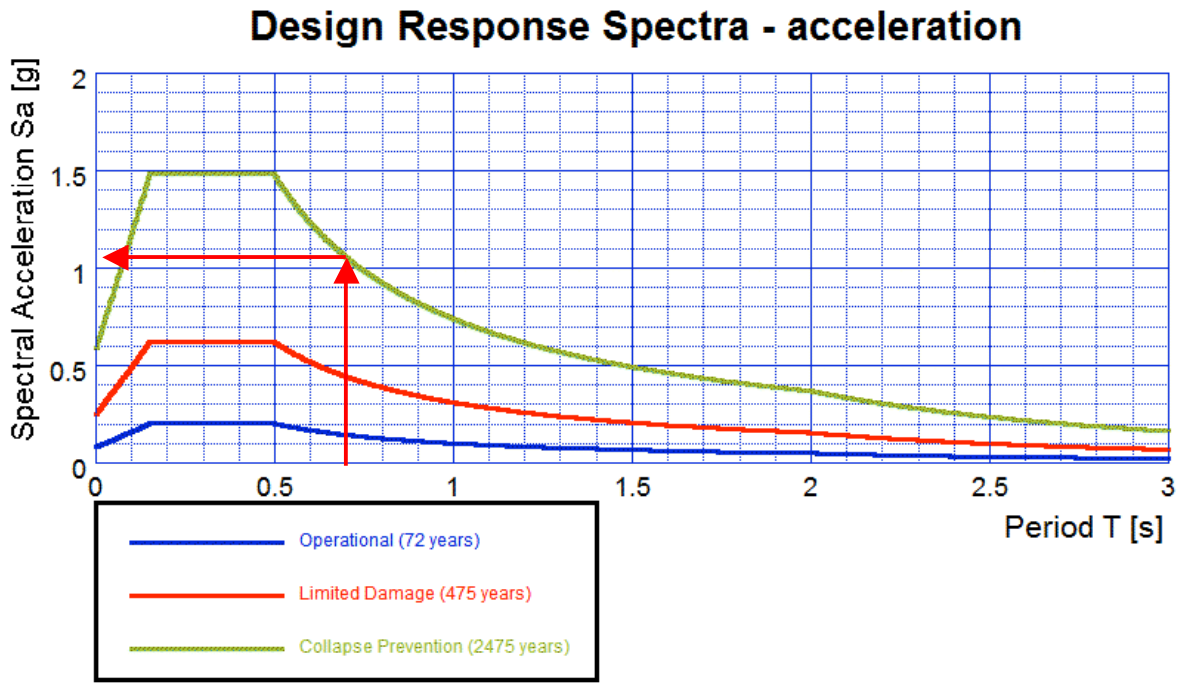


**Figure 6.23** Design response spectra for the BHO-structure in Bern

The first periods of vibration are for both, the flexible and rigid model under 1 second. For masonry structures low periods are common. Hence these values are realistic. The computation also shows lower first periods of vibration for the rigid model. This could be expected.

**Table 6.4** Demands and Capacities of the BHO-structure

| Reference node 259 | Period | Parti. Factor | Demands | | | Capacities | | Ult. acceleration resistance |
|---|---|---|---|---|---|---|---|---|
| | $T_1$ | $\Gamma_1$ | $u_{OP}$ | $u_{LD}$ | $u_{CP}$ | $\Delta_Y$ | $\Delta_{ult}$ | $a_{ULSPG}$ |
| | [s] | [-] | [mm] | [mm] | [mm] | [mm] | [mm] | [m/s2] |
| *flexible* | | | | | | | | |
| x-direction (1st mode) | 0.706 | 0.30 | 1.8 | 5.5 | 13.2 | 9.5 | 15.0 | 1.88 |
| y-direction (mass) | 0.614 | 1.57 | 1.6 | 4.9 | 11.6 | 224.9 | 256.7 | 7.01 |
| *rigid* | | | | | | | | |
| x-direction (1st mode) | 0.696 | 0.36 | 1.8 | 5.5 | 13.1 | 17.4 | 43.4 | 4.54 |
| y-direction (1st mode) | 0.600 | 1.36 | 1.5 | 4.7 | 11.3 | 22.5 | 44.5 | 1.44 |

### 6.3.3 Story Drifts

Story drifts are presented in Figure 6.24. They are computed in a conservative way, using the results of two analyses combinations in both, the x- and the y-direction. First the decisive analysis combination with the first-mode-of-vibration-horizontal-load-pattern is determined and then the decisive analysis with the mass-proportional-horizontal-load-pattern. For both analyses the story drifts are analyzed and for each floor the larger deformation is chosen (see Appendix E.1). These values are assembled and form the curves in Figures 6.24. In Tables 6.5 and 6.6 the values are shown. When story drifts are discussed, the story drifts are delivered in percent. The

yellow-marked columns show the displacements in the loading direction. For the model with flexible floors, the largest deformation is observed in the ground floor (EG) with 0.17% drift in the x-direction and a 0.5% drift in the y-direction. These values indicate a reduced stiffness on the ground floor and a potential soft-story behavior. However, the values are in an acceptable range. According to EC8-3, Chapter 4.3, the drift of a wall controlled by shear can be assumed to be 0.4% and for the performance level of near collapse even 0.53 %.

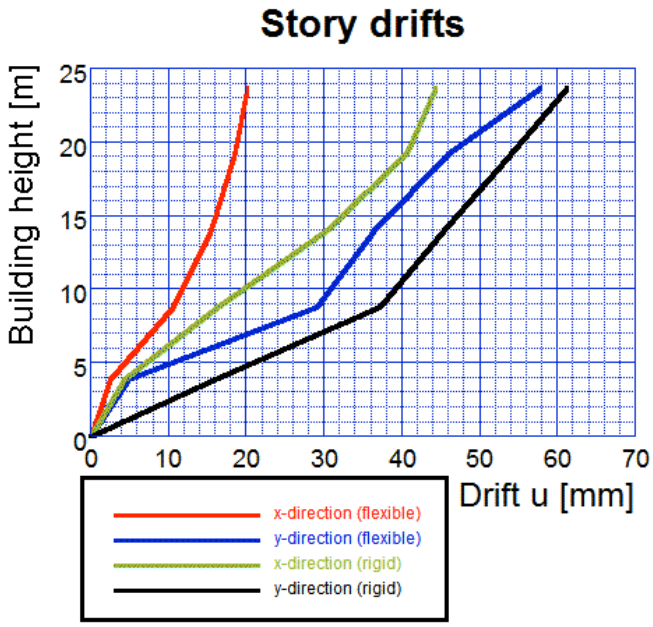


**Figure 6.24** Story drifts of the BHO-structure

**Table 6.5** Story drifts of the BHO-structure with flexible floors (nodes 60-64)

| **Flexible floors** | | | | | | | | |
|---|---|---|---|---|---|---|---|---|
| *loading in x-direction* | | | | | | | | |
| Floor | Node-Nr. | Storeyheight | Heigth | $\Delta_X$ | $\Delta_{X,ratio}$ | $u_X$ | $\Delta_Y$ | $\Delta_Z$ |
| [-] | [-] | [m] | [m] | [mm] | [%] | [mm] | [mm] | [mm] |
| - | - | 0.0 | 0.0 | 0.00 | 0.00 | 0.00 | 0.00 | 0.00 |
| TP | 60 | 3.9 | 3.9 | 2.43 | 0.06 | 2.43 | 0.40 | 1.43 |
| EG | 61 | 4.9 | 8.8 | 8.23 | 0.17 | 10.66 | 1.72 | 1.25 |
| 1.OG | 62 | 5.2 | 14.0 | 4.77 | 0.09 | 15.43 | 1.88 | 1.04 |
| 2.OG | 63 | 5.16 | 19.2 | 3.08 | 0.06 | 18.51 | 1.45 | 1.06 |
| 3.OG | 64 | 4.5 | 23.7 | 1.59 | 0.04 | 20.1 | 0.43 | 0.27 |
| *loading in y-direction* | | | | | | | | |
| Floor | Node-Nr. | Storeyheight | Heigth | $\Delta_X$ | $\Delta_Y$ | $\Delta_{Y,ratio}$ | $u_Y$ | $\Delta_Z$ |
| [-] | [-] | [m] | [m] | [mm] | [mm] | [%] | | [mm] |
| - | - | 0.0 | 0.0 | 0 | 0 | 0 | 0 | 0 |
| TP | 60 | 3.9 | 3.9 | 0.1 | 4.89 | 0.13 | 4.89 | 0.85 |
| EG | 61 | 4.9 | 8.8 | 0.45 | 24.26 | 0.50 | 29.15 | 1.04 |
| 1.OG | 62 | 5.2 | 14.0 | 0.74 | 7.34 | 0.14 | 36.49 | 0.83 |
| 2.OG | 63 | 5.16 | 19.2 | 1.05 | 9.52 | 0.18 | 46.01 | 0.92 |
| 3.OG | 64 | 4.5 | 23.7 | 0.67 | 11.75 | 0.26 | 57.76 | 0.32 |

The story drifts for the rigid structure in the x-direction are constantly larger than those of the flexible structure. This leads to a total top drift of 44 mm, which is twice as big as the top drift of the flexible structure. However, if the shapes of the drifts in the x-direction are compared in Figures 6.24, a similar shape is recognizable. Also the two curves showing the drifts in the y-direction seem to have a similar shape. The main difference can be found in the drift of the underground-floor (TP). The underground-floor-drift of the rigid structure is considerably larger than the one of the flexible structure. In Appendix E.1 it becomes clear that the considerably larger value derives from the analysis with the uniform mass-distribution pattern while the drift of the other floors is based on the first mode of vibration load-distribution.

**Table 6.6** Story drifts of the BHO-structure with rigid floors (nodes 60-64)

| **Rigid floors** | | | | | | | | |
|---|---|---|---|---|---|---|---|---|
| *loading in x-direction* | | | | | | | | |
| Floor | Node-Nr. | Storeyheight | Heigth | $\delta_X$ | $\Delta_{X,ratio}$ | $u_X$ | $\delta_Y$ | $\delta_Z$ |
| [-] | [-] | [m] | [m] | [mm] | [%] | [mm] | [mm] | [mm] |
| - | - | 0.0 | 0.0 | 0.00 | 0.00 | 0.00 | 0.00 | 0.00 |
| TP | 60 | 3.9 | 3.9 | 4.33 | 0.11 | 4.33 | 0.25 | 0.09 |
| EG | 61 | 4.9 | 8.8 | 12.07 | 0.25 | 16.4 | 1.17 | 0.52 |
| 1.OG | 62 | 5.2 | 14.0 | 13.9 | 0.27 | 30.3 | 1.12 | 0.71 |
| 2.OG | 63 | 5.16 | 19.2 | 10.28 | 0.20 | 40.58 | 0.19 | 1.31 |
| 3.OG | 64 | 4.5 | 23.7 | 3.77 | 0.08 | 44.35 | 0.35 | 0.22 |
| *loading in y-direction* | | | | | | | | |
| Floor | Node-Nr. | Storeyheight | Heigth | $\delta_X$ | $\delta_Y$ | $\Delta_{Y,ratio}$ | $u_Y$ | $\delta_Z$ |
| [-] | [-] | [m] | [m] | [mm] | [mm] | [%] | [mm] | [mm] |
| - | - | 0.0 | 0.0 | 0 | 0 | 0 | 0 | 0 |
| TP | 60 | 3.9 | 3.9 | 0.1 | 15.96 | 0.41 | 15.96 | 0.77 |
| EG | 61 | 4.9 | 8.8 | 0.23 | 21.21 | 0.43 | 37.17 | 0.75 |
| 1.OG | 62 | 5.2 | 14.0 | 0.27 | 8.27 | 0.16 | 45.44 | 0.6 |
| 2.OG | 63 | 5.16 | 19.2 | 0.19 | 8.6 | 0.17 | 54.04 | 0.22 |
| 3.OG | 64 | 4.5 | 23.7 | 0.74 | 7.19 | 0.16 | 61.23 | 0.14 |

## 6.4 Local Performance

3Muri offers a tool to investigate local mechanisms. As a condition, the model of the BHO-structure needs to be developed as defined in Chapter 5. Out-of-plane failure is rather difficult to analyze because the user is requested to define possible mechanisms. The program estimates the first period of vibration of the structure using the following, empirical equation, where H is equal to the building's height.

In Figure 6.26 the two analyzed walls of the BHO-structure are marked in yellow. From all the walls of the structure they appear to be the most exposed to an out-of-plane failure. The out-of-plane failure of the two outside-walls marked in orange color is prevented by the total BHO-structure and hence, they are not analyzed. Wall 1 and 4 are both analyzed starting with the top floor. Once the top floor is analyzed, the next floor below is additionally considered, until the whole wall is investigated (see Figure 6.25).

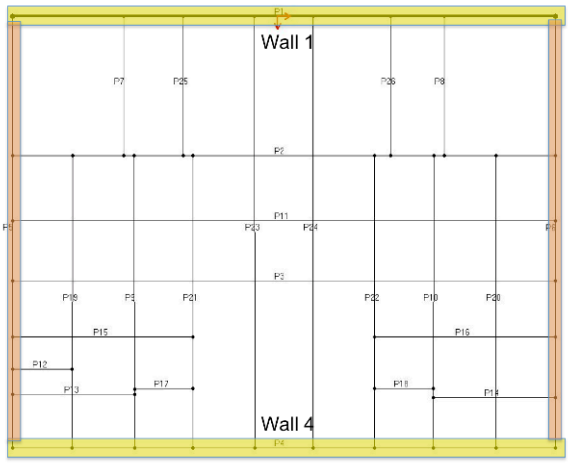


**Figure 6.26:** Ground plan pointing out Wall 1 and 4

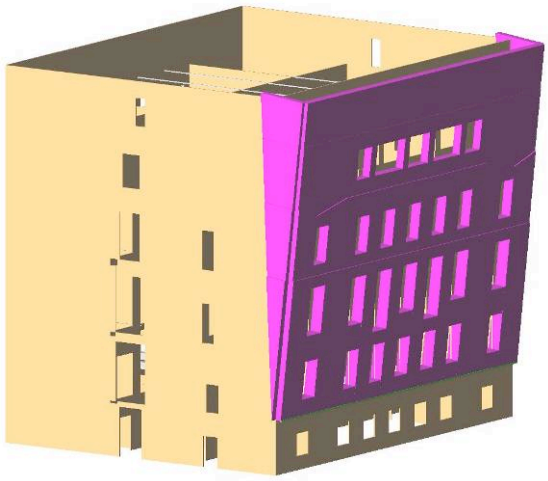

**Figure 6.25:** 3D-model of local mechanism

The user needs to select the resistance-check of interest. He has two options. First, he can conduct a land-constraint-check, which verifies a single element or portion of the building that rests on the ground. Therefore equation (6.7) is applied. Secondly, the user can perform a quote-constraint-check, where a local mechanism is analyzed at a certain quote over the ground. This check is based on equation (6.8). Therefore an estimation of the first period and mode of vibration, based on equation (6.5) and equation (6.6), are required. As user-defined wall-block can be performed based on the following two equations (6.6) and (6.7):

$$T_1 = 0.005 \cdot H^{3/4} \tag{6.5}$$

$$\Psi = \frac{Z}{H} \tag{6.6}$$

$H$ is equal to the building's height and $Z$ is the height, compared to the foundation of the building. $Z$ is not exactly described in the user manual of 3Muri [25].

$$a^*_{0-\min} = \frac{a_{gd} \cdot S}{q} \tag{6.7}$$

$$a^*_{0-\min} = \frac{S_e(T_1) \cdot \Psi(Z) \cdot \gamma}{q} \tag{6.8}$$

$a^*_{0-\min}$: The spectral seismic acceleration of the activation of the mechanism

$a_g$: Function of the probability of exceeding the selected Limit State

$S$: Coefficient taking into account the soil type and the topographical conditions

$q$: Structure factor

$S_e(T_1)$: Value, based on elastic spectrum in accordance with the selected Limit State

$\Psi(Z)$: First vibration mode
$\gamma$: Modal coefficient participation

In Table 6.7, the achieved resistance of the different out-of-plane mechanisms investigated on Wall 1 and 4 are presented. For the walls both the land constraint and quote constraint is computed. Only for the base floor TP the land constraint is relevant. For the other mechanism the quote constraint is of relevance. All the analyzed mechanisms show enough resistance against the estimated action. The resistance of the underground floor is not investigated for the Wall 4 because this wall lies below the ground level on this side of the building. The definitions of the single mechanisms can be found in Appendix E.2.

The action resistances of the local mechanisms, expressed in terms of acceleration, are supposed to amount lower then the maximal acceleration resistance of the global performance. In Table 6.4 the ultimate acceleration resistance of the global performance evaluation can be found. Comparing these values with those of the local performance evaluation proves this expectation correct.

**Table 6.7** Results for the investigated Walls 1 and 4 of the BHO-structure concerning out-of-plane failure

| **Wall 1** | Land constraint | | Quote constraint | |
|---|---|---|---|---|
| | resistance | action | resistance | action |
| Floor | [m/s$^2$] | [m/s$^2$] | [m/s$^2$] | [m/s$^2$] |
| 4.OG | 1.38 | 0.43 | 1.38 | 1.12 |
| 3.OG | 0.94 | 0.43 | 0.94 | 0.9 |
| 2.OG | 0.75 | 0.43 | 0.75 | 0.66 |
| 1.OG | 0.64 | 0.43 | 0.64 | 0.42 |
| EG | 0.53 | 0.43 | 0.53 | 0.19 |
| TP | 0.52 | 0.43 | - | - |
| **Wall 4** | Land constraint | | Quote constraint | |
| | resistance | action | resistance | action |
| Floor | [m/s$^2$] | [m/s$^2$] | [m/s$^2$] | [m/s$^2$] |
| 4.OG | 1.38 | 0.43 | 1.38 | 1.12 |
| 3.OG | 0.94 | 0.43 | 0.94 | 0.9 |
| 2.OG | 0.67 | 0.43 | 0.67 | 0.66 |
| 1.OG | 0.44 | 0.43 | 0.44 | 0.42 |
| EG | 0.54 | 0.43 | - | - |
| TP | - | - | - | - |

The global evaluation in the previous chapter showed a diaphragm deflection on the third floor for the flexible model with loading in the y-direction. Thus, a local evaluation is performed for this section of the Wall 1.

Figures 6.27 and 6.28 visualize the analyzed section.

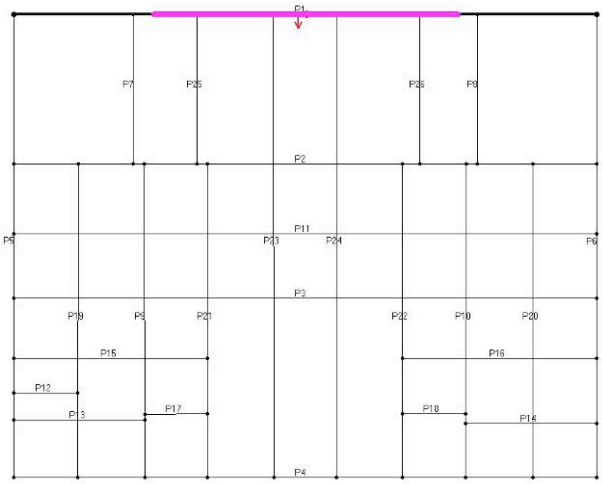

**Figure 6.28:** Floor plan showing the analyzed section

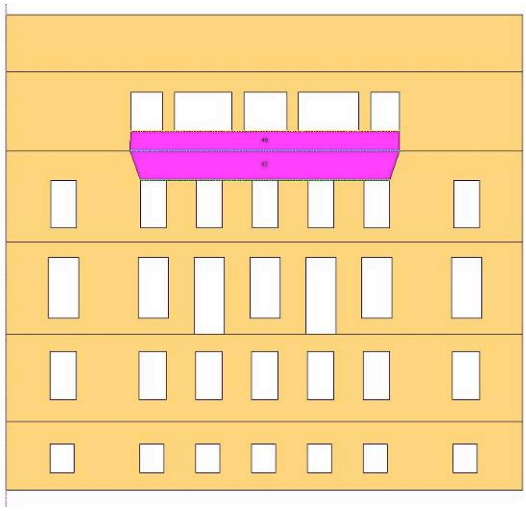

**Figure 6.27** Front view of the wall showing the analyzed section

The analysis results in a resistance acceleration amounting to 6.19 m/s$^2$ against an action of 0.9 m/s$^2$. This resistance acceleration is rather high but still lower than the ultimate acceleration resistance of the global evaluation of 7 m/s$^2$ according to Table 6.4. Figure 6.29 shows the local collapse mechanism. Apparently the diaphragm deflection is not caused by a local collapse but rather by the horizontal loads, acting from the third floor components.

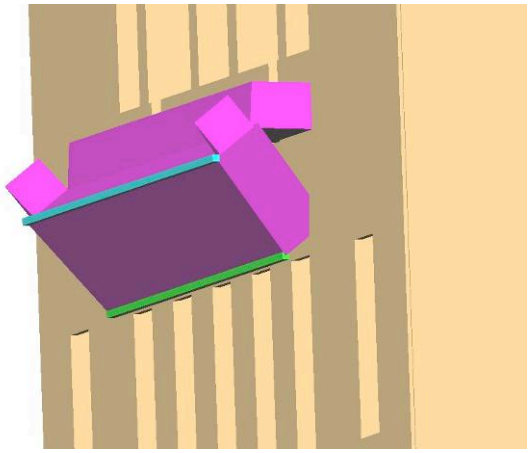

**Figure 6.29** Local collapse mechanism for section on the third floor

## 6.5 Conclusion

The global analysis shows that the BHO-structure satisfies the design requirements concerning the global performance under seismic loading. However, the BHO-structure shows a large deformation in the y-direction, while reaching the yield base shear. In order to reduce the displacement an improvement of the diaphragms could help obtain a better building integrity. It is also questionable if all the timber floors, which are immured about 24 cm deep in the walls would still remain there with deformations of over 25 cm in the third floor, where the diaphragm deflection occurs. The walls that are connected with these floors would need to move rather equally. In order to ensure their connection to the walls, it would be reasonable to create better connections between the walls and the ceilings. The other thing to do is to create stiffer floors, especially in the third floor. This way the floor deflection can be reduced.

The BHO-structure satisfies all the response requirements according to the 3Muri calculation. However, it is rather difficult do know how reliable the results are. The results are based on a model, which is based on masonry parameters according to code provisions and assumptions. It would be interesting to run the same model with the masonry parameters from the ongoing material survey of the BHO-structure. Further it would be helpful to compute by hand the shear capacity and first period of vibration of some single walls.

Since the stiffness of the floors have quite an influence on the response of the structure, especially concerning the nonlinear behavior, a more detailed knowledge of the floor-compositions would be helpful. This way, they could be modeled in 3Muri more close to the reality and improve the reliability of the responses.

Another point that may diminish the reliability of the results is the lack of 3Muri to compute the changes of the connections of the diaphragms to the wall structures, while the lateral loads are increased monotonically. The floors are inserted in 3Muri with a specific stiffness and some options in order to respect the type of connection exist as well.

If the structure would fail to satisfy the response requirements, several measurements exist in order to improve its behavior. They vary from strengthening masonry walls over strengthening diaphragms and improvements of the structural integrity. A reason for a poor seismic behavior of a building may also be a bad foundation. In this case an improvement of the foundation may be required. Further, damage to non-structural elements often presents a large portion of the overall building damage. Nevertheless, this aspect of BHO performance was not considered in this study.

## 6.6 Strengthening of Masonry Structures

Depending on the buildings earthquake resistance, a strengthening may be required. This chapter introduces ways of strengthening of masonry structures based on the explanations according to Tomazevic [21]. There are also other methods of strengthening existing that are not mentioned by Tomazevic.

### 6.6.1 Methods of Strengthening of Masonry Walls

For stone-masonry, an efficient intervention is simply injecting the grout into the void parts of the walls. However, for brick- and block-masonry walls, there are several ways of strengthening available.

**Crack Repairs**

For brick and block masonry, the buildings resistance may be improved by sealing existing cracks. If the cracks width is about 1 cm, they can be sealed with mortar. However, if the width is larger than 1 cm, it may be necessary to reconstruct the

damaged part. In the case of thin cracks under 1 mm, epoxy can be injected. Often cement grouts are preferred, since they are less expensive compared to the effectiveness. For cracks between 5 and 10 mm, fine sand can be added to the grouting mixture existing out of 90% Portland cement and 10% Pozzolana. Experiments have shown that injecting the cracks with cement or epoxy grout can even improve the original load-bearing capacity of the walls in case of poor quality masonry. However, the rigidity is mostly not improved and conservators may not be satisfied with solutions existing out of cement or epoxy.

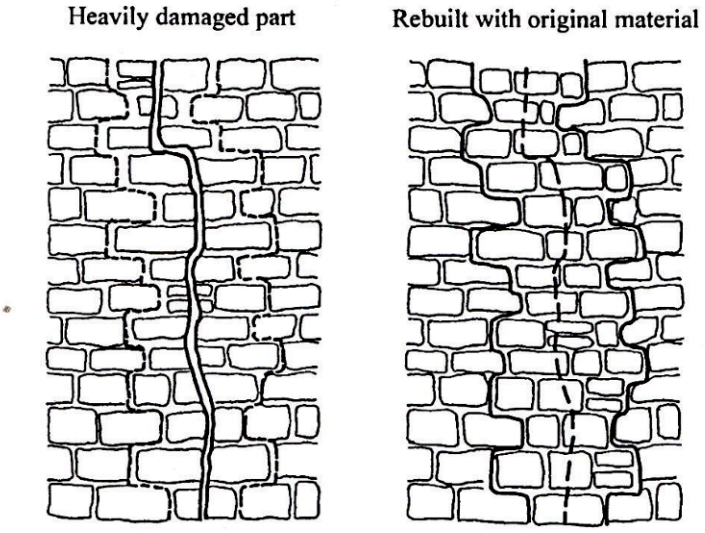


**Figure 6.30** Reconstruction of the central part of a heavily cracked stone-masonry wall [21]

For stone-masonry walls, in contrast, reconstruction of parts or complete walls is often necessary, where severe cracks are found in the middle parts of the wall. For a reconstruction original material should be used in order to maintain the integrity of the wall. If for instance a damaged part is replaced with concrete, the concrete part may be responsible for the damage of neighboring masonry during a future earthquake event [21].

### Repointing

Under repointing an improvement of the wall resistance against vertical and horizontal loading is understood, where a part of the existing poor mortar is replaced with mortar of significantly better quality such as cement mortar. On one or both sides of the wall the mortar is removed up to approximately 1/3 of the wall's thickness (see Figure 6.32) [21].

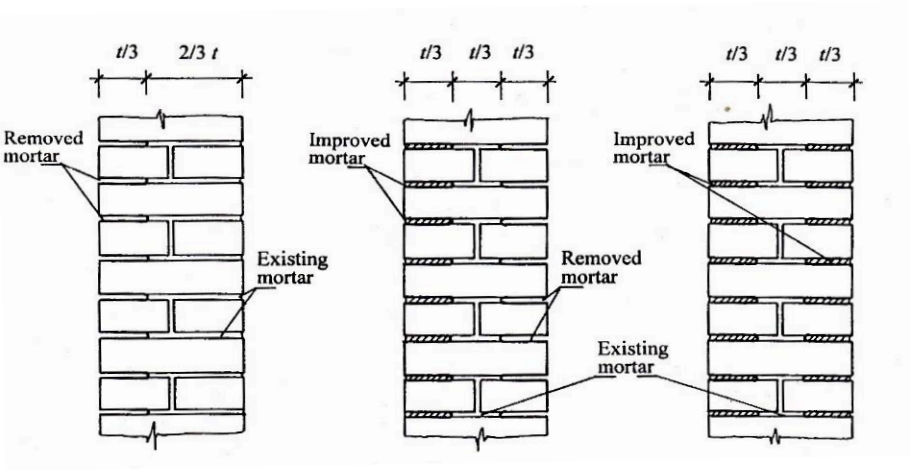


**Figure 6.31** Repointing of a brick-masonry wall [21]

### Reinforced-cement Coating

This is a useful method for seriously damaged brick- and block-masonry walls as well as for strengthening existing structures. The lateral resistance is improved by applying reinforced-cement coating on one or both sides of the wall. It is easy to apply and quite efficient. There have been studies about the possibilities of using ferro-cement or carbon fiber coating instead of reinforcing steel [21].

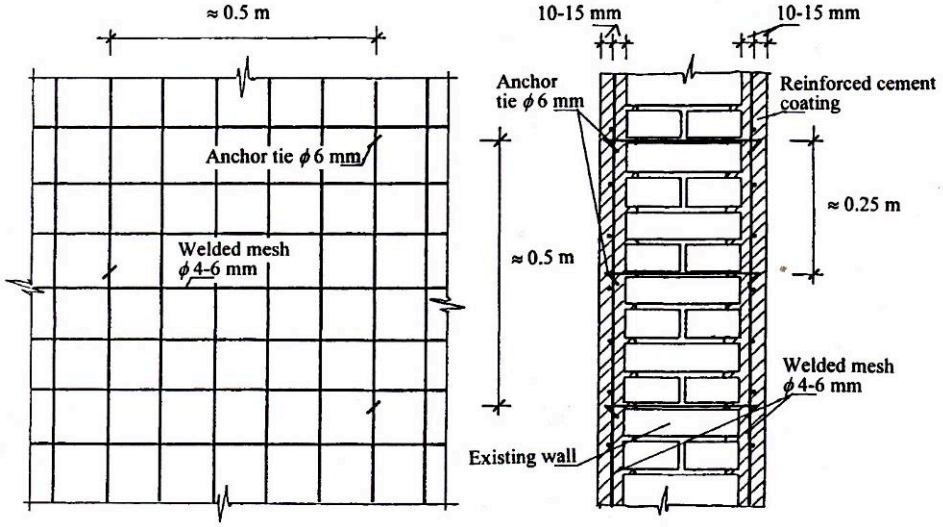


**Figure 6.32** Application of r.c. coating to brick-masonry walls [21]

### Grouting

Existent stone and mixed stone-and-brick masonry often have two outer leaves of uncoursed stones and an inner infill of smaller pieces of stones. Further a poor-quality lime mortar is used as bonding material. Therefore many voids are distributed over the walls. Obviously, systematically injecting cementitious grout is an efficient method of strengthening. Unfortunately, only a limited number of laboratory and in situ tests have been performed so far. Hence, values of basic parameters of cement-grouted masonry walls are combined with uncertainties.

One of the main advantages of this intervention is its invisibility. Therefore it is ideal for historical structures, where principles of preservation and restoration should be regarded. If applied, the effect of cement on traditional masonry, caused by impurities of the cement, which dissolve in the water and may cause damage to decorations, should be considered. However, it is believed that the composition of the grout mix can be designed for each particular type of masonry and therefore each specific problem of this type can be solved [21].

**Prestressing**

By prestressing the wall in vertical or horizontal direction, the shear resistance of the wall can be improved, since the principal tensile stress is a function of the stress state in the wall. Many types of prestressing are existent and can be applied [21].

**Reconstruction**

If a brick- or stone-masonry wall is heavily damaged, it may be necessary to reconstruct that section of the wall. In such a situation, it is important to carefully remove the old masonry in order to prevent additional damage. The reconstruction material should be of improved quality, but needs to be compatible with the original masonry. Further the unit-dimension should match the original dimensions.

Reconstruction is often required for stone-masonry, where a layer has bulged excessively or collapsed. In order to avoid bulged walls to collapse, it may be helpful to use transverse connectors and with steel profiles the wall can be placed in its original position. Then, after grouting, the steel profiles can be removed. However, the transverse connectors are left in the wall to prevent future bulging [21].

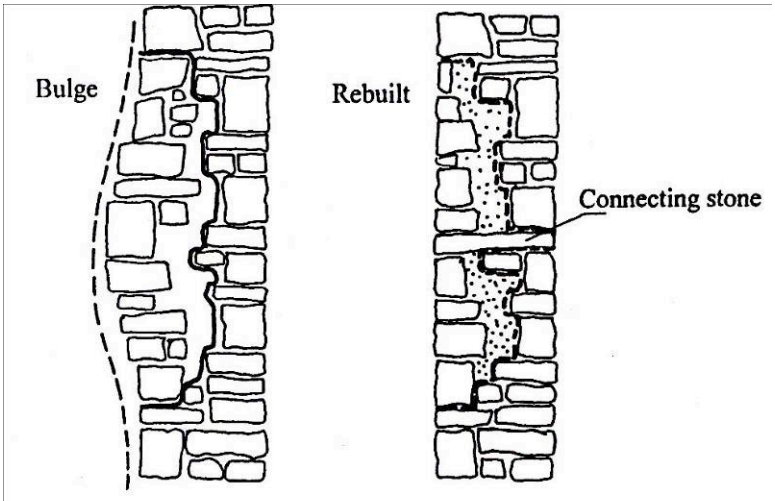


**Figure 6.33** Reconstruction of a bulged stone-masonry wall [21]

## 6.6.2 Methods of Improving Structural Integrity

Next to strengthening individual structural components such as single walls it may be more efficient to study and improve the structural integrity. The structural integrity can be improved with the following methods.

### Tying of Walls with Steel Ties

Steel or wooden ties have been known as improvements for structural integrity for centuries. Observations on ties applied in old masonry buildings have shown a significant improvement of the earthquake resistance. Steel ties are usually inserted immediately under the floor structure. Therefore usual reinforcing steel bars are used. Threading them at the ends allows them to be bolted to steel anchor plates at the ends of the walls.

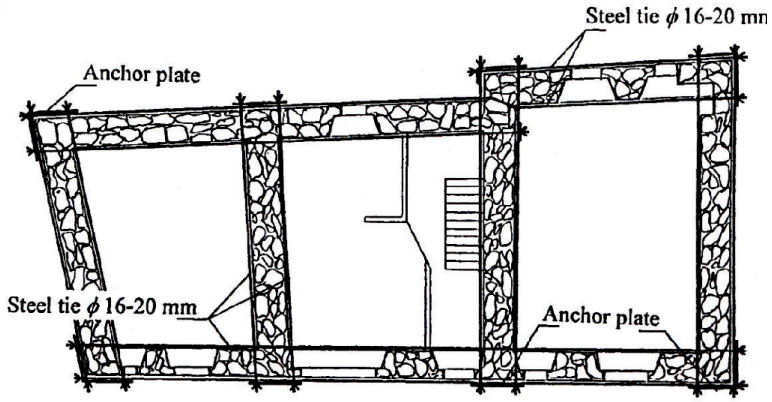


**Figure 6.34** Position of steel ties in plan of a rural stone-masonry house [21]

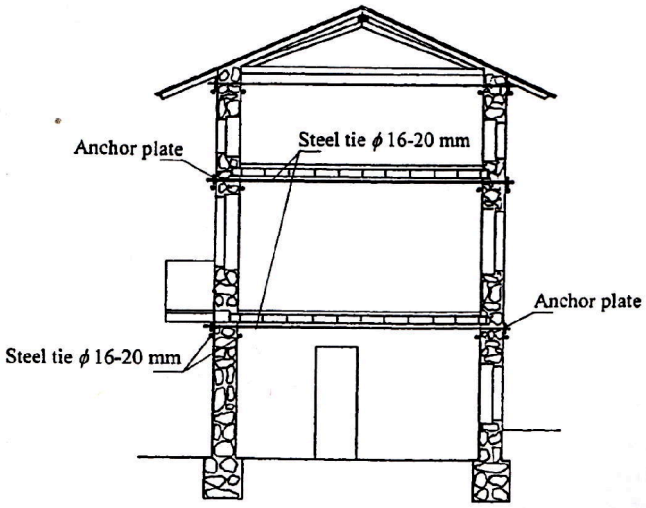


**Figure 6.35** Position of steel ties in elevation of a rural stone-masonry house [21]

If they are applied in historical buildings, they are placed in carefully cut notches in the walls and after installment the notches are filled with the bricks and stones at their original position. This way the intervention is invisible [21].

### Interventions in Floor Structures and Roofs

Another way to improve the structural integrity is to improve the horizontal diaphragm action and the connections of the horizontal diaphragms to the structural walls. As a matter of fact, this is one of the main reasons for the poor seismic behavior of existing masonry buildings. New masonry buildings should have a r.c. tie-beam provided along the structural walls at each story level. Then, tie-beams should connect the floor to the walls and provide a monolithic behaving structural system. Rigid floor diaphragms and tie-beams prevent possible out-of-plane collapse mechanisms. Often timber floors are replaced by reinforced concrete or prefabricated slabs. However, this measure provoked a large number of failure of old buildings in L'Aquilla. Another way to reinforce timber floors is by using steel ties. The bond-beams of timber floors that do not pass entirely over the section of the walls should be connected together and anchored to the walls. They should be immured at least 15 cm deep into the supporting wall [21].

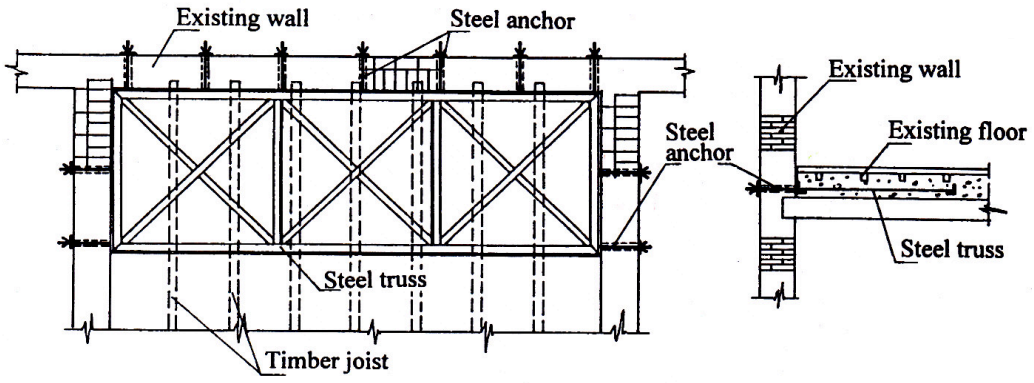


**Figure 6.36** Bracing of a large-span wooden floor with metallic truss [21]

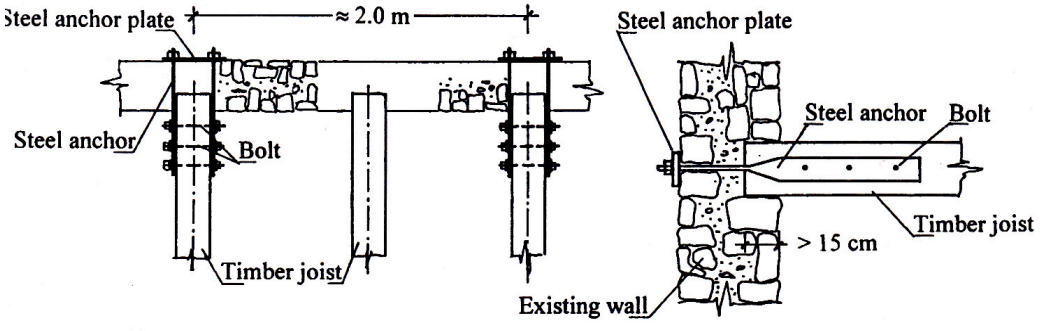


**Figure 6.37** Detail of anchoring of a wooden floor into a stone-masonry wall [21]

### Repair of Corners and Wall Intersection Zones

Corners and wall intersection zones are constantly heavily damaged during earthquakes. Therefore, damaged corners need frequently strengthening. Sometimes stitching is the method applied for stone or metal. Next to stitching, vertical confining elements are used for brick-masonry structures. Alternatively, steel strips welded to anchor plates at the outside ends can be used [21].

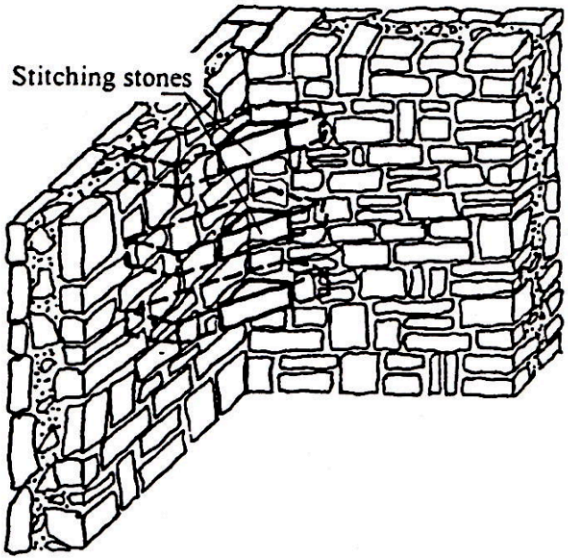


**Figure 6.38** Strengthening of the corner zone of a stone-masonry wall with stone stitching [21]

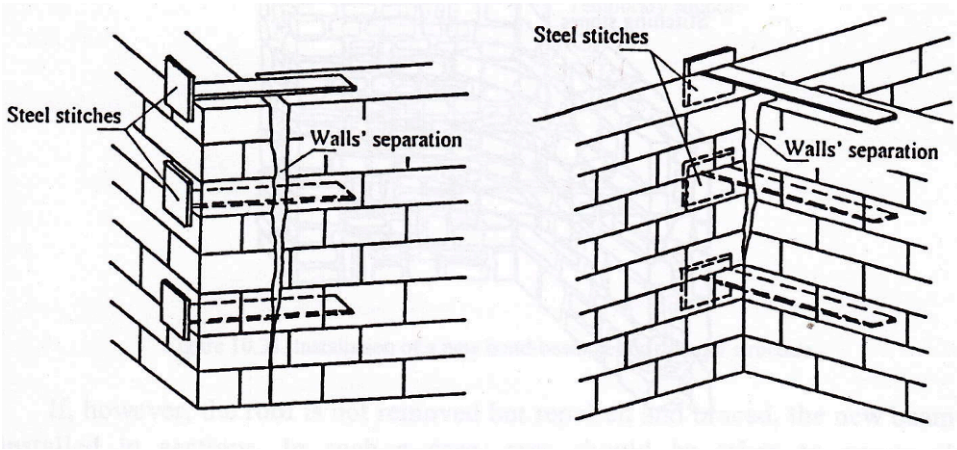


**Figure 6.39** Strengthening of the corner zone of a stone-masonry wall with metal stitching [21]

### Strengthening of Walls by Confinement

The resistance capacity of a masonry structure can be improved significantly by confining plain masonry walls with vertical confining elements, which are placed at all corners and wall intersections. Further they should be placed along vertical borders of large wall openings. This way the structural integrity is improved. Unfortunately, not all buildings are appropriate for installing tie-columns. Rigid floors and horizontal r.c. tie-beams should already exist in the masonry building.

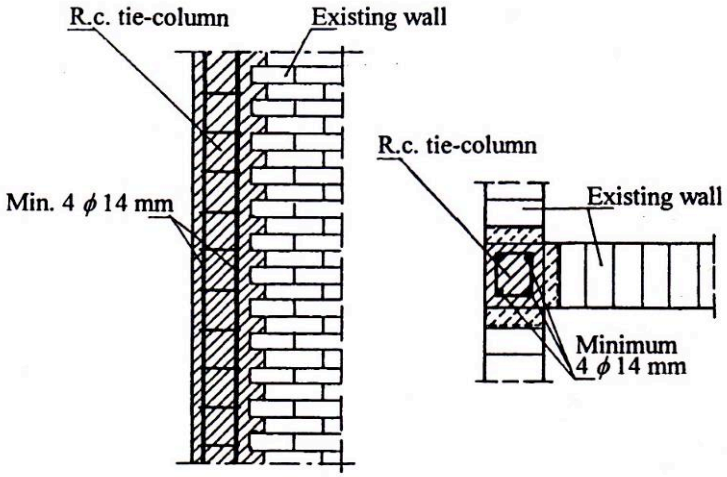


**Figure 6.40** Placement of new tie-columns in a brick-masonry wall [21]

In case of stone-masonry buildings, it is not recommended to strengthen the walls with r.c. tie-columns. In general, for the critical zones such as corners and wall intersections the masons used larger and frequently cut stones to connect both leaves and therefore they form the best parts of the structure [21].

### 6.6.3 Foundation

In some cases, the foundation or ground failure may cause severe damage or even the collapse of a building under earthquake forces. However, existing foundations are rarely the reason for bad behavior of existing masonry buildings during earthquakes. More probably is a damage of masonry walls due to soil phenomena, such as liquefaction or soil sliding, which cause differential settlements, tilting and sinking of the building. These phenomena can be avoided with adequate geotechnical measures.

If interventions are required in the foundation it is mostly because of too excessive vertical loading or washing out of subsoil due to inadequate maintenance of the building's drainage system. Another reason is the deterioration of foundation systems, which are based on wooden piles, due to the effects of time [21].

### 6.6.4 Non-Structural Elements

Non-structural elements such as chimneys, attics and ornamentations do normally not influence the seismic resistance of a structure. Nevertheless the collapse of these non-structural elements can damage structural elements or cause the loss of lives. Therefore non-structural elements should be properly secured [21].

# 7 Pilot Guideline for Seismic Evaluation of Historic Masonry Building Structures

This chapter discusses the evaluation steps used in this dissertation. They are presented in terms of a list. In each step the important tasks are pointed out. The idea of this list is that it could be used as guidance for further evaluations of existing masonry structures. Chapter 7.2 discusses some alternatives.

## 7.1 Proposed Evaluation Procedure

The evaluation can be divided into four phases. In Phase A the survey of the building is carried out, including all tasks performed to gain information about the structure of relevance. In Phase B a numerical program is selected and the structure of relevance is modeled. This also includes the process of getting familiar with the software. Following, the evaluation process starts, described with Phase C. In this stage, the achieved performance of the structure of relevance is analyzed and compared with the expected and required performance. If the performance is not satisfactory, Phase D follows suggesting measures of improvement.

### A. Survey of the Building

#### 1. Seismic Properties of the Building of Relevance

It is helpful to collect the seismic site information of the building of relevance at the beginning. This way, the design professional knows from the beginning with which seismic properties he is dealing with. As visible in Chapter 3.1 these seismic properties consist out of the seismic zone, the ground class defining the soil on which the building stands and the importance class, which describes the importance of the structure. With the knowledge of the ground class, the seismic parameters $S$, $T_B$, $T_C$ and $T_D$ can be found using the correspondent code. Next to the seismic properties based on the codes, it is also useful to seek for possible local earthquake events that may be found in historical records or in national papers handling these matters. They can help to understand the local situation.

#### 2. Geometrical Properties

The knowledge of the geometrical properties is of great importance for a successful analysis. Ideally, the original plans of construction of the building as well as plans of any structural modifications can be found. These old plans can also include useful structural information. However, old plans have to be verified on-site since they may not correspond to the actual situation anymore. If no plans are available, as it was the case for

the BHO-structure, it becomes necessary to create new geometrical plans of the structure even though this is rather time-consuming. They are created by collecting the correspondent information during site visits. Thanks to the ongoing renovation of the BHO-structure, an architectural office already created geometrical plans. This way the plans of the building permit were available for the purpose of the seismic performance evaluation of this work as explained in Chapter 3.2.

**3. Structural Properties**

For a structural analysis, the structural properties are required. Therefore original plans of construction and modifications are very useful. It is one of the most difficult tasks to completely understand the load-carrying system of an old, existing structure. Thus, studying the available documents may not give enough understanding of the structural composition of the building and further measures are required in order to obtain a higher knowledge level. Often, more detailed information about connections between floors and walls or between different walls are required. As explained in Chapter 3.4, knowledge of the composition of floors and their connections is of great importance in respect to their rigidity and to the general performance of the building. Since these parts are mostly hidden, it can be rather challenging to obtain this information. It may be necessary to apply some of NDT (Non Destructive Tests), MDT (Minor Destructive Tests) or DT (Destructive Tests). The chosen measures need to stand in relation with their benefit.

Another issue is to understand the foundation and the soil quality. In some cases the foundation or soil phenomena may be the reason for severe damage of the structure during an earthquake. Historical reports may help to figure out if such phenomena occurred in the region.

In order to create in a later phase a qualitative numerical model of the building's structure, the structural components of the real structure need to be understood (see Chapter 5.3).

Further, the vertical loads should be computed in this step. The dead loads can be computed based on the composition of the floors and walls. To calculate the live loads the use of the different rooms is required.

**4. Mechanical Properties**

Once the structural components are known, the mechanical properties of the used materials need to be defined. There are two ways to define material characteristics if the necessary information of the used materials is lacking. The first way is to estimate the required values based on the experience of similar cases or using recommendations described in codes.

The second way is to perform an experimental investigation. For the BHO-structure the definition of the masonry parameters was challenging. As visible in Chapter 3.5, the masonry characteristics are estimated using provisions described in Eurocode and Swisscode. Many of these formulas are empirical. However, if possible and economically responsible, the second way should be applied, since it delivers more certainty and therewith a higher knowledge level. A good knowledge of the mechanical properties of the materials is of great importance as it is essential for the performance of the structure. Changing the mechanical properties in a later step of the simulation will show that the results change in a rather sensitive way.

**5. Site Visit**

For the evaluation of an old existing building it is necessary to conduct a site visit. As explained in the previous steps, more then one site visit may be required. Connected with step 2 it is at least necessary to verify the available plans of the building on their actuality. If no plans are available several site visits are required in order to create new ones. To understand the structural components and their connections site visits may also be necessary as described in step 3. Then, as discussed in step 4 it is recommended to perform experimental investigations in order to obtain material characteristics such as the characteristic compression strength of masonry. Unless the precise composition of the masonry walls is explained in the present data, the arrangement of the masonry units, their seizes and the dimensions of the bed and head joints need to be studied during a site visit. These knowledge is required if code provisions are applied (see Chapter 3.5). For the purpose of this dissertation only one site visit was performed. As seen in Chapter 3.6 it served to verify the received data. Further, additional information was collected that could not be discovered by studying the plans, e.g. the vaulted openings in the walls between the stairs (see Figure 3.3).

In order to be efficient during the site visit, it is important to study the collected data in advance. Then, an outlet containing the uncertainties and details of further interest should be created. On the site visit this outline serves as guidance. The site visit may also reveal differences between the received data and the real situation. Moreover, unexpected situations may show up.

Having some general knowledge of the surroundings of the building is also important. Sometimes, they can cause difficulties that could not be discovered by studying the received data of the building of relevance, e.g. the accessibility to the building site.

## B. Numerical Simulation

### 1. Choice of Numerical Software

There are multiple programs available on the market, which include tools for seismic analysis. For the purpose of this dissertation, the 3Muri software was selected. As explained in Chapter 5.1, 3Muri is a numerical computation program created for the seismic analysis of masonry structures. Further it has, next to Eurocode and Italian code, also Swisscode implemented. Hence, it seemed appropriate for the purpose of the seismic performance evaluation of the BHO-structure. The program delivers deformation-based results with a capacity curve of the structure.

### 2. Verification

A program needs to be verified, especially if used for the first time. The user needs to get familiar with the software. A good way is to conduct test computations on simple structures. They can be verified with some hand calculations. Simple structures offer good opportunities to vary single parameters and to test their sensitivity. In Chapter 5.2 a simple test structure is defined. Then, a simple analysis is performed using the equivalent lateral force method and the response spectrum method. Additionally, a hand-calculated pushover curve is computed. This hand-calculated pushover curve is ideal for comparing with the pushover curve computed by 3Muri.

### 3. Development of a Model of the Structure of Relevance

Once the verification phase is concluded, the development of the structure of relevance starts. The development of a multiple-story structure can be time-consuming if the stories contain different elements. As experienced while modeling the BHO-structure, small mistakes may later cause the program to crash (see Chapter 5.3). Therefore it is important to develop the structure in multiple steps and to test after each step if the simulation still works. This allows to directly identify new problems and to find solutions.

As explained in Phase A under structural properties, the structural components need to be known in advance. The user may be forced to make some simplifications while developing the model, which is easier if the structural system is understood.

Further, there may some modifications be required because of the limits of the program. During the development of the BHO-structure for example, some windows in the staircase needed to be moved upwards to the next story-level because there would be two windows located over each other in

the same story-level (see first floor in Figure 5.11). But this is something the program refuses.

After the model is developed, the vertical loads of the floors need to be added. Ideally, they are already calculated and summarized in Phase A, step 3. This accelerates the model-developing process.

## C. Evaluation

### 1. Computation of Demands

In order to verify the obtained capacities of the evaluation, the required demands need to be computed. The simplest way is to use the seismic design code. Therefore the seismic properties defined in Phase A, step 1, are required. With these parameters, a design response spectrum can be computed using the correspondent formulas of the code.

A more precise way to compute the demands is to use the UHS for the corresponded region. With the UHS the desired demands can be computed using FEMA 750 [31]. Therefore the spectral acceleration values are required for the natural periods of 0.2 s and 1 s.

If less precision is allowed, the demand can be computed as shown in Chapter 6.1. For the natural period of one second, the spectral accelerations are obtained from the UHS for the requested performance levels. Then, these values are used as the constant $S$ in SIA 261 in order to compute the seismic design spectra.

Eventually, the demand capacities obtained with the seismic design spectra need to be transformed into the same scale as the achieved response capacities delivered by 3Muri. This transformation occurs by using the participation factor as shown in Chapter 6.3. Once this is done, the capacities can be compared with each other.

### 2. Local Evaluation

3Muri offers a tool to investigate local failure mechanisms. With this tool the out-of-plane behavior can be investigated. It is rather difficult to suggest detailed or realistic out-of-plane mechanisms. Maybe some cracks are known from the site visit, which may indicate weak sections. Furthermore, an experienced design professional may be able to predict realistic failure mechanisms. Another way is to investigate in general the façade walls of the building as performed in Chapter 6.4. Based on the global evaluation an additional mechanism is investigated in the third floor, where the diaphragm deflection could be found. In general, the local evaluation should occur before the global one. If a structure collapses

already under local mechanisms, the benefit of a global evaluation is limited.

## 3. Global Evaluation

The general performance of the building is investigated with a global analysis. Unlike in this dissertation, the global evaluation should be carried out after the local evaluation. With 3Muri, 24 pushover curves are delivered for all 24 analyses combinations described in Chapter 5.1.4. 3Muri marks the decisive analysis combination in the x- and y-direction with a yellow bar (see Appendix E). However, it is necessary to verify them. As in Chapter 6.2, the ultimate displacement needs eventually to be redefined manually once a certain damage of the building is achieved. The front façade of the BHO-structure collapses for example long before the reference point reaches its ultimate displacement. Thus, the ultimate displacement of the structure needs to be manually redefined. This manual verification of the collapse mechanisms needs to be done for all relevant analysis combinations. Until then, it is not always clear which analysis combination that is relevant. Then, the achieved displacement capacity of the relevant combination needs to be verified with the correspondent displacement demands in order to check if the buildings performance satisfies its requirements according to the performance levels.

At this point it may be of interest to compute the story drifts. In 3Muri the displacements can be found for each node during every time-step. The comparison of the displacements between the single floors requires the existence of reference nodes at the same location in each floor (such as nodes 60-64 in Figure 6.4). By subtracting the displacement of the lower story from the displacement of the higher one, the drift is obtained. Figure 6.24 visualizes the accumulated story drifts.

Studying the global performance may help find critical sections of the structure, which may be of interest for a local analysis. This way the potential local collapse mechanism of the third floor, visible in Figure 6.29, was found and investigated.

In addition to the global evaluation of the structure it could be of interest to create a rigid-floor model of the structure as in Chapter 6.3. The evaluation of a rigid-floor model may help to understand the influence and effect of the rigidity of the floors on the global performance of the structure. Eventually, it may show that a relatively small improvement of the floor-stiffness might improve the global performance considerably.

**D. Measures of Improvement**

If a structure requires improvement, there are numerous methods. They can generally be divided into the following groups: strengthening masonry walls, improving structural integrity, foundation and non-structural elements.

The analysis of the BHO-structure has shown that there are no serious improvements required. However, if an old structure undergoes a renovation, it may be reasonable to investigate those components that collapsed first with the pushover curve in detail. This way the structure might still be improved.

In order to figure out the requested degree of improvement so that the structure satisfies the required performance, it may be useful to develop a new numerical model of the structure, which includes the improvements. This way the effect of the improvements can be investigated and compared to the original structure.

Generally, tying of the structure is always recommended as well as improving details and connections.

## 7.2 Alternatives

Alternatively to the here presented evaluation method, an old masonry building could be analyzed according to standard SIA 2018. However, this standard does not specify very detailed how to analyze such a structure. In SIA D0237, two examples show the use of SIA 2018. Another way would be to analyze a structure strictly using EC8. This way the advantages of the Eurocode in relation to Swisscode could be considered. Especially the use of knowledge levels and performance levels is explained in this code. In any case EC8 is probably needed if standard SIA 2018 is used. Standard SIA 2018 states that for the analysis of a masonry structure with a deformation-based method, SIA 266 and EC8 should be applied.

Most important is to define at the beginning of an evaluation how detailed a structure should be investigated. If only the basic behavior of a building is required, it may be suitable to perform a simple analysis based on some checklists, such as described in Tier 1 of FEMA 310 or the checklists published by the Federal Office for Water and Geology (FOWG) [12].

Further, evaluation of the seismic performance of non-structural elements is important. Recent earthquake experience shows that, in aggregate, non-structural damage often exceeds the costs of structural damage. Nevertheless, the scope of this dissertation is limited to structural damage. It should be noted that the proposed evaluation procedure should be extended to cover the performance of non-structural elements.

# 8 Conclusion

Previous to the evaluation of the BHO-structure, evaluation procedures are compared. Generally, seismic evaluation procedures can be divided into two groups: configuration based checks and strength checks (see Figure 2.1). As mentioned in Chapter 1, configuration based checks serve to figure out quickly the general behavior of a structure while strength checks serve to compute the load carrying capacity of the structure.

Comparing Swisscode, Eurocode and FEMA 310 shows that FEMA 310 includes the most advanced evaluation procedure for the evaluation of existent building structures. In Swisscode the definition of performance levels is missing compared to Eurocode and FEMA 310. Further, a safety factor expressing the knowledge level as known in Eurocode is missing in Swisscode as well. For the analysis of old masonry structures the partial factor for material $\gamma_M$ according to SIA 266 appears to be the only factor regarding uncertainties. It is rather hard to understand how this material safety factor can be equal to the factor of the knowledge level as defined in EC8. This is an issue that might be of interest for a future investigation.

The evaluation procedure described in Standard SIA 2018 is similar to the one described in EC8, since many issues of Swisscode are based on Eurocode. In order to examine the seismic resistance of existing buildings on a quick way, the Federal Office for Water and Geology (FOWG) of Switzerland developed an evaluation procedure based on checklists, similar to Tier 1 of FEMA 310.

The survey of the middle part of the *Bundeshaus Ost* building was connected with some difficulties. Unfortunately, it was only possible to get limited knowledge of the building because of security reasons. Some information, such as the seismic parameters were available from the example in documentation SIA 0237. Of the composition of floors and walls only limited information is existent. Further, some connections could only be suggested and since the material characteristics of the ongoing material survey were not available yet, they needed to be estimated using code provisions. Therefore, several assumptions were necessary in order to obtain all required values needed for the following simulation. After studying the collected data, a site visit was performed in order to verify the obtained plans of the building permit of the ongoing renovation and to answer other questions. Also some new facts were discovered. Therefore the importance of a site visit can only be emphasized.

After the survey of the building, a numerical model of the building was created using 3Muri-software. As mentioned in Chapter 5.1, 3Muri is a numerical computation program created for the seismic analysis of masonry structures. The verification of the program showed almost matching pushover curves between the 3Muri computed and the hand-calculated one. During the development of the numerical model of the

BHO-structure, some problems and limits of the program could be detected (see Chapter 5.3). Therefore, it is believed that the software can still be improved in terms of model development.

The evaluation of the BHO-structure has shown that it satisfies the design requirements concerning the global and local performance under seismic loading for the performance levels operational (72years), limited damage (475years) and collapse prevention (2475years). As mentioned in Chapter 6.5, the BHO-structure undergoes a large deformation in the y-direction, while reaching the yield base shear. It is questionable if all the structural elements would remain intact under a displacement of 25 cm. It could be interesting to investigate in more detail the diaphragm deflection in the third floor using more detailed information of the floor composition and connections. An improvement of the diaphragms would improve the building integrity in general. Even though the program showed very good results during the program verification in Chapter 5.2, it would be helpful to analyze the BHO-structure with another seismic program and to compare the results. It remains difficult to know how realistic the results are, considering that several assumptions and estimations needed to be done in order to obtain the necessary structural components and the material characteristics. In a next step, it would be interesting to run the same simulation using the masonry parameters obtained from the ongoing material survey and to compare the results to the ones in this dissertation.

Following the analysis of the flexible-floor model, a rigid-floor model was developed. In this model rigid floors replaced all the flexible floors. The load distribution remained the same. Comparing the results of the rigid-floor model with the results of the flexible-floor model demonstrate that a more rigid-floor structure shows a better integrity with a more uniform deformation behavior. The comparison of the deformation capacity in the y-direction is rather difficult since the reference point lies in the diaphragm deflection, determined in the third floor.

Next, the story drifts of both models were computed. The largest drift of 0.5% is found to be in the expected area between 0.4% and 0.6%. The rigid-floor structure shows a higher story drift capacity than the flexible-floor one.

With 3Muri, the out-of-plane behavior of the two outside façades was analyzed for each floor (see Chapter 6.4). In addition a partial local mechanism was investigated in the third floor, where the diaphragm deflection was detected during the global evaluation. All these investigations show that the BHO-structure has enough resistance.

Conclusively, a pilot guideline for seismic evaluation of historic masonry building structures was created. It is based on the experiences collected during the evaluation of the BHO-structure, which excludes the evaluation of the seismic performance of non-structural elements. It should be noted that the proposed evaluation procedure should be extended to cover the performance of non-structural elements.

# 9 References

[1] SIA D0237 (2010), Beurteilung von Mauerwerksgebäuden bezüglich Erdbeben, Swiss Society of Engineers and Architects, Zürich, pp. 106.

[2] Bachmann, H. and Lang, K. (2002). Zur Erdbebensicherung von Mauerwerksbauten, Institute of Structural Engineering, Swiss Federal Institute of Technology Zürich, Zürich, pp. 3.

[3] Merkblatt SIA 2018 (2004), Überprüfung bestehender Gebäude bezüglich Erdbeben

[4] Wenk, T. (2006). Application of Eurocode 8 in Switzerland, First European Conference on Earthquake Engineering and Seismology, paper number 1399, Geneva

[5] Rai. D. C. (2003), Review of Documents on Seismic Evaluation of Existing Buildings, Indian Institute of Technology Kanpur, Document Nr. IITK-GSDMA-EQ03-V1.0, Kanpur

[6] SIA 160 (1970) and (1989), Einwirkungen auf Tragwerke, Swiss Society of Engineers and Architects, Zürich

[7] Empfehlung SIA 160/2 (1975), Praktische Massnahmen zum Schutze der Bauwerke gegen Erdbeben, Swiss Society of Engineers and Architects, Zürich

[8] Wenk, T. (2000), Erdbeben-Baunormen der Schweiz, 15. NDK Blockkurs, Institute of Structural Engineering, Swiss Federal Institute of Technology Zürich, Zürich

[9] SIA 261 (2003), Actions on Structures, Swiss Society of Engineers and Architects, Zürich, pp. 114.

[10] SIA 266 (2003), Masonry, Swiss Society of Engineers and Architects, Zürich, pp. 44.

[11] EN 1998-3 (2005), Eurocode 8: Design of structures for earthquake resistance – Part 3: Assessment and retrofitting of buildings, Brussels, pp. 89.

[12] Richtlinien des BWG (2005), Beurteilung der Erdbebensicherheit bestehender Gebäude – Konzept und Richtlinien für die Stufen 1-3, Federal Office for Water and Geology FOWG, Bern, pp. 133.

[13] FEMA-310 (1998), Handbook for the Seismic Evaluation of Buildings, Federal Emergency Management Agency and American Society of Civil Engineers, pp. 218.

[14] EN 1998-1 (2003), Eurocode 8: Design of structures for earthquake resistance – Part 1: General rules, seismic actions and rules for buildings, Brussels, pp. 227.

[15] Tena-Colunga, A. and Abrams, D. P. (1996), Seismic Behavior of Structures with Flexible Diaphragms, Journal of Structural Engineering, 122:439-445, pp. 439-445.

[16] FEMA-356 (2000), Prestandard and Commentary for the Seismic Rehabilitation of Buildings, Federal Emergency Management Agency, Washington D.C., pp. 518.

[17] EN 1996-1-1 (2004), Eurocode 6: Design of masonry structures – Part 1-1: Common rules for reinforced and unreinforced masonry structures, Brussels, pp. 123.

[18] SIA V178 (1996), Naturstein-Mauerwerk, Swiss Society of Engineers and Architects, Zürich, p. 40.

[19] SIA 266/2 (2012), Natural Stone Masonry, Swiss Society of Engineers and Architects, Zürich, pp. 14-22.

[20] EN 1052-1 (1998), Methods of test for masonry – Part 1: Determination of compressive strength

[21] Tomaževič, M. (2006), Earthquake-Resistant Design of Masonry Buildings, Slovenian National Building and Civil Engineering Institute, Imperial Collage Press, p.46, p.121. pp. 203-251.

[22] Lang, K. (2002). Seismic vulnerability of existing buildings, Dissertation ETH No. 14446. Swiss Federal Institute of Technology Zürich, Zürich, pp. 16-18.

[23] Chopra, A. K. (2007). Dynamics of Structures, Theory and Applications to Earthquake Engineering, 3rd Edition. Prentice Hall. p. 556.

[24] 3Muri General Description, Version 4, S.T.A. DATA, Torino, pp. 78.

[25] 3Muri User Manual, Release: 5.0.1, S.T.A. DATA, Torino, pp. 136.

[26] D.M. 14 gennaio 2008, Norme Tecniche per le Costruzioni, pp. 438.

[27] Turnšek, V. and Cacovic, F. (1971). Some experimental results on the strength of brick masonry walls, Proceedings of the 2nd IBBMC, Stoke-on-Trent, pp. 149-156.

[28] SIA V177, Mauerwerk, Swiss Society of Engineers and Architects, Zürich, pp. 52.

[29] Wikipedia (visited 01.07.2013). http://en.wikipedia.org/wiki/Hazard

[30] Giardini, D. and Wiemer, S. and Fäh, D. and Deichmann, N. (2004). Seismic Hazard Assessment of Switzerland, Swiss Seismological Service, Swiss Federal Institute of Technology Zürich, Zürich, pp. 95.

[31] FEMA P-750 (2009), NEHRP Recommended Seismic Provisions for New Buildings and Other Structures, Federal Emergency Management Agency of the U.S. Department of Homeland Security, Washington D.C., pp. 21-35.

# Appendix

## A Site Visit

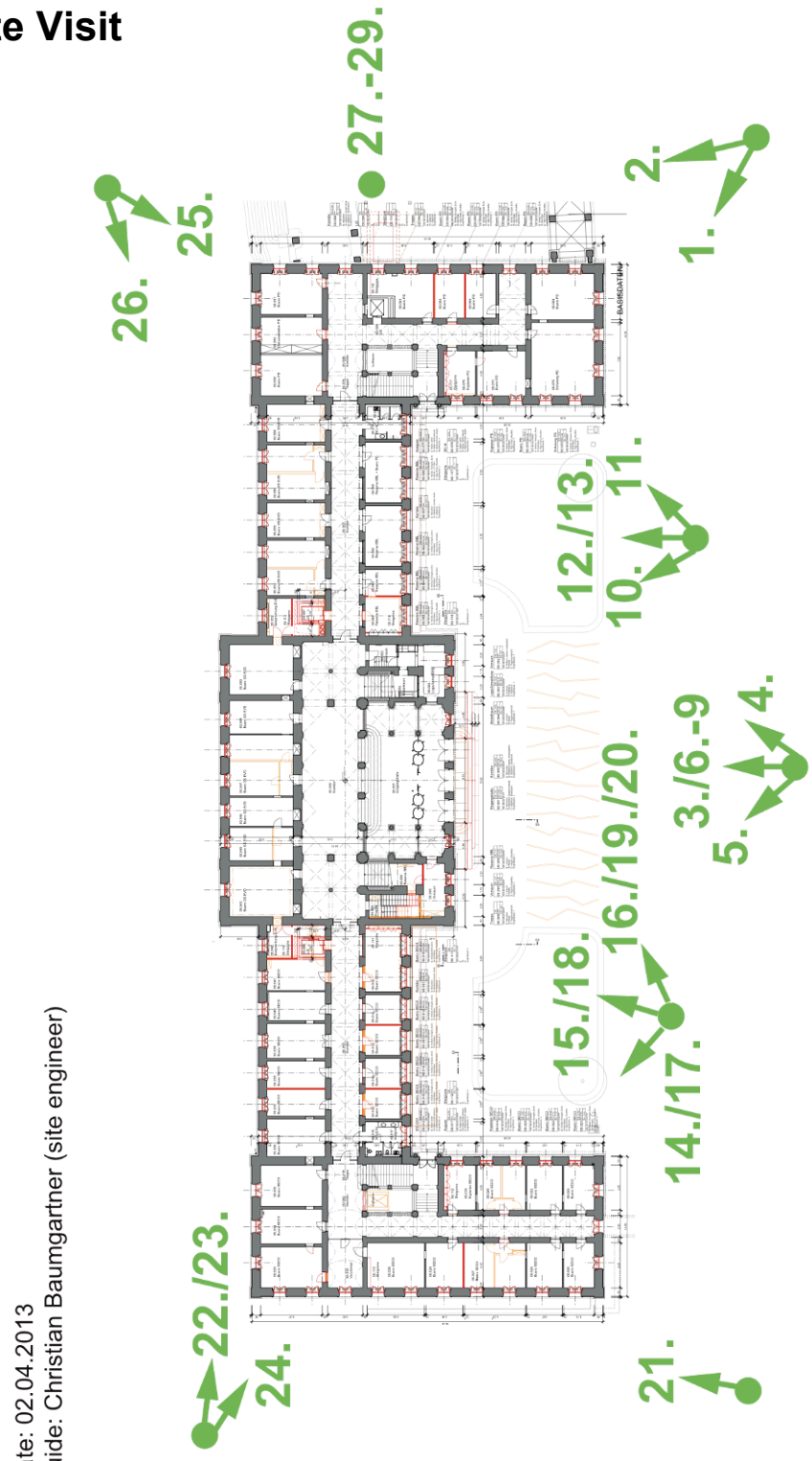


**Figure A.1** Picture recording positions

**Figure A.2** Picture 1

**Figure A.3** Picture 2

**Figure A.4** Picture 3

**Figure A.5** Picture 4

**Figure A.6** Picture 5

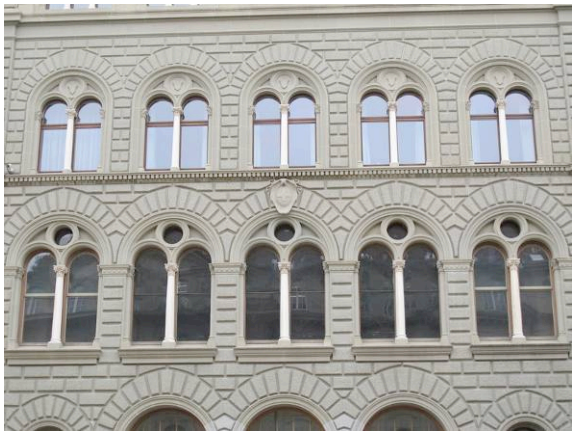

**Figure A.7** Picture 6

**Figure A.8** Picture 7

**Figure A.10** Picture 9


**Figure A.13** Picture 12


**Figure A.9** Picture 8

**Figure A.11** Picture 10


**Figure A.12** Picture 11

**Figure A.14** Picture 14

**Figure A.15** Picture 15

**Figure A.16** Picture 16

**Figure A.17** Picture 17

**Figure A.18** Picture 18

**Figure A.19** Picture 19

**Figure A.20** Picture 20

**Figure A.21** Picture 21

**Figure A.22** Picture 22

**Figure A.23** Picture 23

**Figure A.24** Picture 24

**Figure A.25** Picture 25

**Figure A.26** Picture 26

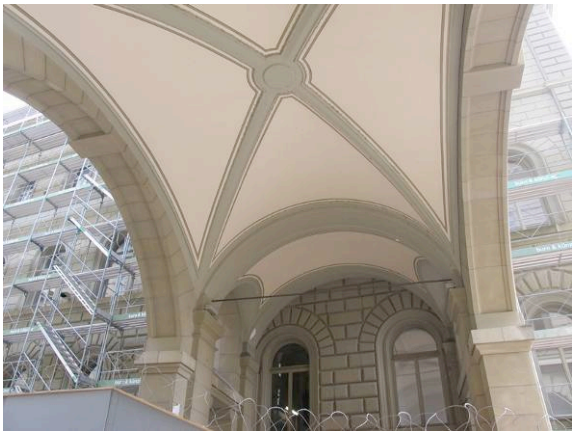

**Figure A.28** Picture 28

**Figure A.27** Picture 27

**Figure A.29** Picture 29

# B BHO-structure

## B.1 Geometry

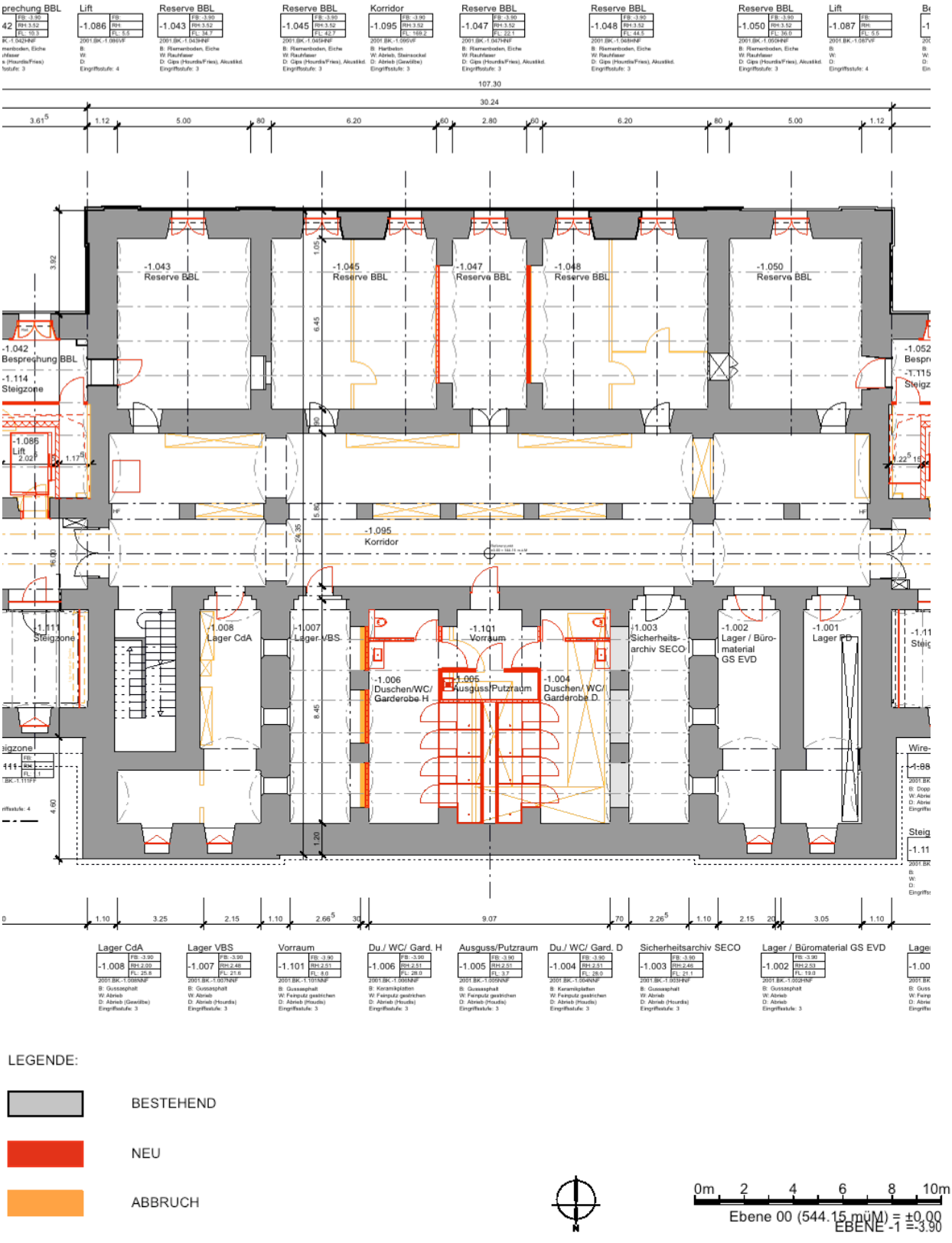


**Figure B.1** Ground plan of the underground floor (TP) of the middle part of the BHO-structure

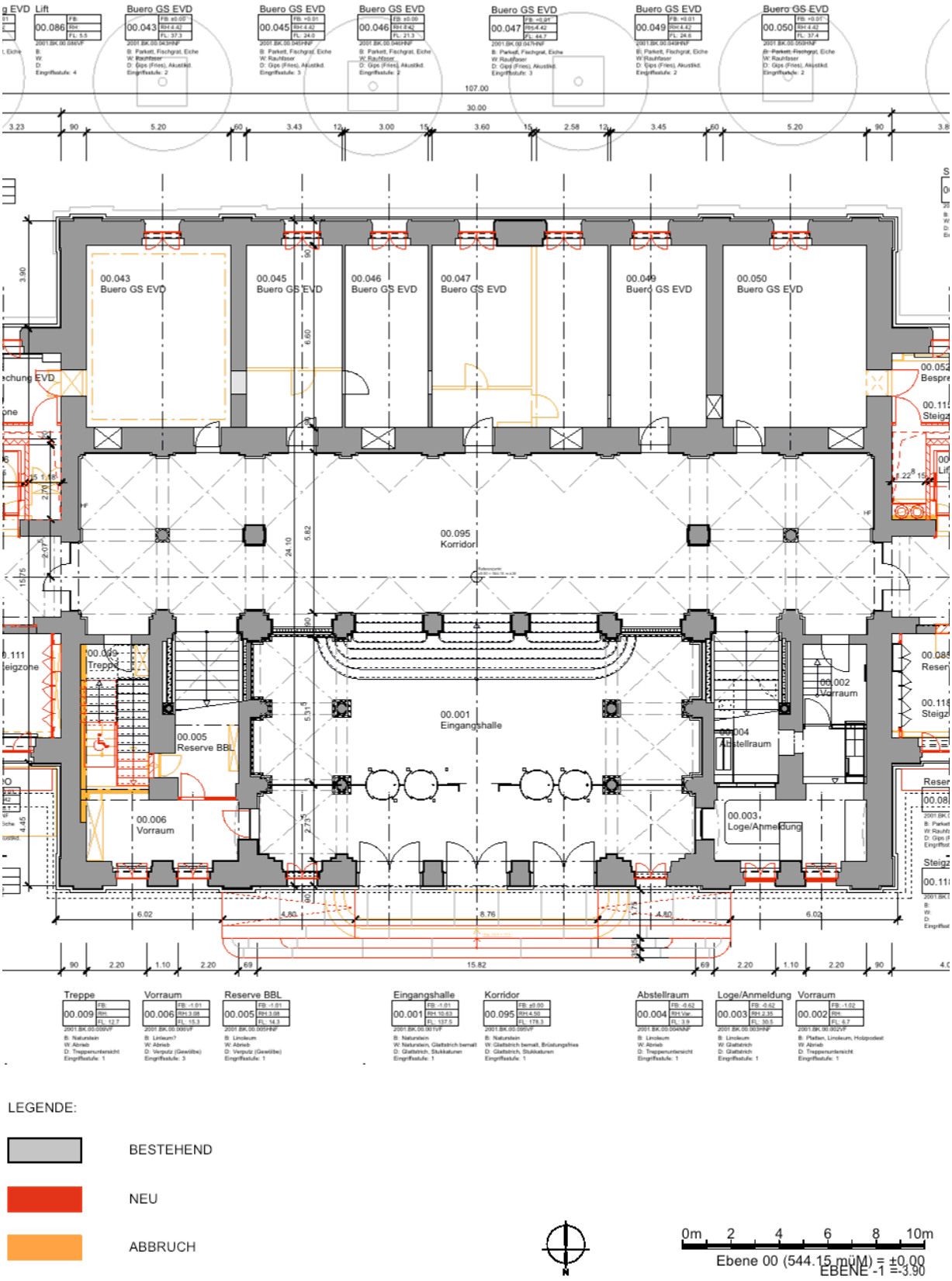


**Figure B.2** Ground plan of the ground floor (EG) of the middle part of the BHO-structure

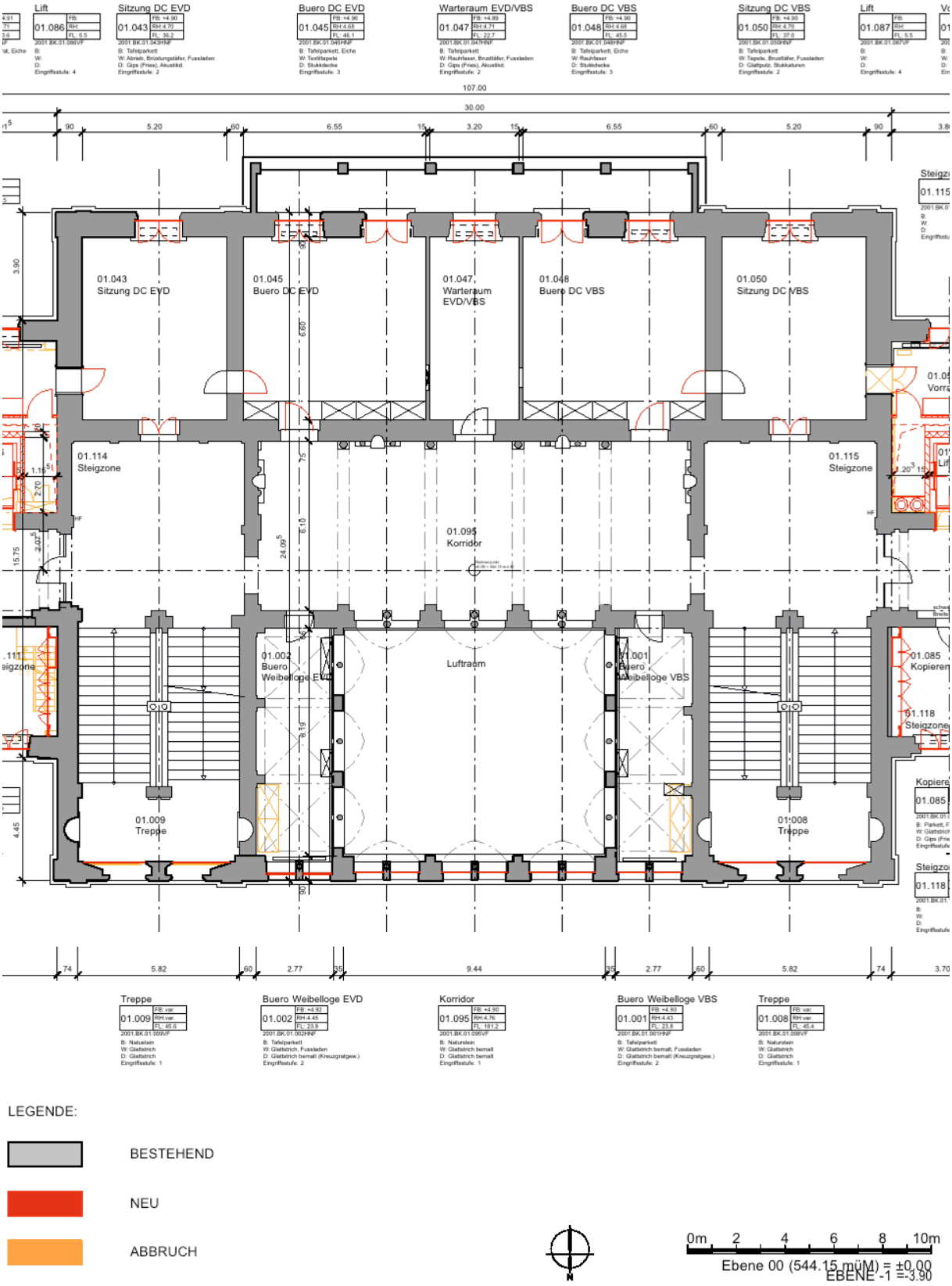


**Figure B.3** Ground plan of the first floor (1.OG) of the middle part of the BHO-structure

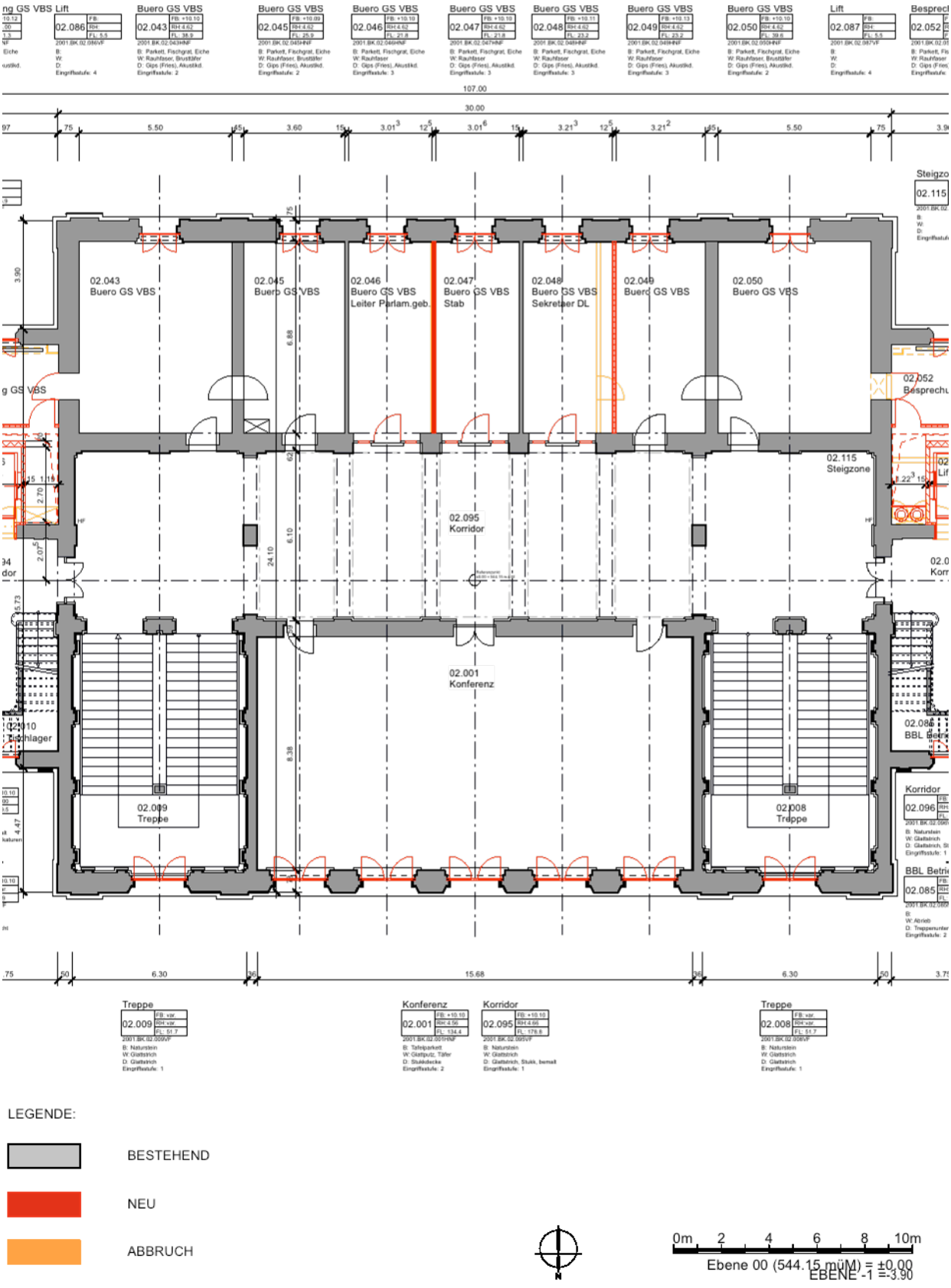


**Figure B.4** Ground plan of the second floor (2.OG) of the middle part of the BHO-structure

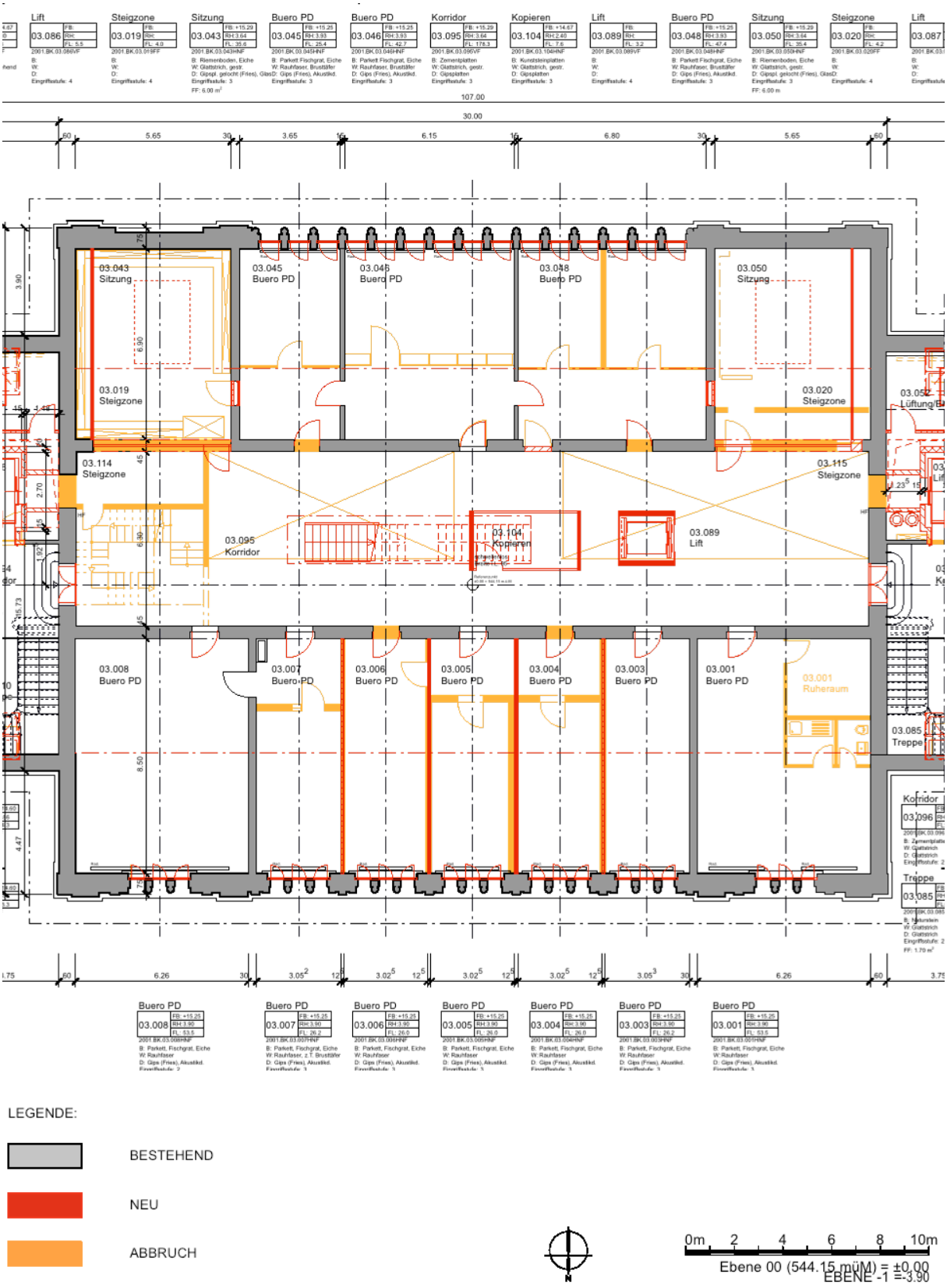


**Figure B.5** Ground plan of the third floor (3.OG) of the middle part of the BHO-structure

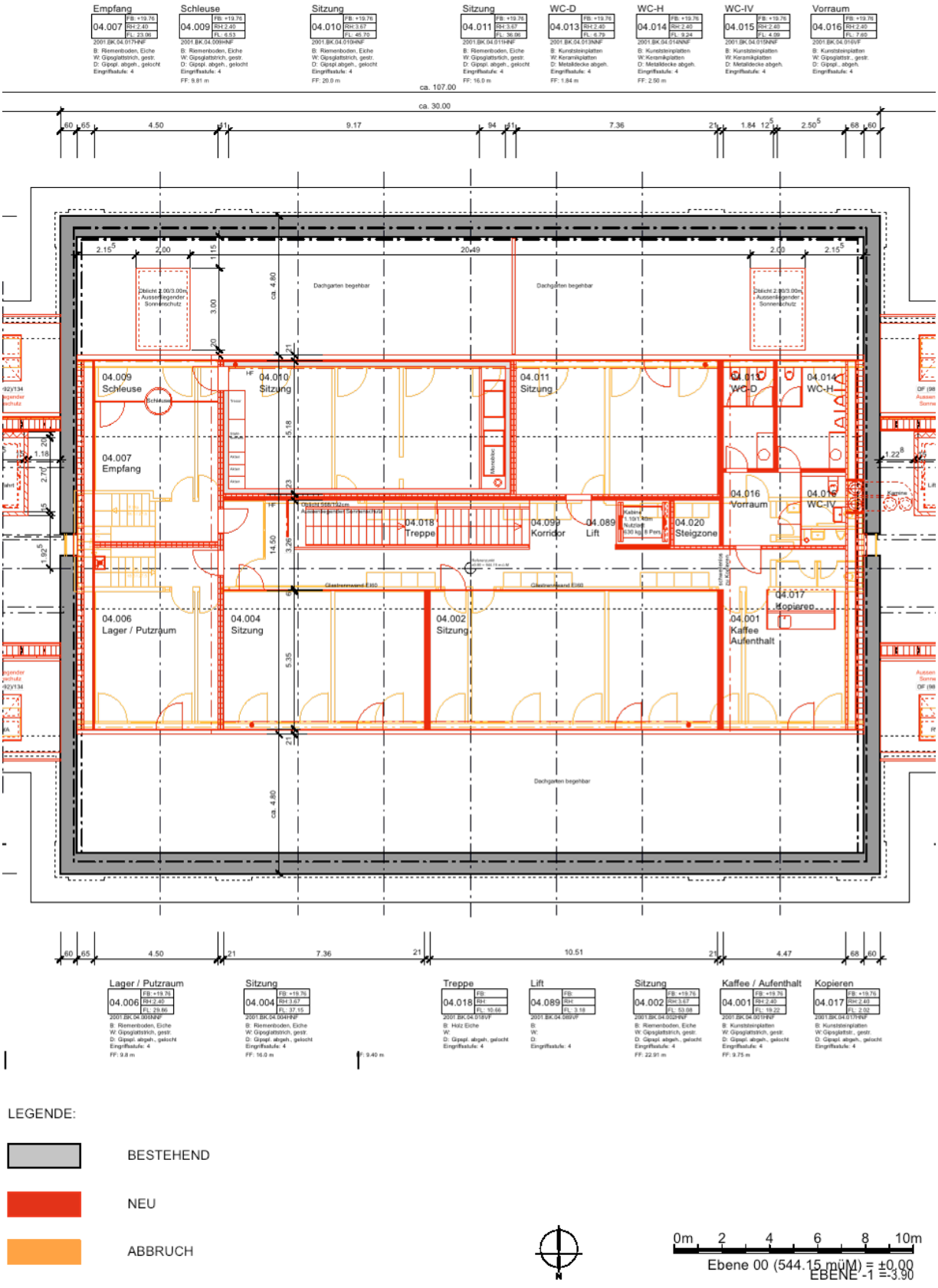


**Figure B.6** Ground plan of the fourth floor (4.OG) of the middle part of the BHO-structure

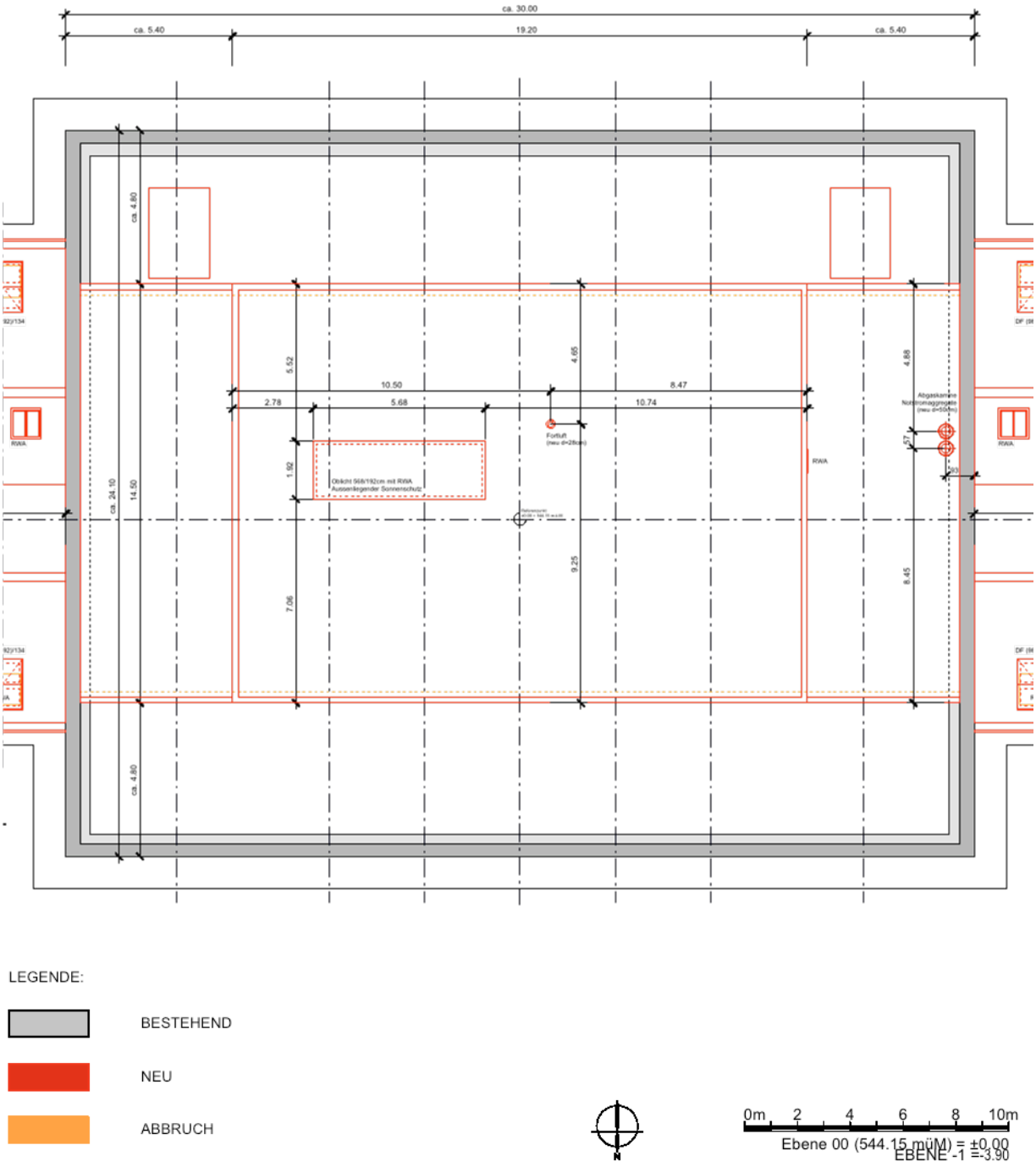


**Figure B.7** Top view of the roof of the middle part of the BHO-structure

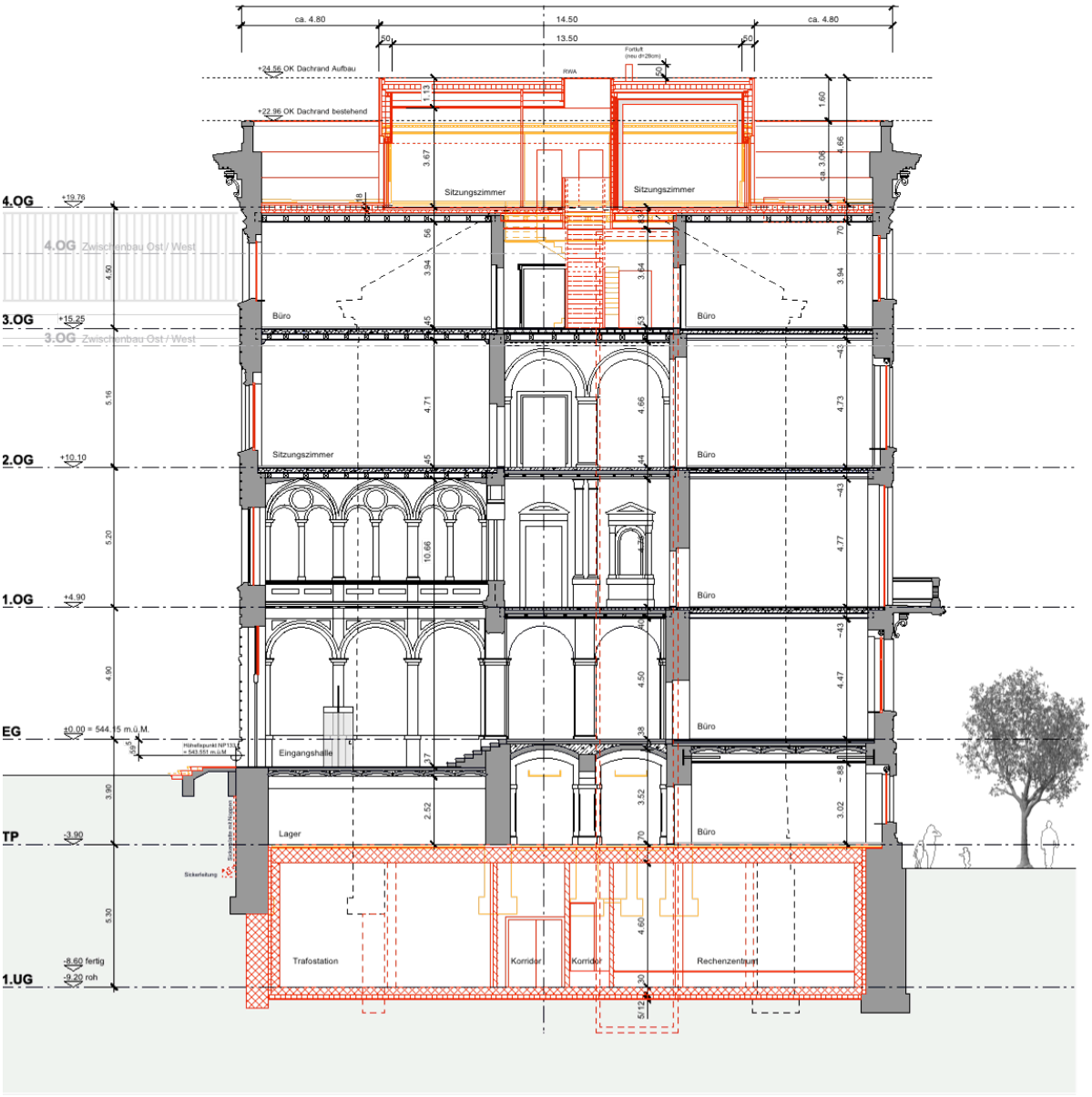


Querschnitt - Mittelbau

LEGENDE:

BESTEHEND

NEU

ABBRUCH

**Figure B.8** Cross section of the middle part of the BHO-structure

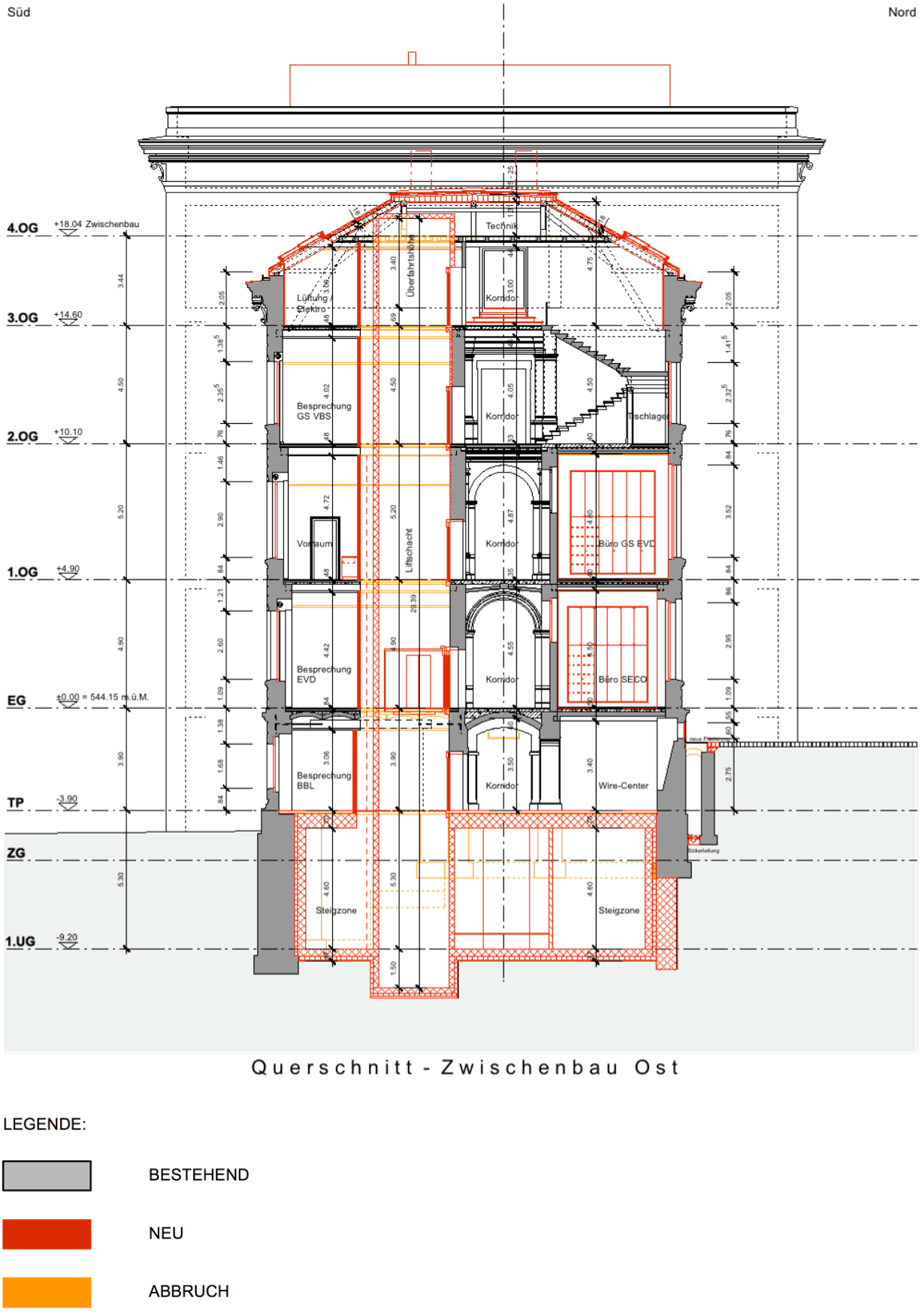


Querschnitt - Zwischenbau Ost

**Figure B.9** Cross section of the east corridor part of the BHO-structure


Laengsschnitt - Mittelbau

LEGENDE:

BESTEHEND

NEU

ABBRUCH

**Figure B.10** Longitudinal section of the middle part of the BHO-structure with the entrance hall and the staircases

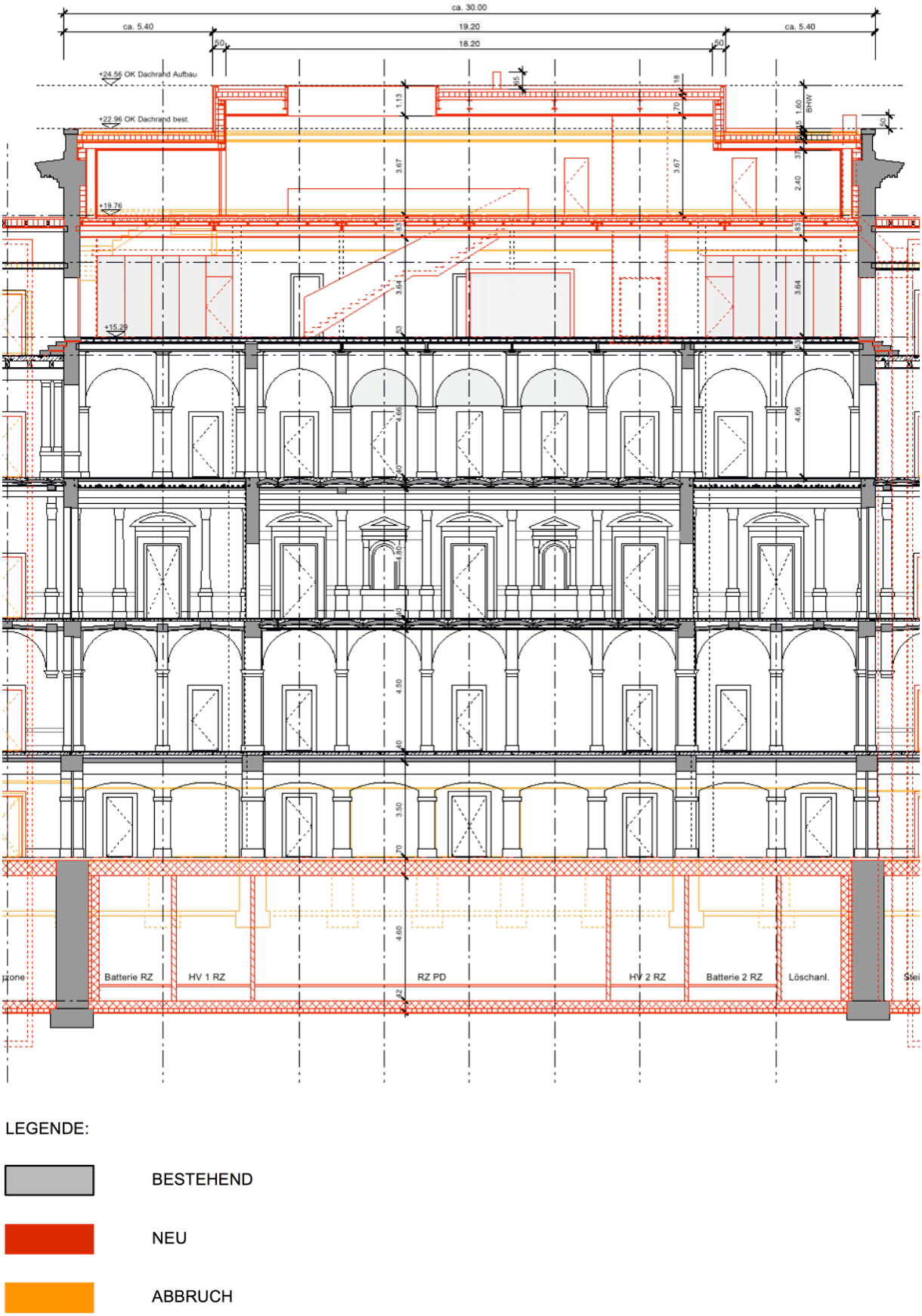


**Figure B.11** Longitudinal section of the corridors of the BHO-structure

## B.2 Vertical Load Assignments and Floor Types

In each floor the load-carrying direction is shown with black arrows. Only the blue and red marked parts have a 50%-load distribution in both directions.

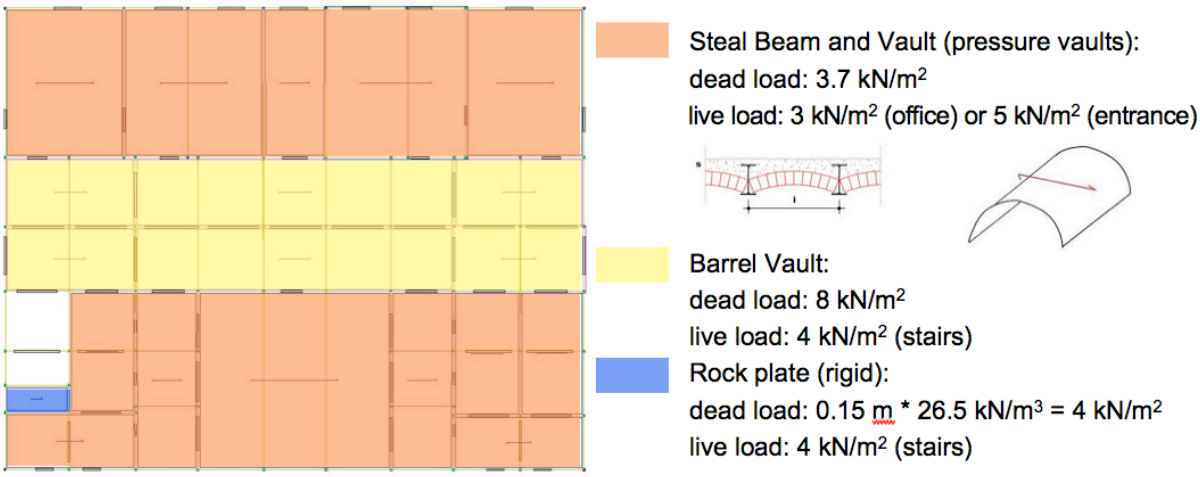


**Figure B.12** Ground floor on base floor (EG on TP)

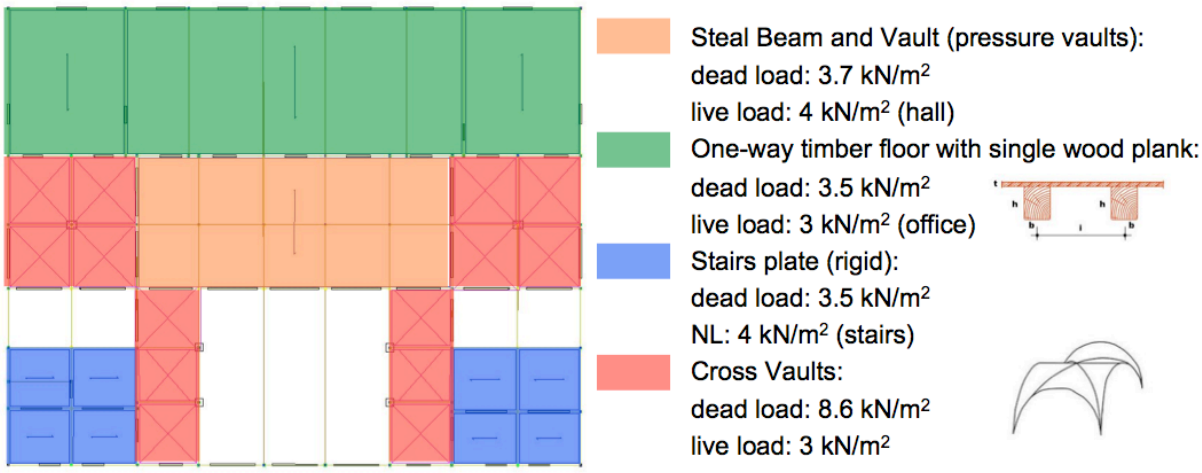


**Figure B.13** First floor on ground floor (1.OG on EG)

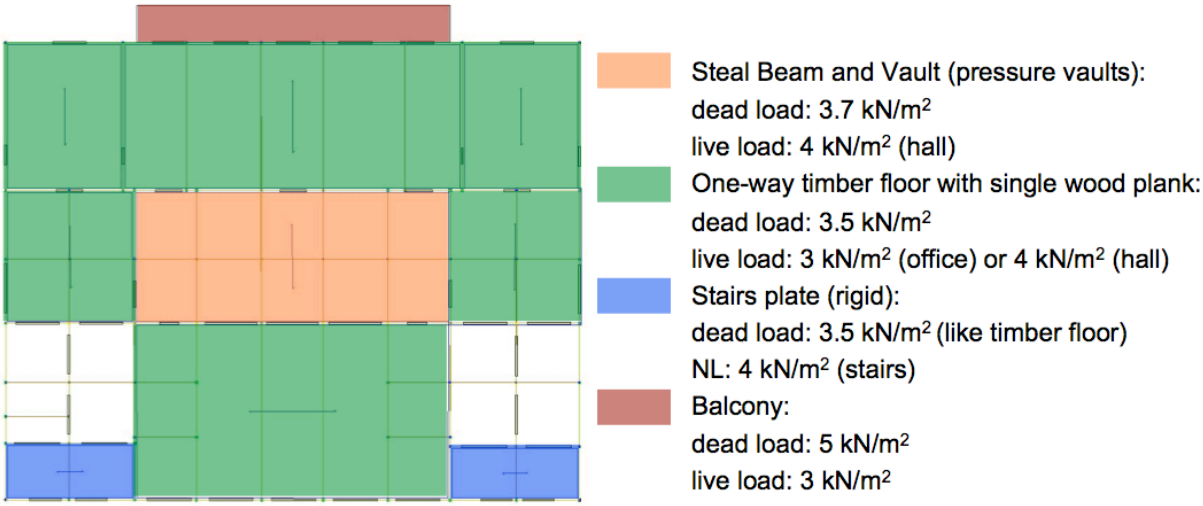


**Figure B.14** Second floor on first floor (2.OG on 1.OG)

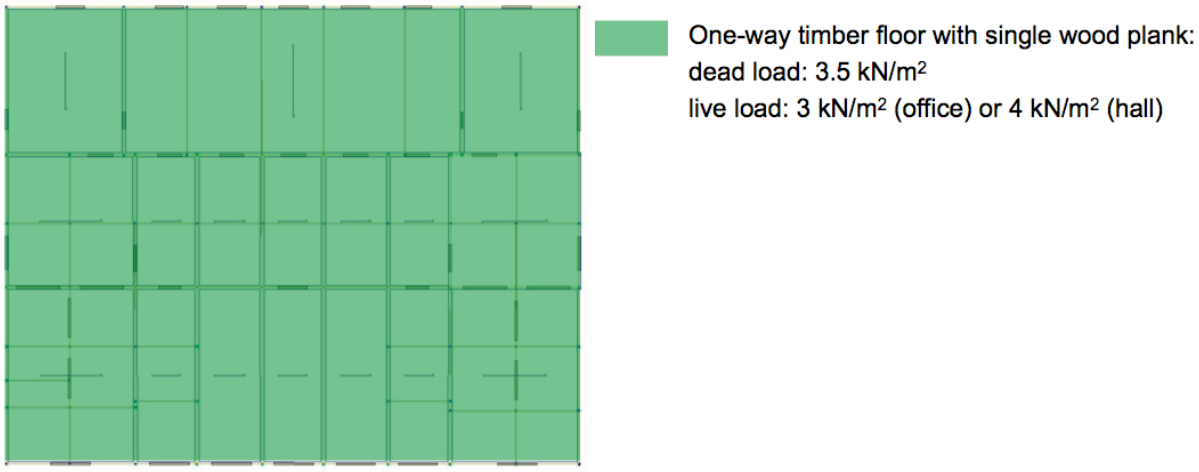


**Figure B.15** Third floor on second floor (3.OG on 2.OG)

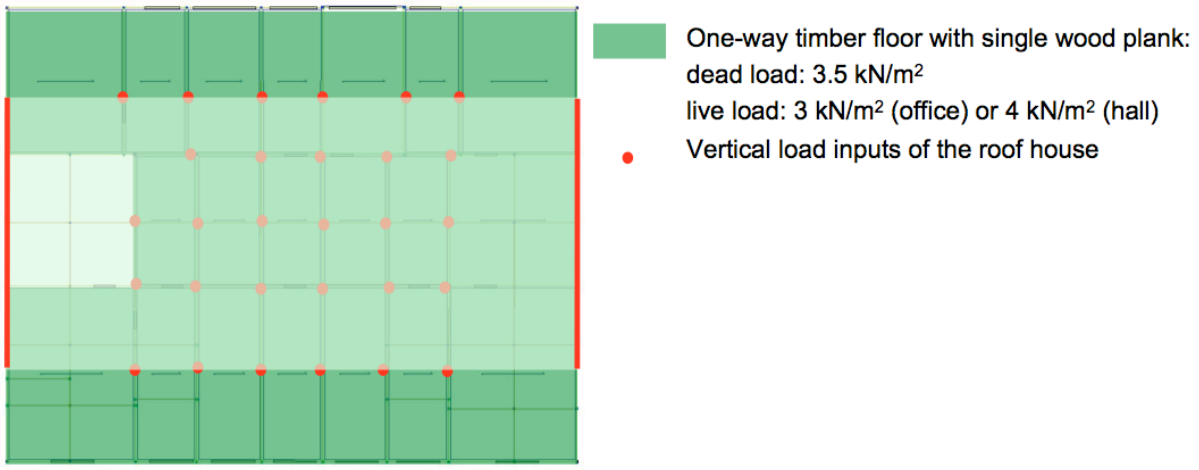


**Figure B.16** Fourth floor on third floor (4.OG on 3.OG)

## B.3 Floor types and its components

| | |
|---|---|
| **Steal-beam (IPE 160) and Vault** 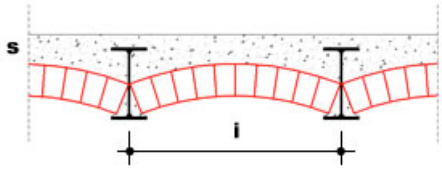  | i 115 [cm]<br>$E_{IPE}$ 210000 [N/mm$^2$]<br>$A_{IPE}$ 2010 [mm$^2$]<br>- iron beams well connected to masonry<br>- brick<br>- without additional concrete topping |
| **Steal-beam (IPE 240) and Vault** 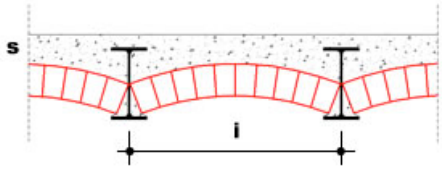  | i 130 [cm]<br>$E_{IPE}$ 210000 [N/mm$^2$]<br>$A_{IPE}$ 3910 [mm$^2$]<br>- iron beams well connected to masonry<br>- brick<br>- without additional concrete topping |
| **One-way timber floor** 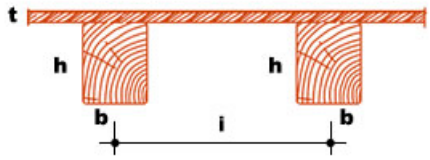  | i 60 [cm]<br>b 20 [cm]<br>h 28 [cm]<br>E 11000 [N/mm$^2$]<br>- beams sufficiently connected to the perimeter walls |

**Figure B.17** Floor types with their components

| | | | | |
|---|---|---|---|---|
| **Cross vault** | | | | 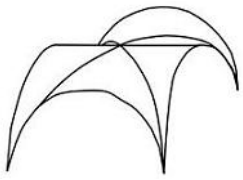 |
| Vault thickness at the key | $S_{tot}$ | 32 | [cm] | |
| Rise | f | 115 | [cm] | |
| Average structural thickness | $S_{medi}$ | 20 | [cm] | |
| Filling density | ρ | 20 | [kN/m$^3$] | |
| Structural filling | masonry | | | |
| Degree of connection | absent | | | |
| Vault material | sandstone masonry | | | |
| **Barrel vault** | | | | 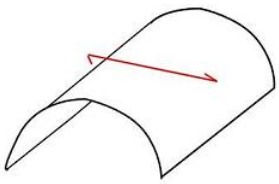 |
| Vault thickness at the key | $S_{tot}$ | 32 | [cm] | |
| Rise | f | 38 | [cm] | |
| Average structural thickness | $S_{medi}$ | 20 | [cm] | |
| Filling density | ρ | 20 | [kN/m$^3$] | |
| Structural filling | masonry | | | |
| Degree of connection | absent | | | |
| Vault material | sandstone masonry | | | |

**Figure B.18** Vault types with their components

# C Mass Center Calculation

**Table D.1** Mass center calculation of the ground floor (EG)

| **EG** (only half-side of the structure analyzed since buidling is symmetric) | | | | | storey height = | | 4.9 [m] | |
|---|---|---|---|---|---|---|---|---|
| ***Floors*** | | | | surface | surface load | load | lever | moment |
| | | | | [$m^2$] | [$kN/m^2$] | [kN] | [m] | [kNm] |
| office | | | | 108.8 | 3.5 | 380.6 | 3.6 | 1370.3 |
| corridor | | | | 94.3 | 4.0 | 377.0 | 11.5 | 4335.5 |
| gallery | | | | 27.0 | 3.0 | 81.0 | 19.3 | 1563.3 |
| floors of stairs | | | | 39.0 | 4.0 | 156.0 | 21.5 | 3354.0 |
| | | | | | **Total floors** | 994.6 | | 10623 |
| ***Walls*** | width | length | openings | volume | density | load | lever | moment |
| | [m] | [m] | [m] | [$m^3$] | [$kN/m^3$] | [kN] | [m] | kNm |
| 1 | 0.9 | 7.5 | 1.0 | 29.5 | 25 | 738.6 | 3.8 | 2770 |
| 2 | 0.6 | 7.5 | 1.0 | 19.7 | 25 | 492.4 | 3.8 | 1846 |
| 3 | 0.6 | 6.5 | 2.5 | 12.1 | 25 | 303.0 | 10.8 | 3257 |
| 4 | 0.65 | 6.5 | 5.0 | 4.9 | 26 | 128.0 | 10.8 | 1376 |
| 5 | 0.9 | 9.5 | 0.0 | 43.2 | 25 | 1079.4 | 18.8 | 20239 |
| 6 | 0.75 | 6.0 | 3.0 | 11.4 | 25 | 284.1 | 17.2 | 4876 |
| 7 | 0.45 | 9.5 | 3.0 | 14.8 | 25 | 369.3 | 18.8 | 6924 |
| 8 | 0.9 | 14.5 | 4.5 | 45.5 | 28 | 1272.6 | 0.0 | 0 |
| 9 | 0.9 | 14.5 | 4.8 | 44.1 | 25 | 1102.2 | 7.5 | 8266 |
| 10 | 0.9 | 14.5 | 10.2 | 19.5 | 26 | 508.1 | 14.0 | 7114 |
| 11 | 0.9 | 14.5 | 7.0 | 34.1 | 27 | 920.4 | 22.0 | 20248 |
| | | | | | **Total wallls** | 7198.0 | | 76917 |
| | | | | | **Total floors** | 994.6 | | 10623 |
| | | | | | **Total** | ***8192.6*** | | ***87540*** |
| | | | | | ***mass center point*** | | 10.7 | ***[m]*** |

**Table D.2** Mass center calculation of the first floor (1.OG)

| **1.OG** (only half-side of the structure analyzed since buidling is symmetric) | | | | | storey height = | | 5.2 [m] | |
|---|---|---|---|---|---|---|---|---|
| ***Floors*** | | | | surface | surface load | load | lever | moment |
| | | | | [$m^2$] | [$kN/m^2$] | [kN] | [m] | [kNm] |
| office | | | | 108.75 | 3.5 | 380.625 | 3.6 | 1370.25 |
| corridor | | | | 94.25 | 4 | 377 | 11.5 | 4335.5 |
| gallery | | | | 65.94 | 3 | 197.82 | 19.3 | 3817.926 |
| floors of stairs | | | | 22.05 | 4 | 88.2 | 21.5 | 1896.3 |
| | | | | | **Total floors** | 1043.6 | | 11420 |
| ***Walls*** | width | length | openings | volume | density | load | lever | moment |
| | [m] | [m] | [m] | [$m^3$] | [$kN/m^3$] | [kN] | [m] | kNm |
| 1 | 0.9 | 7.5 | 1 | 29.5 | 25 | 738.56 | 3.75 | 2769.6 |
| 2 | 0.6 | 7.5 | 1 | 19.7 | 25 | 492.38 | 3.75 | 1846.4 |
| 3 | 0.55 | 6.5 | 2.5 | 11.1 | 25 | 277.75 | 10.75 | 2985.8 |
| 4 | 0.5 | 6.5 | 1.3 | 13.1 | 26 | 341.38 | 10.75 | 3669.8 |
| 5 | 0.75 | 9.5 | 0 | 36.0 | 25 | 899.53 | 18.75 | 16866.2 |
| 6 | 0.6 | 14.5 | 0 | 43.9 | 25 | 1098.38 | 7.5 | 8237.8 |
| 7 | 0.9 | 14.5 | 6 | 38.6 | 25 | 965.81 | 0 | 0.0 |
| 8 | 0.75 | 14.5 | 3.75 | 40.7 | 25 | 1017.89 | 14 | 14250.5 |
| 9 | 0.65 | 14.5 | 9.2 | 17.4 | 25 | 434.93 | 23.5 | 10220.9 |
| 10 | 0.9 | 14.5 | 9.4 | 23.2 | 26 | 602.67 | 23.5 | 14162.7 |
| | | | | | **Total wallls** | 6869.28 | | 75009.7 |
| | | | | | **Total floors** | 1043.65 | | 11420.0 |
| | | | | | **Total** | 7912.92 | | 86429.7 |
| | | | | | ***mass center point*** | | 10.9 | ***[m]*** |

**Table D.3** Mass center calculation of the second floor (2.OG)

| **2.OG** | | | | | | | | |
|---|---|---|---|---|---|---|---|---|
| (only half-side of the structure analyzed since buidling is symmetric) | | | | | storey height = | | 5.19 | [m] |
| ***Floors*** | | | | surface | surface load | load | lever | moment |
| | | | | [$m^2$] | [$kN/m^2$] | [kN] | [m] | [kNm] |
| office | | | | 108.75 | 3.5 | 380.63 | 3.6 | 1370.3 |
| corridor | | | | 94.25 | 3.7 | 348.73 | 11.5 | 4010.3 |
| gallery | | | | 65.94 | 3.5 | 230.79 | 19.3 | 4454.2 |
| floors of stairs | | | | 22.05 | 4 | 88.20 | 21.5 | 1896.3 |
| | | | | | **Total floors** | 1048.3 | | 11731 |
| ***Walls*** | width | length | openings | volume | density | load | lever | moment |
| | [m] | [m] | [m] | [$m^3$] | [$kN/m^3$] | [kN] | [m] | kNm |
| 1 | 0.75 | 7.5 | 1 | 25.3 | 25 | 633.14 | 3.5 | 2216.0 |
| 2 | 0.45 | 7.5 | 1 | 15.2 | 25 | 379.88 | 3.5 | 1329.6 |
| 3 | 0.55 | 6.5 | 1.7 | 13.7 | 25 | 342.87 | 10.75 | 3685.9 |
| 4 | 0.45 | 6.5 | 5 | 3.5 | 25 | 87.67 | 10.75 | 942.4 |
| 5 | 0.5 | 9.5 | 0 | 24.7 | 25 | 616.91 | 18.75 | 11567.0 |
| 6 | 0.35 | 9.5 | 0 | 17.3 | 25 | 431.83 | 18.75 | 8096.9 |
| 7 | 0.75 | 14.5 | 5 | 37.0 | 25 | 925.36 | 0 | 0.0 |
| 8 | 0.6 | 14.5 | 8.5 | 18.7 | 25 | 467.55 | 7.5 | 3506.6 |
| 9 | 0.6 | 14.5 | 6.5 | 24.9 | 25 | 623.40 | 14 | 8727.6 |
| 10 | 0.7 | 14.5 | 9 | 20.0 | 25 | 500.02 | 23.5 | 11750.4 |
| | | | | | **Total wallls** | 5008.63 | | 51822.4 |
| | | | | | **Total floors** | 1048.34 | | 11731.1 |
| | | | | | **Total** | 6056.97 | | 63553.5 |
| | | | | | ***mass center point*** | | 10.3 | ***[m]*** |

**Table D.4** Mass center calculation of the third floor (3.OG)

| **3.OG** | | | | | | | | |
|---|---|---|---|---|---|---|---|---|
| (only half-side of the structure analyzed since buidling is symmetric) | | | | | storey height = | | 4.47 | [m] |
| ***Floors*** | | | | surface | surface load | load | lever | moment |
| | | | | [$m^2$] | [$kN/m^2$] | [kN] | [m] | [kNm] |
| office | | | | 108.75 | 3.5 | 380.63 | 3.6 | 1370.3 |
| corridor | | | | 94.25 | 3.7 | 348.73 | 11.5 | 4010.3 |
| gallery | | | | 65.94 | 3.5 | 230.79 | 19.3 | 4454.2 |
| floors of stairs | | | | 22.05 | 4 | 88.20 | 21.5 | 1896.3 |
| | | | | | **Total floors** | 1048.3 | | 11731 |
| ***Walls*** | width | length | openings | volume | ρ | | | |
| | [m] | [m] | [m] | [$m^3$] | kN/m3 | kN | m | kNm |
| 1 | 0.6 | 7.5 | 0 | 21.7 | 25 | 543.38 | 3.5 | 1901.8 |
| 2 | 0.3 | 7.5 | 1 | 9.4 | 25 | 235.46 | 3.5 | 824.1 |
| 3 | 0.55 | 6.5 | 1.5 | 13.3 | 25 | 332.06 | 10.75 | 3569.7 |
| 4 | 0 | 6.5 | 5 | 0.0 | 25 | 0.00 | 10.75 | 0.0 |
| 5 | 0.55 | 9.5 | 0 | 25.2 | 25 | 630.92 | 18.75 | 11829.7 |
| 6 | 0.3 | 9.5 | 1 | 12.3 | 25 | 307.91 | 18.75 | 5773.4 |
| 7 | 0.6 | 14.5 | 6.2 | 24.1 | 25 | 601.34 | 0 | 0.0 |
| 8 | 0.6 | 14.5 | 0 | 42.0 | 25 | 1050.53 | 7.5 | 7878.9 |
| 9 | 0.6 | 14.5 | 2.75 | 34.1 | 25 | 851.29 | 14 | 11918.0 |
| 10 | 0.7 | 14.5 | 7.1 | 25.0 | 25 | 625.49 | 23.5 | 14698.9 |
| | | | | | **Total wallls** | 5178.36 | | 58394.5 |
| | | | | | **Total floors** | 1048.34 | | 11731.1 |
| | | | | | **Total** | 6226.70 | | 70125.7 |
| | | | | | ***mass center point*** | | 11.3 | ***[m]*** |

# D Test Building Structure

## D.1 Equivalent Force Analysis according to SIA 261

### Ersatzkraftverfahren gemäss SIA 261

| | | | | |
|---|---|---|---|---|
| Seismic Zone | $a_{gd}$ = | 0.6 | [m/s$^2$] | |
| Soil Class B | S = | 1.2 | [-] | |
| | $T_B$ = | 0.15 | [s] | |
| | $T_C$ = | 0.5 | [s] | |
| | $T_D$ = | 2 | [s] | |
| Importance factor II | $\gamma_f$ = | 1.2 | [-] | |
| Einwirkung Dach: | $q_{d,Decke}$ = | 3.33 | [kN/m$^2$] | |
| Einwirkung Wand: | $g_{Wand}$ = | 2.6 | [kN/m$^2$] | |
| Gebäudemasse | $m_{tot}$ = | 6336 | [kg] | |
| | G = | 63.36 | [kN] | |
| Dämpfungsfaktor | μ = | 1 | [-] | (SIA 261, equation (29)) |
| Eigenperiode abgeschätzt | $C_t$ = | 0.05 | [-] | |
| | h = | 2.625 | [m] | |
| | $T_1$ ~ | 0.103 | [s] | < $T_B$ |
| | $\omega_1$ = | 60.934 | [s$^{-1}$] | |
| Elastic spectra | $S_a$ = | 0.149 | [-] | |
| Horizontale Ersatzkraft | $F_d$ = | 9.45 | [kN] | |
| Horizontale Verschiebung | | | | |
| | $S_d$ = | 0.394 | [mm] | |

# D.2 Response Spectra Analysis according to SIA 261

## Antwortspektrenverfahren gemäss SIA 261

| | | | | |
|---|---|---|---|---|
| | $a_{gd}$ = | 0.6 | [m/s$^2$] | |
| Soil class B | S = | 1.2 | [-] | |
| | $T_B$ = | 0.15 | [s] | |
| | $T_C$ = | 0.5 | [s] | |
| | $T_D$ = | 2 | [s] | |
| Importance class II | $\gamma_f$ = | 1.2 | [-] | |
| Einwirkung Dach: | $q_{d,Decke}$ = | 3.33 | [kN/m$^2$] | |
| Einwirkung Wand: | $g_{Wand}$ = | 2.6 | [kN/m$^2$] | |
| Raumgewicht | $\rho_m$ = | 13 | [kN/m$^3$] | |
| Gebäudemasse | $m_{tot}$ = | 6336 | [kg] | |
| Weight | W = | 63.36 | [kN] | |
| Dämpfungsfaktor | $\mu$ = | 1 | [-] | (SIA 261, equation (29)) |

**Modalanalyse:**

| | | | |
|---|---|---|---|
| h = | 2.625 | [m] | |
| $l_w$ = | 1 | [m] | |
| $A_w$ = | 200000 | [mm$^2$] | |
| E = | 7000 | [N/mm$^2$] | |
| G = | 2800 | [N/mm$^2$] | 0.83 (fixed-ended) ≤ α' ≤ 3.33 (cantilever) |
| α' = | 3.33 | [-] | |
| $k_e$ = | 17466 | [kN/m] | Tomazevic |
| $m_{tot}$ = | 6336 | [kg] | |

Steifigkeit mit Statik:

| | | | |
|---|---|---|---|
| Q = | 1 | [kN] | |
| $M_1$* = | 0.2 | [kNm] | |
| $M_2$* = | 2.4 | [kNm] | |
| $w_c$ = | 28.43 | [mm] | |
| $w_b$ = | 1.68 | [mm] | |
| $w_{tot}$ = | 58.54 | [mm] | |
| k = | 17081 | [kN/m] | |

Eigenperiode:

| | | | |
|---|---|---|---|
| $\omega_1$ = | 105.008 | [s$^{-1}$] | |
| $T_1$ = | 0.0598 | [s] | < $T_B$ |
| $S_a$ = | 0.117 | [-] | Formel (30) |

horizontale Ersatzkrafteinwirkung

| | | | |
|---|---|---|---|
| $F_d$ = | 7.43 | [kN] | |

Horizontale Verschiebung

| | | | |
|---|---|---|---|
| $S_d$ = | 0.106 | [mm] | |

# D.3 Hand calculation to Bachmann and Lang

## Kapazitätskurven der Wände mit MB (normal)

### 1) Geometrie

| | | | |
|---|---|---|---|
| Gebäudefläche | $A$ = | 12 | [$m^2$] |
| Gebäudehöhe | $H_{tot}$ = | 3 | [m] |
| Geschosshöhe | $h_{st}$ = | 2.625 | [m] |
| Fensterhöhe | $h_p$ = | 2.25 | [m] |

| Wände | $L_w$ [m] | t [m] |
|---|---|---|
| 1 | 1 | 0.2 |
| 5 | 1 | 0.2 |

**Materialparameter (Masonry with bricks in clay)**

| | | | |
|---|---|---|---|
| | $\gamma_m$ = | 2.0 | [-] |
| charakteristic compression strenght | $f_k$ = | 7.0 | [$N/mm^2$] |
| design compression strenght in x-direction | $f_{xd}$= | 3.5 | [$N/mm^2$] |
| design compression strenght in y-direction (0.3*fxd) | $f_{yd}$ = | 1.05 | [$N/mm^2$] |
| mean compression strength of masonry | $f_m$ = | 10 | [$N/mm^2$] |
| | $f_{vm0}$ | 0.29 | [$N/mm^2$] |
| | $f_{vlim}$ | 2.2 | [$N/mm^2$] |
| | $\mu$ = | 0.6 | [-] |
| Young elasticity modulus | $E$ = | 7000 | [$N/mm^2$] |
| Shear modulus (0.4 * E) | $G$ = | 2800 | [$N/mm^2$] |
| masonry density | $\rho_m$ = | 13 | [$kN/m^3$] |
| cracked stiffness ratio | $k_{eff}/k_0$ = | 0.6 | [-] |

**Einwirkungen**

| | | | |
|---|---|---|---|
| Eigengewicht Decke | $g_{mD}$ = | 2.43 | [$kN/m^2$] |
| Eigengewicht Wand | $g_{mW}$ = | 2.6 | [$kN/m^2$] |
| Eigengewicht Wandaufbau | $g_{AW}$ = | 0.5 | [$kN/m^2$] |
| Nutzlast | $q_{NL}$ = | 3 | [$kN/m^2$] |
| | $\psi_2$ = | 0.3 | [-] |

### 2) Identifikation der tragenden Wände

| | Wandnr. | 1 | | |
|---|---|---|---|---|
| Wandlänge | $L_w$ | 1.0 | [m] | |
| Pfeilerhöhe | $H_{op}$ | 2.25 | [m] | |
| Wanddicke | $t_w$ | 0.2 | [m] | |
| Trägheitsmoment Wand | $I_w$ | 1.67E+10 | [$mm^4$] | |
| Wandsteifigkeit | $EI_w$ | 1.17E+14 | [$Nmm^2$] | |
| Kopplungssteifigkeit | $EI_K$ | 1.97E+13 | [-] | |
| Steifigkeitsverhältnis | $EI_K/EI_W$ | 1.69E-01 | [-] | |
| Distanz zwischen Wände (Öffungen) | $l_0$ | 2 | [m] | |
| Verhältnis | $h_{st}/l_o$ | 1.31 | [-] | |
| | | 0.221 | [-] | --> Diagramm |
| aus Diagramm | $h_0/h_{st}$ | 0.730 | [-] | |

### 3) Berechnung der Normalkräfte und Stockwerksmassen

| | | | |
|---|---|---|---|
| Totale Vertikalkraft | $N_{tot}$ = | 63.36 | [kN] |
| | $q_{d,Decke}$ = | 3.33 | [$kN/m^2$] |

| Stockwerk | N1 [kN] |
|---|---|
| 1 | 15.8 |
| 1 | - |
| 1 | 7 |

Decke ist nur mit Wände in x-Richtung verbunden.
Decke ist nur mit Wände in y-Richtung verbunden.
Decke ist gleichmässig verbunden.

Kontrolle:

| | | |
|---|---|---|
| Vertikallast aus Wandeinnormalkräfte: | 63.36 | [kN] |
| Vertikallast aus Deckeneinwirkung auf Gesamtfläche: | 39.96 | [kN] |

## 4) Kapazitätskurve der Wände

a) Ermittlung der relativen Höhe des Momentennullpunktes

| Wand | 1 | |
|---|---|---|
| $h_{op}/h_p$ | 0.852 | [-] |
| $h_{op}$ | 1.91625 | [m] |

b) horizontaler **Widerstand**

$V_m$ = 3.96

c) Momente

$V_{bm}$ = 15.83 [kN]
$M_1$ = -1.3 [kNm]
$M_2$ = 7.6 [kNm]

d) Winkel der Druckstrebe alpha

$l_{2v}$ = 0.04 [m]
$\tan \alpha_{max}$ = 0.43 if ≥ $\tan \Phi_d = \mu$ = 0.6

e) Spannung in vertikale Druckstrebe:

$N_v$ = 9.30 [kN]
$N_n$ = 6.5 [kN]
$\sigma_n$ = 0.77 [N/mm$^2$]
if < fxd - fyd = 2.45 [N/mm$^2$]

f) Gleitkriterium
(Am obersten Stock, wo Normalkräfte am kleinsten sind.

$V_{OG}$ = 3.96 [kN]
$\tan \alpha$ = 0.25 < $\tan \Phi d = \mu$ = 0.6

g) Steifigkeitsermittlung:
(einfaches Rahmensystem)
(mit Q = 1kN)

| | | |
|---|---|---|
| Q = | 1 | [kN] |
| $M_1$* = | -0.3 | [kNm] |
| $M_2$* = | 1.9 | [kNm] |
| $w_{Stütze}$ = | 28.43 | [mm] |
| $w_{Kopplung}$ = | 1.68 | [mm] |
| $w_{tot}$ = | 58.54 | [mm] |
| $k_0$ = | 17081 | [kN/m] |

$k_{eff}$ = 10249
$k_{tot}$ = 40995.56

h) Fliessverschiebung

$\Delta_y$ = (ratio 1) 0.232 [mm]
$\Delta_y$ = (ratio 0.6) 0.386 [mm]

i) plastisches Verformungsvermögen

$\delta_u$ = 0.78 [%] (0.5 bis 0.7)
$\delta_y$ = (ratio 0.6) 0.0147 [%]
$\mu = \delta u/\delta y$ (ratio 1) 101.05 [-]
$\mu = \delta u/\delta y$ (ratio 0.6) 60.63 [-]

j) Verschiebeduktilität
k) Bruchverschiebung

$\Delta_u$ = (ratio 1) 20.10 [mm]
$\Delta_u$ = (ratio 0.5) 20.12 [mm]

l) Duktilität

$\mu = \Delta_u/\Delta_y$ (ratio 1) 86.76 [-]
$\mu = \Delta_u/\Delta_y$ (ratio 0.5) 52.11 [-]

6534
m = 6336 kg
omega = 80.44 s$^{-1}$
f = 16.53 s$^{-1}$
T = (stiffness ratio 1) 0.0605 s
f = 12.80 s$^{-1}$
T = (stiffness ratio 0.5) 0.0781

| | k | $\omega_1$ | $T_1$ |
|---|---|---|---|
| | [kN/m] | [s-1] | [s] |
| Lang (1) | 68326 | 103.84 | 0.061 |
| Lang (0.7) | 47828 | 86.88 | 0.072 |
| Lang (0.6) | 40996 | 80.44 | 0.078 |
| Lang (0.5) | 34163 | 72.31 | 0.087 |

| | uncracked stiffness | | cracked stiffness (0.5) | | cracked stiffness (0.6) | | cracked stiffness (0.7) | |
|---|---|---|---|---|---|---|---|---|
| | d [mm] | $V_b$ [kN] | d [mm] | $V_b$ [kN] | d [mm] | $V_b$ [kN] | d [mm] | $V_b$ [kN] |
| $\Delta_0$ = | 0.00 | 0.00 | 0.00 | 0.00 | 0.00 | 0.00 | 0.00 | 0.00 |
| $\Delta_y$ = | 0.23 | 15.83 | 0.46 | 15.83 | 0.39 | 15.83 | 0.33 | 15.83 |
| $\Delta_u$ = | 20.10 | 15.83 | 20.13 | 15.83 | 20.12 | 15.83 | 20.11 | 15.83 |

| | | |
|---|---|---|
| $\Delta_{u,\alpha=0.6}$ = | 12.10 | 15.83 |

## D.4. 3Muri Computation

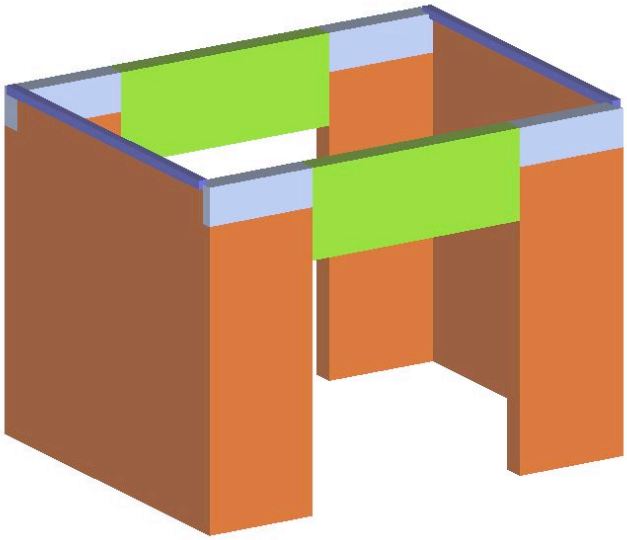

**Figure D.1** 3D-mesh model of test structure

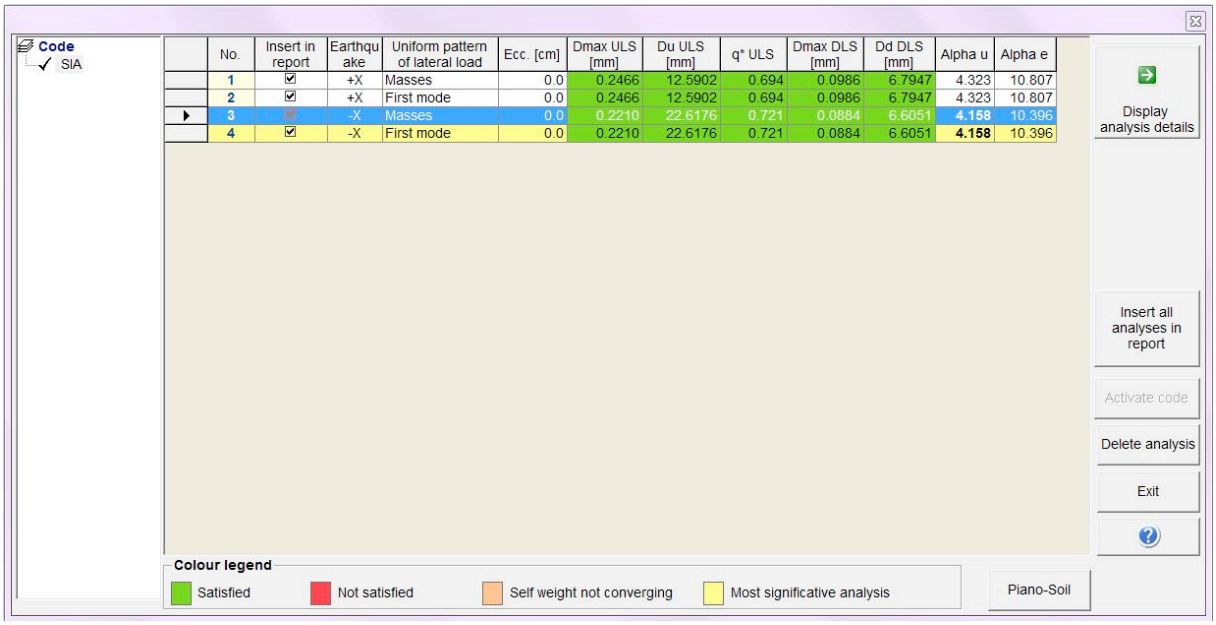


**Figure D.2** Analysis combinations of the test structure

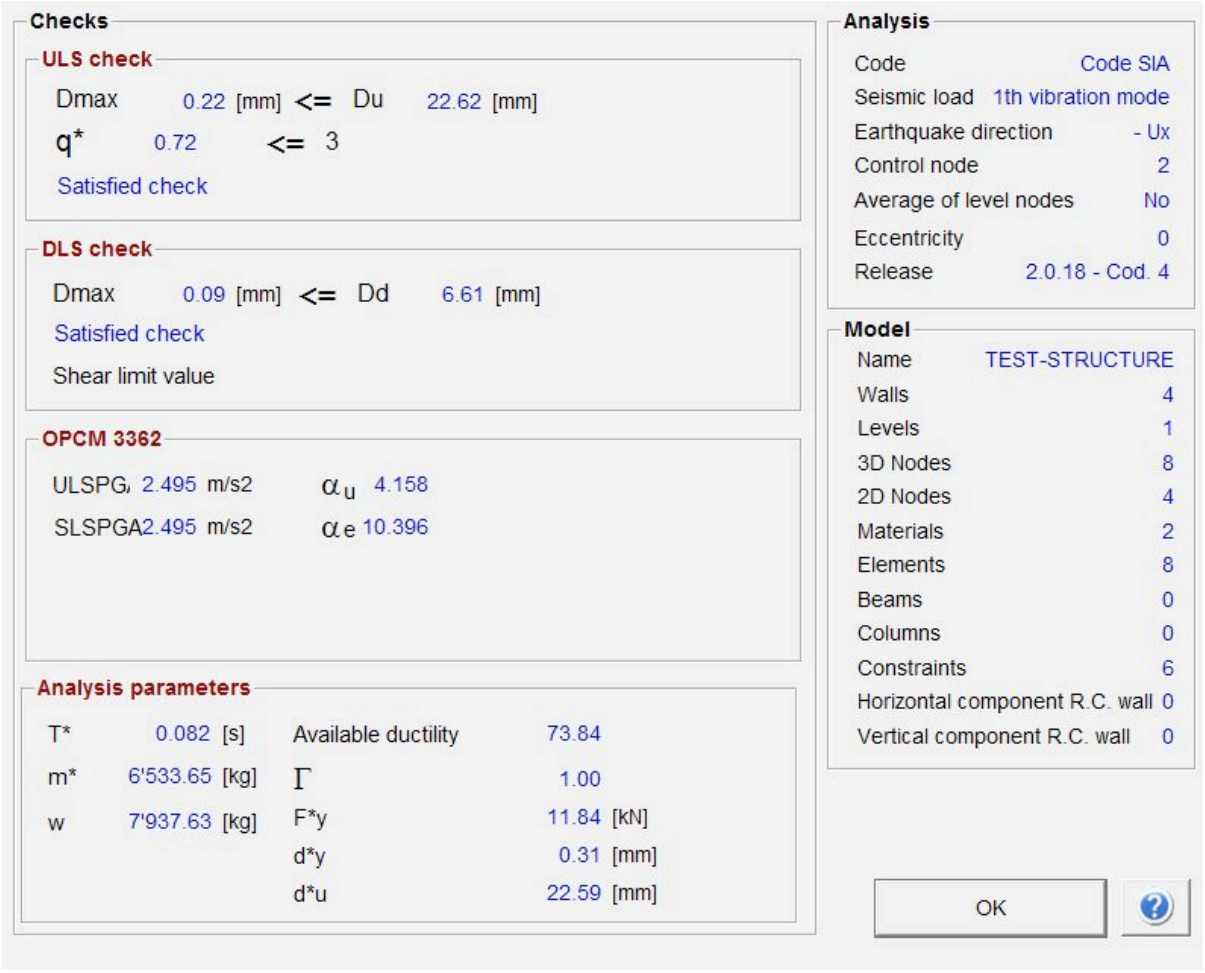


**Figure D.3** Results of the decisive analysis combination for the test structure

# E Evaluation

## E.1 Global Analysis

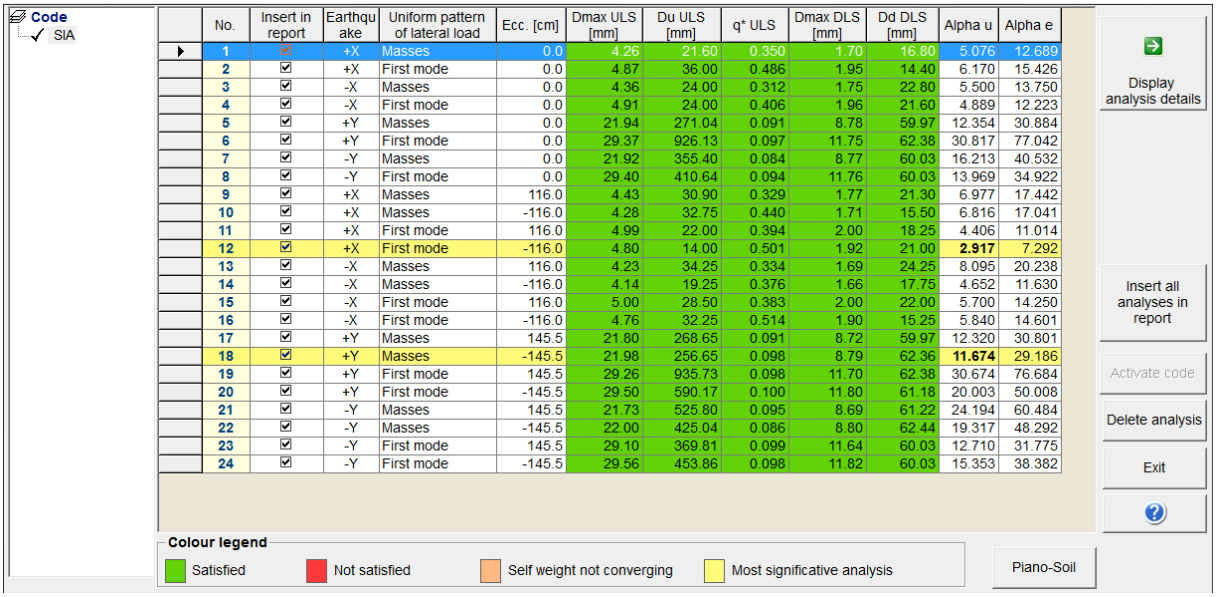

Code: SIA

| | No. | Insert in report | Earthquake | Uniform pattern of lateral load | Ecc. [cm] | Dmax ULS [mm] | Du ULS [mm] | q* ULS | Dmax DLS [mm] | Dd DLS [mm] | Alpha u | Alpha e |
|---|---|---|---|---|---|---|---|---|---|---|---|---|
| ▶ | 1 | ☑ | +X | Masses | 0.0 | 4.26 | 21.60 | 0.350 | 1.70 | 16.80 | 5.076 | 12.689 |
| | 2 | ☑ | +X | First mode | 0.0 | 4.87 | 36.00 | 0.486 | 1.95 | 14.40 | 6.170 | 15.426 |
| | 3 | ☑ | -X | Masses | 0.0 | 4.36 | 24.00 | 0.312 | 1.75 | 22.80 | 5.500 | 13.750 |
| | 4 | ☑ | -X | First mode | 0.0 | 4.91 | 24.00 | 0.406 | 1.96 | 21.60 | 4.889 | 12.223 |
| | 5 | ☑ | +Y | Masses | 0.0 | 21.94 | 271.04 | 0.091 | 8.78 | 59.97 | 12.354 | 30.884 |
| | 6 | ☑ | +Y | First mode | 0.0 | 29.37 | 926.13 | 0.097 | 11.75 | 62.38 | 30.817 | 77.042 |
| | 7 | ☑ | -Y | Masses | 0.0 | 21.92 | 355.40 | 0.084 | 8.77 | 60.03 | 16.213 | 40.532 |
| | 8 | ☑ | -Y | First mode | 0.0 | 29.40 | 410.64 | 0.094 | 11.76 | 60.03 | 13.969 | 34.922 |
| | 9 | ☑ | +X | Masses | 116.0 | 4.43 | 30.90 | 0.329 | 1.77 | 21.30 | 6.977 | 17.442 |
| | 10 | ☑ | +X | Masses | -116.0 | 4.28 | 32.75 | 0.440 | 1.71 | 15.50 | 6.816 | 17.041 |
| | 11 | ☑ | +X | First mode | 116.0 | 4.99 | 22.00 | 0.394 | 2.00 | 18.25 | 4.406 | 11.014 |
| | 12 | ☑ | +X | First mode | -116.0 | 4.80 | 14.00 | 0.501 | 1.92 | 21.00 | **2.917** | 7.292 |
| | 13 | ☑ | -X | Masses | 116.0 | 4.23 | 34.25 | 0.334 | 1.69 | 24.25 | 8.095 | 20.238 |
| | 14 | ☑ | -X | Masses | -116.0 | 4.14 | 19.25 | 0.376 | 1.66 | 17.75 | 4.652 | 11.630 |
| | 15 | ☑ | -X | First mode | 116.0 | 5.00 | 28.50 | 0.383 | 2.00 | 22.00 | 5.700 | 14.250 |
| | 16 | ☑ | -X | First mode | -116.0 | 4.76 | 32.25 | 0.514 | 1.90 | 15.25 | 5.840 | 14.601 |
| | 17 | ☑ | +Y | Masses | 145.5 | 21.80 | 268.65 | 0.091 | 8.72 | 59.97 | 12.320 | 30.801 |
| | 18 | ☑ | +Y | Masses | -145.5 | 21.98 | 256.65 | 0.098 | 8.79 | 62.36 | **11.674** | 29.186 |
| | 19 | ☑ | +Y | First mode | 145.5 | 29.26 | 935.73 | 0.098 | 11.70 | 62.38 | 30.674 | 76.684 |
| | 20 | ☑ | +Y | First mode | -145.5 | 29.50 | 590.17 | 0.100 | 11.80 | 61.18 | 20.003 | 50.008 |
| | 21 | ☑ | -Y | Masses | 145.5 | 21.73 | 525.80 | 0.095 | 8.69 | 61.22 | 24.194 | 60.484 |
| | 22 | ☑ | -Y | Masses | -145.5 | 22.00 | 425.04 | 0.086 | 8.80 | 62.44 | 19.317 | 48.292 |
| | 23 | ☑ | -Y | First mode | 145.5 | 29.10 | 369.81 | 0.099 | 11.64 | 60.03 | 12.710 | 31.775 |
| | 24 | ☑ | -Y | First mode | -145.5 | 29.56 | 453.86 | 0.098 | 11.82 | 60.03 | 15.353 | 38.382 |

Colour legend: Satisfied | Not satisfied | Self weight not converging | Most significative analysis

Buttons: Display analysis details | Insert all analyses in report | Activate code | Delete analysis | Exit | Piano-Soil

**Figure E.1** 24 analyses combinations for the flexible-floor model

**Checks**

**ULS check**

Dmax 4.80 [mm] <= Du 14.00 [mm]

q* 0.50 <= 3

Satisfied check

**DLS check**

Dmax 1.92 [mm] <= Dd 21.00 [mm]

Satisfied check

Shear limit value

**OPCM 3362**

ULSPGA 1.750 m/s2 $\alpha_u$ 2.917

SLSPGA 1.750 m/s2 $\alpha_e$ 7.292

**Analysis parameters**

T* 0.706 [s] Available ductility 1.46

m* 9'483'940.56 [kg] Γ 0.30

w 10'201'693.43 [kg] F*y 24'147.13 [kN]

d*y 32.14 [mm]

d*u 46.95 [mm]

**Analysis**

| | |
|---|---|
| Code | Code SIA |
| Seismic load | 1th vibration mode |
| Earthquake direction | + Ux |
| Control node | 259 |
| Average of level nodes | No |
| Eccentricity | -116.010200500488 |
| Release | 2.0.18 - Cod. 4 |

**Model**

| | |
|---|---|
| Name | BHO_FF-MC |
| Walls | 26 |
| Levels | 6 |
| 3D Nodes | 268 |
| 2D Nodes | 71 |
| Materials | 4 |
| Elements | 549 |
| Beams | 55 |
| Columns | 6 |
| Constraints | 67 |
| Horizontal component R.C. wall | 0 |
| Vertical component R.C. wall | 0 |

OK

**Figure E.2** Analysis results for the decisive analysis nr. 12 in the x-direction

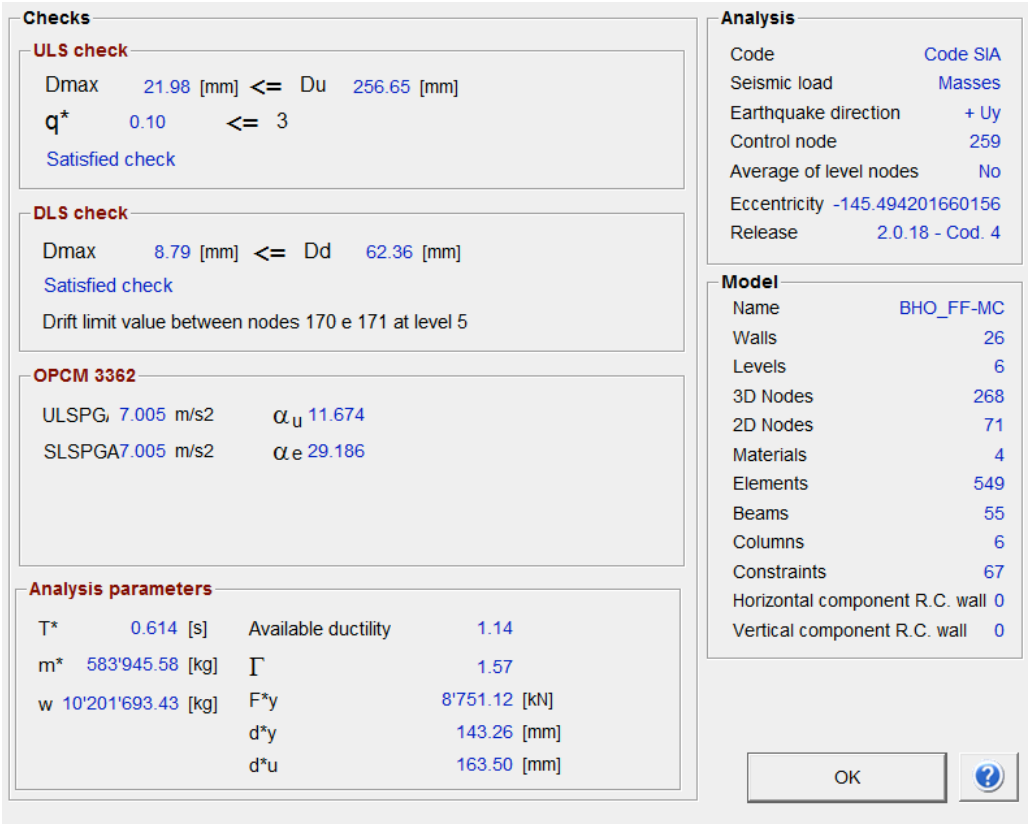


**Figure E.3** Analysis results for the decisive analysis nr. 18 in the y-direction

The following tables contain the values of the story-drift evaluation. Two analyses combinations have been used to determine the maximal story drift in each direction. The green fields show the decisive drift in the correspondent analysis.

**Table E.1** Story drift determination for the model with flexible floors

**Flexible Floors Analysis - reference node 259 (3.OG) close to mass center**

| 1st Modus | loading in X-direction (analysis nr.12) | | | | | | |
|---|---|---|---|---|---|---|---|
| T = 0.732 s | Node-Nr. | $U_x$ | $U_y$ | $U_z$ | $\Delta_X$ | $\Delta_Y$ | $\Delta_Z$ |
| Floor | [-] | [mm] | [mm] | [mm] | [mm] | [mm] | [mm] |
| EG | 60 | 1.87 | -0.31 | -1.43 | 1.87 | -0.31 | -1.43 |
| 1.OG | 61 | 5.72 | -2.03 | -2.68 | 3.85 | -1.72 | -1.25 |
| 2.OG | 62 | 10.49 | -3.91 | -3.37 | 4.77 | -1.88 | -0.69 |
| 3.OG | 63 | 13.57 | -5.36 | -3.35 | 3.08 | -1.45 | 0.02 |
| 4.OG | 64 | 15 | -5.79 | -3.58 | 1.43 | -0.43 | -0.23 |
| Masses | loading in X-direction (analysis nr. 14) | | | | | | |
| T = 0.609 s | Node-Nr. | $U_x$ | $U_y$ | $U_z$ | $\Delta_X$ | $\Delta_Y$ | $\Delta_Z$ |
| Floor | [-] | [mm] | [mm] | [mm] | [mm] | [mm] | [mm] |
| EG | 60 | -2.43 | 0.40 | -0.26 | -2.43 | 0.40 | -0.26 |
| 1.OG | 61 | -10.66 | 1.81 | -1.06 | -8.23 | 1.41 | -0.80 |
| 2.OG | 62 | -14.95 | 2.87 | -2.10 | -4.29 | 1.06 | -1.04 |
| 3.OG | 63 | -17.16 | 3.30 | -3.16 | -2.21 | 0.43 | -1.06 |
| 4.OG | 64 | -18.75 | 3.14 | -3.43 | -1.59 | -0.16 | -0.27 |
| 1st Modus | loading in Y-direction (analysis nr.23) | | | | | | |
| T = 0.813 s | Node-Nr. | $U_x$ | $U_y$ | $U_z$ | $\Delta_X$ | $\Delta_Y$ | $\Delta_Z$ |
| Floor | [-] | [mm] | [mm] | [mm] | [mm] | [mm] | [mm] |
| EG | 60 | 0.07 | -1.91 | -0.85 | 0.07 | -1.91 | -0.85 |
| 1.OG | 61 | 0.33 | -9.67 | -1.89 | 0.26 | -7.76 | -1.04 |
| 2.OG | 62 | 0.44 | -16.16 | -2.72 | 0.11 | -6.49 | -0.83 |
| 3.OG | 63 | 0.32 | -24.10 | -3.64 | -0.12 | -7.94 | -0.92 |
| 4.OG | 64 | 0.16 | -35.85 | -3.96 | -0.16 | -11.75 | -0.32 |
| Masses | loading in Y-direction (analysis nr. 18) | | | | | | |
| T = 0.614 s | Node-Nr. | $U_x$ | $U_y$ | $U_z$ | $\Delta_X$ | $\Delta_Y$ | $\Delta_Z$ |
| Floor | [-] | [mm] | [mm] | [mm] | [mm] | [mm] | [mm] |
| EG | 60 | -0.10 | 4.89 | -0.61 | -0.10 | 4.89 | -0.61 |
| 1.OG | 61 | -0.55 | 29.15 | -1.51 | -0.45 | 24.26 | -0.90 |
| 2.OG | 62 | 0.19 | 36.49 | -2.34 | 0.74 | 7.34 | -0.83 |
| 3.OG | 63 | 1.24 | 46.01 | -2.71 | 1.05 | 9.52 | -0.37 |
| 4.OG | 64 | 1.91 | 54.78 | -2.87 | 0.67 | 8.77 | -0.16 |

**Table E.2** Story drift determination of the model with rigid floors

**Rigid Floors Analysis - reference node 259 (3.OG) close to mass center**

| 1st Modus | loading in X-direction (analysis nr.16) | | | | | | |
|---|---|---|---|---|---|---|---|
| T = 0.696 s | Node-Nr. | $U_x$ | $U_y$ | $U_z$ | $\Delta_X$ | $\Delta_Y$ | $\Delta_Z$ |
| Floor | [-] | [mm] | [mm] | [mm] | [mm] | [mm] | [mm] |
| EG | 60 | -3.32 | 0.29 | 0.04 | -3.32 | 0.29 | 0.04 |
| 1.OG | 61 | -15.01 | 1.51 | -0.33 | -11.69 | 1.22 | -0.37 |
| 2.OG | 62 | -28.91 | 2.94 | -0.40 | -13.9 | 1.43 | -0.07 |
| 3.OG | 63 | -39.19 | 3.19 | -1.71 | -10.28 | 0.25 | -1.31 |
| 4.OG | 64 | -42.96 | 3.71 | -1.91 | -3.77 | 0.52 | -0.2 |
| Masses | loading in X-direction (analysis nr. 14) | | | | | | |
| T = 0.580 s | Node-Nr. | $U_x$ | $U_y$ | $U_z$ | $\Delta_X$ | $\Delta_Y$ | $\Delta_Z$ |
| Floor | [-] | [mm] | [mm] | [mm] | [mm] | [mm] | [mm] |
| EG | 60 | -4.33 | 0.25 | 0.09 | -4.33 | 0.25 | 0.09 |
| 1.OG | 61 | -16.40 | 1.42 | -0.43 | -12.07 | 1.17 | -0.52 |
| 2.OG | 62 | -28.43 | 2.54 | -1.14 | -12.03 | 1.12 | -0.71 |
| 3.OG | 63 | -36.24 | 2.73 | -2.07 | -7.81 | 0.19 | -0.93 |
| 4.OG | 64 | -39.2 | 3.08 | -2.29 | -2.96 | 0.35 | -0.22 |
| 1st Modus | loading in Y-direction (analysis nr.20) | | | | | | |
| T = 0.6 s | Node-Nr. | $U_x$ | $U_y$ | $U_z$ | $\Delta_X$ | $\Delta_Y$ | $\Delta_Z$ |
| Floor | [-] | [mm] | [mm] | [mm] | [mm] | [mm] | [mm] |
| EG | 60 | 0.10 | 4.90 | -0.58 | 0.1 | 4.9 | -0.58 |
| 1.OG | 61 | 0.10 | 26.11 | -1.31 | 0 | 21.21 | -0.73 |
| 2.OG | 62 | 0.32 | 34.38 | -1.87 | 0.22 | 8.27 | -0.56 |
| 3.OG | 63 | 0.62 | 42.98 | -1.89 | 0.3 | 8.6 | -0.02 |
| 4.OG | 64 | 1.36 | 50.17 | -2.01 | 0.74 | 7.19 | -0.12 |
| Masses | loading in Y-direction (analysis nr. 18) | | | | | | |
| T = 0.495 s | Node-Nr. | $U_x$ | $U_y$ | $U_z$ | $\Delta_X$ | $\Delta_Y$ | $\Delta_Z$ |
| Floor | [-] | [mm] | [mm] | [mm] | [mm] | [mm] | [mm] |
| EG | 60 | -0.02 | 15.96 | -0.77 | -0.02 | 15.96 | -0.77 |
| 1.OG | 61 | 0.21 | 26.66 | -1.52 | 0.23 | 10.7 | -0.75 |
| 2.OG | 62 | 0.48 | 32.57 | -2.12 | 0.27 | 5.91 | -0.6 |
| 3.OG | 63 | 0.67 | 38.36 | -2.34 | 0.19 | 5.79 | -0.22 |
| 4.OG | 64 | 1.2 | 42.99 | -2.48 | 0.53 | 4.63 | -0.14 |

## E.2 Local Analysis

### Local Collapse Mechanisms of Wall 1

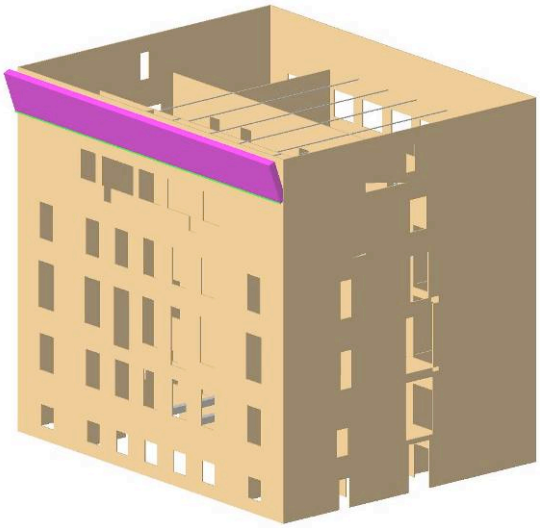

**Figure E.4** Mechanism 1 of Wall 1

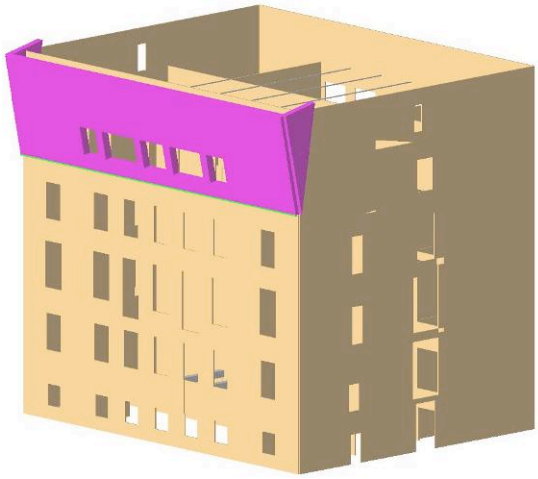

**Figure E.5** Mechanism 2 of Wall 1

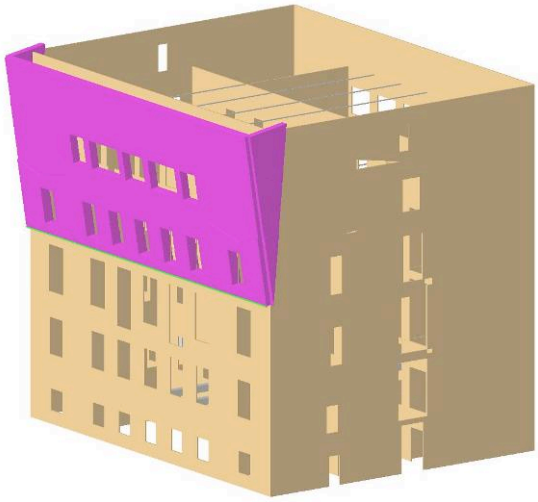

**Figure E.6** Mechanism 3 of Wall 1

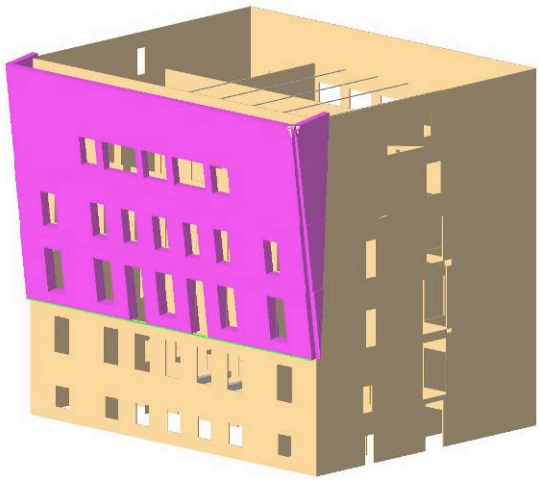

**Figure E.7** Mechanism 4 of Wall 1

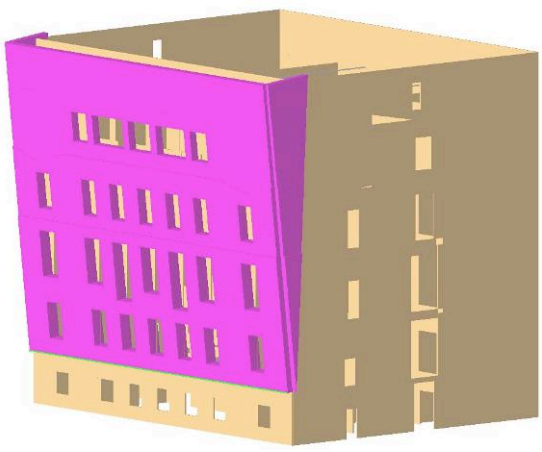

**Figure E.8** Mechanism 5 of Wall 1

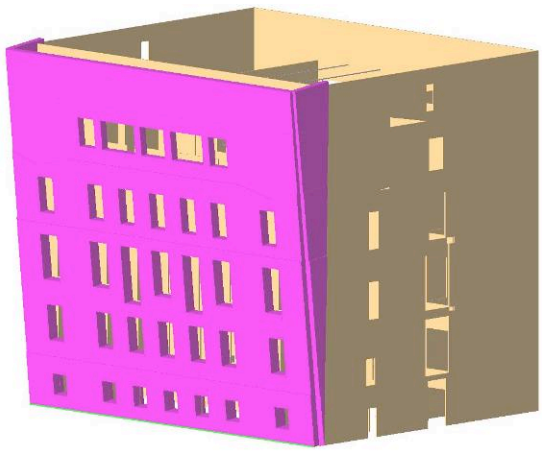

**Figure E.9** Mechanism 6 of Wall 1

**Local Collapse Mechanisms of Wall 2**

**Figure E.10** Mechanism 1 of Wall 2

**Figure E.11** Mechanism 2 of Wall 2

**Figure E.12** Mechanism 3 of Wall 2

**Figure E.13** Mechanism 4 of Wall 2

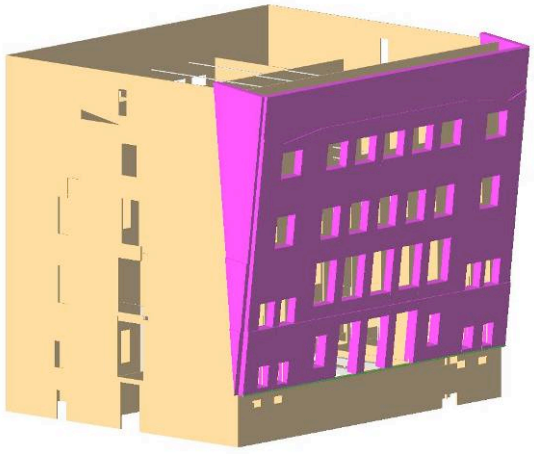

**Figure E.14** Mechanism 5 of Wall 2